MOLECULAR EFFECTS ON THE TRIBOLOGICAL PROPERTIES OF MONOLAYER FILMS

By

Brandon David Booth

Dissertation

Submitted to the Faculty of the

Graduate School of Vanderbilt University

in partial fulfillment of the requirements

for the degree of

DOCTOR OF PHILOSOPHY

in

Chemical Engineering

May, 2011

Nashville, Tennessee

Approved:

Dr. G. Kane Jennings

Dr. Clare McCabe

Dr. Paul E. Laibinis

Dr. Peter Cummings

Dr. Florence Sanchez

To my parents, Jan and David Booth, and my wife, Aubrie

ACKNOWLEDGEMENTS

I would like to thank Kane Jennings for his support as the primary advisor to my graduate research. He was an invaluable resource for both inspiration and guidance and I cannot thank him enough for his help. I would also like to thank Clare McCabe for her countless contributions and discussions regarding my research. I would also like to thank my thesis committee members: Dr. Paul Laibinis, Dr. Peter Cummings, and Dr. Florence Sanchez who provided direction and support in my graduate career. The questions they raised and criticism they provided added depth to this work and helped me grow as a researcher. I wish them continued success at Vanderbilt University.

I would like to thank fellow graduate students Angeline Cione, Steve Vilt, and Ben Lewis, post-docs Dr. Oleg Mayzar and Dr. Jose Rivera, and undergraduates Eddie Buehler and Nate Martin who contributed to this work. All of their contributions to this research were extremely beneficial. I would also like to thank Dr. Brad Berron, Dr. Chris Faulker, Dr. Peter Ciesielski, Juan Carlos Tuberquia, and Carlos Escobar for their helpful discussions and friendship during my time at Vanderbilt. I would also like to thank Dr. Ben Schmidt and Bobby Harl who provided assistance with characterizations in their lab. I was extremely lucky to have been surrounded by so many talented and intelligent individuals. Each enhanced my research experience and for that I am truly grateful.

I thank Dr. Bridget Rogers for the use of ellipsometer and XPS and Dr. David Cliffel for the use of the optical microscope.

There are many friends both within and outside the Chemical Engineering department that helped make my experience at Vanderbilt and in Nashville memorable and entertaining outside of my research.

Finally I would like to thank my family whose unwavering belief in me provided a source of inspiration during difficult times. The support of the Gatlin family was too frequently not fully recognized by me, but whose constant love and support was certainly not overlooked. My parents Jan and David Booth provided frequent pep talks, advice, and a sympathetic ear on countless occasions. I am most grateful to my wife who has stood by me throughout my graduate studies. I thank her for her patience and support and would like her to know that without her love I would not be the person I am today.

This work was supported by the Office of Naval Research under grant numbers N00014-06-1-0624 and N00014-07-1-0843 and the State of Tennessee. I am thankful to the IBM Fellowship Foundation and Vanderbilt University.

TABLE OF CONTENTS

Page

LIST OF TABLES

Table Page

LIST OF FIGURES

CHAPTER I

INTRODUCTION

In recent years the specific problem of lubricating microelectromechanical systems (MEMS) and nanoelectromechanical systems (NEMS) has resulted in the re-emergence of the field of tribology[1-8] with the goal of understanding lubrication at the nanoscale, as well as related concepts of friction and wear. MEMS/NEMS devices (referred to by the generic term MEMS) can be used in areas such as fluidics, information technology, and automotive industries where devices have been fabricated to meet a wide range of applications, including sensors (acceleration, pressure, chemical), gear trains, gas turbines, switches, and tweezers.[9] To date, MEMS devices have been fabricated primarily by photolithography and are emerging in commercial applications such as accelerometers used in automobile air bag deployment, digital micromirrors used in projection displays,[10] and Apple's iPod and iPhones. While accelerometers in air bags have been used for decades and the incorporation of such sensors in handheld devices has been commonplace for several years, these MEMS devices that are now appearing in commercial applications only have point contacts between components due to the lack of effective lubrication schemes between moving parts and the length scales. In the case of micromirrors for projection displays, the device was only made viable by cleverly minimizing stiction at point contacts through use of a small Hookean spring rather than eliminating adhesion at the contact site.[11] Therefore, understanding and controlling the forces acting in MEMS devices where surfaces are in sliding contact is of extreme

importance to the commercial realization and successful operation of MEMS devices, particularly for the future generations of devices in which many more components are necessary for operation and are often in motion relative to one another.

MEMS lubrication poses particular challenges in that, by design, these devices have surfaces that are separated by as few as 1-2 nm[12] and can move with respect to each other at what can be modest velocities from a macroscopic point of view (cm/s) but which correspond to extremely high strain rates ($\sim 10^7$ s^{-1}). Additionally, the phase behavior and physical properties of fluids used as lubricants can be dramatically affected by nanoconfinement. Finally, at the nanoscale, the surface to volume ratio for a typical component is very high, and as a result, surface forces such as adhesion, stiction, friction and wear become significant technological barriers to the successful application of durable devices. As devices become more sophisticated with more complex and demanding design and longevity requirements, particularly associated with rotating or oscillating elements, the need for a fundamental understanding of, and accurate design tools for, lubrication increases.

The sliding contact of two solid surfaces results in friction and wear, the significance of which is emphasized by their annual cost to the United States, estimated at over half a trillion dollars per year.[13] Lubrication is defined as the application of a substance capable of reducing friction, heat, and wear when introduced as a film between solid surfaces. The lubrication of any device must also enable reliable long-term operation with little to no damage to components or accumulation of thermal energy. Fundamentally, the phenomena of friction, wear, and lubrication involve molecular mechanisms occurring on a nanometer scale, and therefore, a good understanding of

lubricant behavior on this scale is critical to developing new technologies for reduction of loss due to friction. Practical examples are numerous and range from applications at the leading edge of lubrication technology (microelectromechanical systems and next generation magnetic disk drives) to the more conventional area of automotive lubrication (where the distances between asperities in moving metal surfaces can be nanometers or less). A lubrication scheme must be durable enough so as to reduce the long-term wear to the device and extend its lifetime. Traditional lubrication strategies are insufficient for MEMS as the microscale dimensions prevent viscous liquids from fully integrating into the device and do not provide ample wear protection or allow for proper functioning. Similarly, polymer films are often too thick to be deposited conformally between and underneath nano- and microscale components, and vapor-deposited films, while ultrathin and straightforward to apply, generally adhere only weakly to the surface and are therefore easily removed, resulting in the need for a constant flow of lubricant molecules in the vapor phase to maintain the function of the lubricant.[14, 15] In general, lubrication of small systems has not been solved, and as the number of these devices increases and their size scale decreases,[16] the need for new lubrication strategies is further emphasized.

Thin organic films prepared by the robust chemical adsorption of molecular components from solution onto the device surface represent an alternative lubrication strategy that lowers friction and has the potential to sustain repeated cycles of operation.[12, 17] Monolayer films represent a potential class of lubrication materials for MEMS devices due to their ease of formation, varying surface functionalities, and robust attachment to substrates. Precursors may be chosen that selectively assemble onto a substrate by matching head group of the assembling molecule to the substrate and can

assemble within complex geometries and intricate components. Figure 1.1 demonstrates the two monolayer systems studied in Chapters III-VI. Silane-based monolayer films

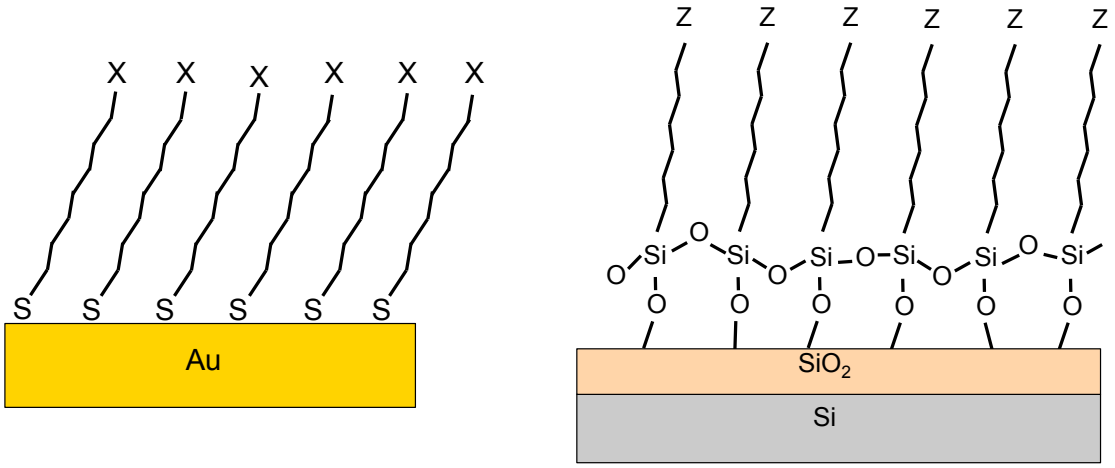

Figure 1.1. Schematic of monolayer films used in this work for lubrication schemes. The length of the film can be controlled by selection of precursor, X represents functionalities of thiolate precursors (CH_3, OH, COOH) and Z represents functionality of silane functionalities (CH_2, CH_3, CF_3, OH).

offer a covalent linkage to the substrate and simple deposition procedures onto a variety of surfaces while being compatible with silicon surfaces currently used for the majority of MEMS fabrication. Similarly, thiolate based monolayers chemisorb to many metal surfaces that are used for micromirrors and switches that also represent a critical need in MEMS development. However, some devices may necessitate the use of a mobile phase lubricant. Ionic liquids represent a unique set of fluids that offer the advantages of being highly tunable and possessing negligible vapor pressures while still having properties beneficial to the reduction of friction. Figure 1.2 shows the imidazolium-based cation and trifluoromethansulfonate and hexafluorophosphate anions studied in Chapter VII that were chosen due to demonstrated lubrication properties.[18-20]

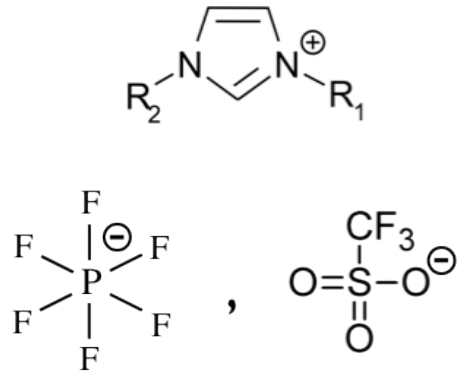

Figure 1.2. General 1,3-imidazolium based cation and three anions (PF_6^-, $CF_3SO_3^-$) that compose ionic liquids studied in this work. In this work R_1= CH_3- and R_2 = $CH_3(CH_2)_3$-

This thesis addresses key issues regarding the successful implementation of silane monolayers on silicon and n-alkanethiolate monolayers on gold as bound molecular lubricant films in tribological applications. While there have been studies addressing the use of monolayer for lubrication, it is my hope that this work provides a more comprehensive set of experiments on a more extensive number of molecules to better understand the molecular interactions in a lubricating film. Chapters IV, V, and VI discuss the tribological properties of monolayer films in lubrication schemes. This work provides a basic understanding of the interfacial interactions between two surfaces in contact and in motion while studying classical monolayer systems, which are straightforward to assemble and characterize, as the lubricant film. Chapter IV focuses on the initial frictional response of silane monolayers and n-alkanethiolate self-assembled monolayers to an applied load sliding across the surface and addresses the intermolecular interactions within the films that contribute to its coefficient of friction. This chapter serves to provide insight into the molecular aspects involved in a molecularly thin film

and provide guidelines for the expected performance of similar molecular layers in a lubricating layer. In Chapter V I describe the long term wear properties of monolyaer films with a focus on silane-based films, which displayed the most promising results in previous chapters, and address specifically the mechanism of failure for these monolayers. Both the durability and mechanism for failure are key factors in the potential application of monolayer films as lubricants and the work in this chapter discusses the molecular aspects of these phenomena. Chapter VI further addresses the role of intermolecular forces on tribological properties by using gradient films that have a varied surface coverage in a particular direction and therefore, varied surface energy in that direction. Potential applications for gradient films include devices such as microfluidics and molecular sensing. Chapter VII begins to address the use of a mobile phase of ionic liquid for further tribological benefit. Challenges in wettability and surface coverage are addressed as well as the sustainability of a mobile phase in microscale devices. While there has been a great deal of interest in the use of ionic liquids in a variety of fields including lubrication, this chapter focuses on the fundamentals of wetting and spreading of ionic liquids on substrates with a few key tribological studies.

References

1. Hu, Y. Z.; Granick, S., *Tribology Letters* **1998,** *5*, 81-88.

2. Feldman, K.; Fritz, M.; Hahner, G.; Marti, A.; Spencer, N. D., *Tribology International* **1998,** *31*, 99-105.

3. Gao, J. P.; Luedtke, W. D.; Landman, U., *Tribology Letters* **2000,** *9*, 3-13.

4. Czichos, H., *Meccanica* **2001,** *36*, 605-615.

5. Blau, P. J., *Tribology International* **2001,** *34*, 585-591.

6. Adams, J. B.; Hector, L. G.; Siegel, D. J.; Yu, H. L.; Zhong, J., *Surface and Interface Analysis* **2001,** *31*, 619-626.

7. Hsu, S. M., *Tribology International* **2004,** *37*, 537-545.

8. Maboudian, R.; Carraro, C., *Annual Review Of Physical Chemistry* **2004,** *55*, 35-54.

9. Muller, R. S., Microdynamic Systems in the Silicon Age. In *Handbook of Micro/Nano Tribology*, 2nd ed.; Bhushan, B., Ed. CRC Press: 1999; pp 673-690.

10. Henck, S. A., *Tribology Letters* **1997,** *3*, 239-247.

11. Israelachvili, J. N., *Intermolecular and Surface Forces*. 2nd ed.; Academic Press London: London, 1992.

12. Maboudian, R.; Ashurst, W. R.; Carraro, C., *Tribology Letters* **2002,** *12*, 95-100.

13. Bhushan, B., *Handbook of Micro/Nanotribology*. Second ed.; CRC Press: Boca Raton, FL, 1998.

14. Asay, D. B.; Dugger, M. T.; Kim, S. H., *Tribology Letters* **2008,** *29*, 67-74.

15. Asay, D. B.; Dugger, M. T.; Ohlhausen, J. A.; Kim, S. H., *Langmuir* **2008,** *24*, 155-159.

16. Bhushan, B., *Microelectronic Engineering* **2007,** *84*, 387-412.

17. Ren, S.; Yang, S. R.; Zhao, Y. P.; Zhou, J. F.; Xu, T.; Liu, W. M., *Tribology Letters* **2002,** *13*, 233-239.

18. Liu, W. M.; Ye, C. F.; Gong, Q. Y.; Wang, H. Z.; Wang, P., *Tribology Letters* **2002,** *13*, 81-85.

19. Ye, C. F.; Liu, W. M.; Chen, Y. X.; Ou, Z. W., *Wear* **2002,** *253*, 579-584.

20. Ye, C. F.; Liu, W. M.; Chen, Y. X.; Yu, L. G., *Chemical Communications* **2001**, 2244-2245.

CHAPTER II

BACKGROUND

Microelectromechanical Systems (MEMS)

Traditionally MEMS devices have been built using silicon as the structural material, due to its good mechanical properties and the availability of highly sophisticated silicon micromachining technology developed within the microelectronics industry.[1] Increasingly, other materials are being adopted for specific applications tailored to their properties, such as aluminum (micromirrors) and gold (optical MEMS/NEMS, microswitches). SiC has excellent mechanical and thermal properties and is optically transparent and chemically inert, making it particularly suited to harsh environments, such as those encountered in many aerospace applications.[2] Similarly, diamond and hard amorphous carbon coatings (known as diamond-like carbon) exhibit low friction and wear and are potential materials for various applications.[3, 4] Friction and wear at extremely light loads, as in MEMS devices, have been shown to be due to surface interaction forces at the atomic or molecular level rather than to the applied load. MEMS devices can have surface contacts which are either point (for example between the meshing teeth in a microgear such as in Figure 2.1) or area contacts (for example between the mirror and landing site in digital micromirror devices). The interaction between these asperities is governed by surface forces, and the resulting adhesion originates from a

combination of different attractive and/or repulsive forces including van der Waals, electrostatic, hydrodynamic, viscous and lubrication forces.[5] While this complication has

Figure 2.1. Scanning electron micrograph from Sandia National Laboratory demonstrating intricate fabrication capabilities for MEMS components. Image courtesy of Sandia National Laboratories, SUMMiT(TM) Technologies, http://www.mems.sandia.gov.

been addressed using techniques such as surface roughening that also helps reduce friction,[6, 7] this procedure alone does not solve many tribological issues such as durability. Hence, the major challenges in the production and use of MEMS include the release of adhesion between components and the substrate or adjacent microstructures, which can occur during both processing and in operation.[8] Traditional lubricants are incompatible with MEMS due to their high viscosities that prevent the desired motion of the device. Solid lubricants such as diamond-like carbon,[3] carbides,[9, 10] nitrides[11] and oxides have been developed for a number of applications; however, they suffer from the drawback of wear and are not easily replenished without destroying the MEMS device.

Thin organic films prepared by self-assembly on the device surface are an alternative strategy and several classes of organic films have been studied as boundary-layer lubricants, the most common being silane monolayers and thiol-based self-assembled monolayers (SAMs).

Tribology

With the recent growth in the development of MEMS, the field of tribology, which is the study of the interactions of surface when in motion, has become increasingly important at the micro- and nanoscales. Several techniques are available to probe the interactions between surfaces including atomic force microscopy (AFM), [12-18] surface force apparatus (SFA), [19, 20] and pin on disk tribometry.[18, 21-23] AFM and friction force microscopy (FFM) have been widely used for tribological studies and can provide information on the roughness,[19, 24] friction,[20, 25, 26] wear,[27] and lubrication[28] of films. AFM experiments are conducted at sliding speeds (~1 m/s) that are several orders of magnitude lower than application speeds for MEMS devices (0.1 m/s to over 500 m/s[29]) resulting in frictional properties that may not be in the correct regime for practical applications. AFM-based studies also lack the ability to investigate normal loads greater than ~100 nN, where the contacting area is approximately 100 nm^2, which corresponds to contact pressures on the order of ~10^9 Pa.[20]

Macro- and microscale friction and wear tests also have been reported in the literature using a pin-on-disk tribometer.[18, 21-23] A microtribometer enables the study of a broad range of sliding speeds (10 m/s to 10 mm/s), normal loads, and tip composition;

the ability to vary both the tip and the normal load, as in the current work, allows for measurements at higher forces while maintaining low to moderate surface pressures (< 300 MPa).

The surface contact pressure in pin on disk tribometry is calculated using the relevant model for contact area and the applied normal force:

$$P_m = \frac{F_N}{A_i} \tag{2-1}$$

where P_m is the mean surface contact pressure and A_i is the area of contact with i representing the model used to estimate the area. To estimate the contact area of the probe tip on the surface, two models will be used: the Hertz equation[30, 31] (equation 2-2) for deformation of a flat surface by a sphere:

$$A_H = \pi a^2 = \pi\left(\frac{3RF_N}{4E_c}\right)^{2/3} \tag{2-2}$$

where a is the radius of contact zone, E_c is the composite Young's modulus, and R is the tip radius. The Johnson-Kendall-Roberts (JKR) model[32] (equation 2-3) which modifies the Hertz equation to account for elastic deformation from adhesive forces by incorporating surface energy:

$$A_{JKR} = \pi\left[\frac{3R}{4E_c}\left(F_N + 6\pi\gamma R + \sqrt{12\pi\gamma RF_N + \left(6\pi\gamma R\right)^2}\right)\right]^{2/3} \tag{2-3}$$

where γ is the surface energy. The JKR theory, while describing the contact mechanics of soft materials with strong short-range adhesion, also provides a limiting case of continuous contact between the two surfaces. A parameter, α, has been developed that indicates a correction model to use based upon properties of the two contacting surfaces[33, 34]:

$$\alpha = \left[\frac{16R\gamma^2}{9E_c^2 z_o^3}\right]^{1/3} \tag{2-4}$$

where z_o is the separation of the surfaces or the range of effective adhesion. The microtribometer used for testing in this work yields an α value between 2.5 and 9.0 where $\alpha > 5$ suggests that the JKR model is relevant. Figure 2.2 shows the relationship between contact pressure and load for the microtribometer used in this work for both the Hertz and JKR models. Using known values of elastic properties for gold (E_{Au} = 77 GPa[35]) and silicon substrates (E_{SiO2} = 70 GPa[36]), a surface pressure for a normal load of 9.8 mN was calculated to be ~ 210 MPa using the Hertz equation and ~ 150 MPa using the JKR model. Since the effect of a monolayer on the elastic properties of a substrate has not been established, this estimate does not account for the monolayer films.

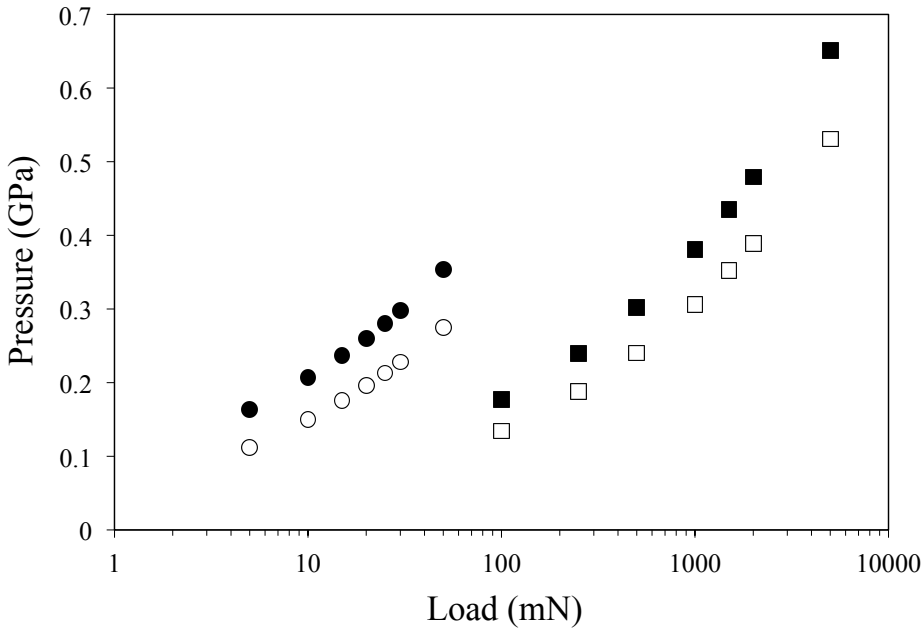

Figure 2.2. The relationship between normal load and contact pressure for tribology testing with microtribometer is shown as calculated from Eq 2-1. Circles represent lower DMF force sensor while squares correspond to DFM-0.5 force sensor. Closed and open symbols represent Hertz and JKR equation calculations, respectively.

Monolayers

Self-assembled monolayers (SAMs) are molecular films that can provide dense, two-dimensional sheets of surface functionality to impact interfacial properties.[37] SAMs have been used in a wide range of applications, such as the mitigation of protein adsorption,[38] promotion of selective attachments,[39, 40] generation of surfaces with varying wettability,[41] and lubrication between contacting surfaces.[25, 42-44] In the latter regard, the lubricating properties of a variety of different monolayer films on silicon[12, 28, 44] and

gold[13, 15, 45, 46] surfaces have been investigated in an effort to reduce friction and prevent wear during operation. The ability to tailor the properties of SAMs by manipulating the composition of the precursor molecule yields a versatile class of materials with which to investigate molecularly thin lubrication schemes. The ability to functionalize the terminus of the SAM and vary the length of the assembling molecules provides a wide range of possible films and surfaces, each with differing tribological properties and interfacial interactions. The role of packing and degree of crystallinity of the resulting film is important in the tribological properties of SAMs where a high degree of order yields a solid film capable of reducing friction while more loosely packed layers have a more liquid-like structure that may exhibit higher friction but provide better long-term wear protection.[12, 47]

Monolayers in Tribology

Monolayer films offer distinct advantages over many classical strategies for lubrication[43] of MEMS devices because the molecular components can assemble onto all surfaces, even within nanoscale crevices between moving components, or onto targeted surfaces by matching the adsorbate head group with the metal or oxide surface. Silane-based films are generally preferred in tribological applications[18] over thiolates because of the stronger covalent attachment of silanes compared to the weaker chemisorption of thiols on gold, silver, or copper. In addition, most MEMS devices are fabricated from silicon,[48] and therefore, interest in lubrication of silicon-based devices has led to several studies on the tribological properties of silane monolayers,[18, 22, 25, 42, 49] which are often

prepared by the reaction of n-alkyltrichlorosilanes with surface silanol groups. Nonetheless, alkanethiolate SAMs on gold are also of keen interest in tribological studies due to their widespread use in the modification of many surfaces,[37, 50] and the requisite, yet varied, mechanical requirements for these films.[26, 51, 52]

Molecular films have shown promise for the lubrication of surfaces, including both alkanethiolate SAMs on coinage metals[14, 15, 23, 26, 53, 54] and silane monolayers on silicon.[18, 25, 42, 44, 49] Individual studies have focused on the effects of chain length, packing, and functionality of contacts. Specifically, Lio et al.[45] and McDermott et al.[13] demonstrated that alkanethiolate monolayers formed from longer precursor molecules are more ordered and possess denser packing than shorter molecules. Their results suggest that the higher order and degree of packing for SAMs with longer chains are correlated with a reduced coefficient of friction. In addition to monolayer thickness, the functionality of the monolayer terminus has been shown to play an important role in frictional properties.[22, 55, 56] Clear and Nealey[25] showed that adhesion and friction were dependent upon monolayer terminus and solvent when performing chemical force microscopy with thiol-coated gold tips and trichlorosilane-coated silicon substrates. The frictional force is larger for polar termini than for nonpolar termini for all solvents studied. Evidence of probe tip influence has also been reported where similar functionalities between two contacting surfaces display greater adhesion and therefore a higher coefficient of friction than when the two have dissimilar termini.[15, 25, 57] Although studies of the frictional properties of monolayers by AFM and pin-on-disk tribometry are performed at vastly different forces and contacting areas, results from both types of testing were shown to be consistent.[18]

The structure and order within a monolayer is extremely important when characterizing the film's tribological properties. Several studies have focused on understanding the order and structure of silane films on silicon using infrared spectroscopy (FTIR,[58, 59] ATR,[60] and transmission IR[47, 61]) and near-edge X-ray absorption fine structure (NEXAFS)[59, 62, 63] and established the relationship between the length of the adsorbing molecule and the organization of the resulting films. Well formed $CH_3(CH_2)_{n-1}SiCl_3$ films derived from molecules where $n \geq 12$ are known to have a highly ordered, crystalline structure with the chains extended in a trans conformation with a 7-8° tilt from the substrate.[58, 60, 61] Similarly, shorter chains ($n < 8$) exhibit liquid-like structure that can be attributed to the lack of sufficient dispersive forces between molecules.[16] Monolayer films formed from silanes with an intermediate chain length ($8 \leq n < 12$) possess both crystalline and disordered, liquid-like regions.[12, 47, 59]

Ionic Liquids

The continuous replenishment of lubricant layers with viscous liquids is the key feature of conventional lubricant processes. While traditional lubricants are generally too viscous for MEMS devices, low-viscosity room-temperature ionic liquids (ILs) have begun to attract attention as potential MEMS lubricants.[64, 65] ILs are composed of poorly coordinating ions, so they can be highly polar yet non-coordinating solvents. In general ILs consist of a large, organic cation with a weakly coordinating inorganic anion, which limits packing and lowers the melting point. Since both the cation and anion can be varied largely independently, ILs are often referred to as "designer" fluids since their

properties, such as melting point, viscosity, density, hydrophobicity and miscibility in water, can be adjusted through changes to the type and structure of the ions. Although their bulk-phase viscosity is comparable to traditional hydrocarbon lubricants, ILs have been shown to exhibit very low friction in lubrication testing.[66, 67] ILs are comprised entirely of ions and have melting points at or below room temperature, (distinguishing them from high temperature molten salts). ILs have unique physical properties:[68-70] negligible vapor pressure, liquid at room temperature with an enormous liquid range (up to 300˚C), good solvents for a wide range of inorganic, organic and polymeric materials, high thermal stability, and non-flammability. While ILs are not new,[71 72] interest in these chemicals has grown considerably in recent years with the synthesis of water-stable ILs.[73, 74] ILs are used in electrochemisty,[75, 76] biochemistry[77, 78] and as solvents in synthesis,[69, 79-81] catalysis,[79, 82, 83] and separations,[68, 84-86] and recently, the first commercial process involving ionic liquids was announced.[87]

Many experimental studies on the tribological behavior of ILs have been carried out, which have demonstrated a number of promising IL lubricant candidates.[64, 66, 67, 88-92] Additionally, studies have been performed on the corrosion behavior of ILs which suggest they will make suitable lubricants for MEMS devices.[93] Lubrication of MEMS devices with ionic liquids has been shown to significantly enhance durability compared to hydrocarbon and fluorocarbon mobile or bound lubricant systems.[66, 88-91, 94-96] The work in Chapter VII focuses on the beneficial lubrication properties of ILs and challenges of deposition of such layers into a film for friction reduction.

References

1. Bhushan, B., Micro/Nano Tribology and Micro/Nano Mechanics of MEMS Devices. In *Handbook of Micro/Nano Tribology*, 2nd ed.; Bhushan, B., Ed. CRC Press: 1999; pp 797-831.

2. Breuer, K., Lubrication in MEMS. In *CRC Handbook on MEMS*, Gad el Hak, M., Ed. CRC Press: 2001.

3. Krauss, A. R.; Auciello, O.; Gruen, D. M.; Jayatissa, A.; Sumant, A.; Tucek, J.; Mancini, D. C.; Moldovan, N.; Erdemir, A.; Ersoy, D.; Gardos, M. N.; Busmann, H. G.; Meyer, E. M.; Ding, M. Q., *Diamond and Related Materials* **2001,** *10*, 1952-1961.

4. Auciello, O.; Birrell, J.; Carlisle, J. A.; Gerbi, J. E.; Xiao, X. C.; Peng, B.; Espinosa, H. D., *Journal of Physics-Condensed Matter* **2004,** *16*, R539-R552.

5. Komvopoulos, K., *Wear* **1996,** *200*, 305-327.

6. Komvopoulos, K., *Journal of Adhesion Science and Technology* **2003,** *17*, 477-517.

7. Lee, C. C.; Hsu, W., *Journal of Vacuum Science & Technology B* **2003,** *21*, 1505-1510.

8. Delrio, F. W.; De Boer, M. P.; Knapp, J. A.; Reedy, E. D.; Clews, P. J.; Dunn, M. L., *Nature Materials* **2005,** *4*, 629-634.

9. Gao, D.; Carraro, C.; Howe, R. T.; Maboudian, R., *Tribology Letters* **2006,** *21*, 226-232.

10. Radhakrishnan, G.; Adams, P. M.; Robertson, R.; Cole, R., *Tribology Letters* **2000,** *8*, 133-137.

11. Hsu, S. M., *Tribology International* **2004,** *37*, 537-545.

12. Sambasivan, S.; Hsieh, S.; Fischer, D. A.; Hsu, S. M., *Journal of Vacuum Science & Technology A* **2006,** *24*, 1484-1488.

13. McDermott, M. T.; Green, J. B. D.; Porter, M. D., *Langmuir* **1997,** *13*, 2504-2510.

14. Sung, I. H.; Kim, D. E., *Tribology Letters* **2004,** *17*, 835-844.

15. Brewer, N. J.; Leggett, G. J., *Langmuir* **2004,** *20*, 4109-4115.

16. Xiao, X. D.; Hu, J.; Charych, D. H.; Salmeron, M., *Langmuir* **1996,** *12*, 235-237.

17. Kim, H. I.; Graupe, M.; Oloba, O.; Koini, T.; Imaduddin, S.; Lee, T. R.; Perry, S. S., *Langmuir* **1999,** *15*, 3179-3185.

18. Bhushan, B.; Kasai, T.; Kulik, G.; Barbieri, L.; Hoffmann, P., *Ultramicroscopy* **2005,** *105*, 176-188.

19. Yoshizawa, H.; Chen, Y. L.; Israelachvili, J., *Journal of Physical Chemistry* **1993,** *97*, 4128-4140.

20. McGuiggan, P. M.; Zhang, J.; Hsu, S. M., *Tribology Letters* **2001,** *10*, 217-223.

21. Nakano, M.; Ishida, T.; Numata, T.; Ando, Y.; Sasaki, S., *Japanese Journal of Applied Physics Part 1-Regular Papers Short Notes & Review Papers* **2003,** *42*, 4734-4738.

22. Song, S. Y.; Zhou, J. F.; Qu, M. N.; Yang, S. R.; Zhang, J. Y., *Langmuir* **2008,** *24*, 105-109.

23. Lee, S.; Heeb, R.; Venkataraman, N. V.; Spencer, N. D., *Tribology Letters* **2007,** *28*, 229-239.

24. Benz, M.; Rosenberg, K. J.; Kramer, E. J.; Israelachvili, J. N., *Journal of Physical Chemistry B* **2006,** *110*, 11884-11893.

25. Clear, S. C.; Nealey, P. F., *Journal of Colloid and Interface Science* **1999,** *213*, 238-250.

26. Akimoto, K.; Sato, F.; Morikawa, T.; Fujihira, M., *Japanese Journal of Applied Physics Part 1-Regular Papers Short Notes & Review Papers* **2004,** *43*, 4492-4498.

27. D'Acunto, M., *Nanotechnology* **2006,** *17*, 2954-2962.

28. Maboudian, R.; Ashurst, W. R.; Carraro, C., *Sensors and Actuators A-Physical* **2000,** *82*, 219-223.

29. Bhushan, B., *Microelectronic Engineering* **2007,** *84*, 387-412.

30. Johnson, K. L., *Contact Mechanics*. Cambridge University Press: New York, 1987.

31. Mate, M. C., *Tribology on the Small Scale*. Oxford University Press: New York, 2008.

32. Johnson, K. L.; Kendall, K.; Roberts, A. D., *Proceedings of the Royal Society of London Series a-Mathematical and Physical Sciences* **1971,** *324*, 301-&.

33. Maugis, D., *Journal of Colloid and Interface Science* **1992,** *150*, 243-269.

34. Carpick, R. W.; Agrait, N.; Ogletree, D. F.; Salmeron, M., *Langmuir* **1996,** *12*, 3334-3340.

35. Piwonka, T. S., *Metals Handbook Desk Edition*. 2nd ed.; ASM International: 1998.

36. Kim, M. T., *Thin Solid Films* **1996,** *283*, 12-16.

37. Love, J. C.; Estroff, L. A.; Kriebel, J. K.; Nuzzo, R. G.; Whitesides, G. M., *Chemical Reviews* **2005,** *105*, 1103-1169.

38. Prime, K. L.; Whitesides, G. M., *Journal of the American Chemical Society* **1993,** *115*, 10714-10721.

39. Mrksich, M.; Chen, C. S.; Xia, Y. N.; Dike, L. E.; Ingber, D. E.; Whitesides, G. M., *Proceedings of the National Academy of Sciences of the United States of America* **1996,** *93*, 10775-10778.

40. Gujraty, K. V.; Ashton, R.; Bethi, S. R.; Kate, S.; Faulkner, C. J.; Jennings, G. K.; Kane, R. S., *Langmuir* **2006,** *22*, 10157-10162.

41. Laibinis, P. E.; Whitesides, G. M., *Journal of the American Chemical Society* **1992,** *114*, 1990-1995.

42. Ashurst, W. R.; Yau, C.; Carraro, C.; Maboudian, R.; Dugger, M. T., *Journal of Microelectromechanical Systems* **2001,** *10*, 41-49.

43. Tsukruk, V. V., *Advanced Materials* **2001,** *13*, 95-108.

44. Srinivasan, U.; Houston, M. R.; Howe, R. T.; Maboudian, R., *Journal of Microelectromechanical Systems* **1998,** *7*, 252-260.

45. Lio, A.; Charych, D. H.; Salmeron, M., *Journal of Physical Chemistry B* **1997,** *101*, 3800-3805.

46. Gellman, A. J. S., N.D. , *Proc. Inst. Mech. Engrs. Part J: Engineering Tribology* **2002**, 443-461.

47. Masuko, M.; Miyamoto, H.; Suzuki, A., *Tribology International* **2007,** *40*, 1587-1596.

48. Maboudian, R.; Ashurst, W. R.; Carraro, C., *Tribology Letters* **2002,** *12*, 95-100.

49. Singh, R. A.; Yoon, E. S.; Han, H. G.; Kong, H., *Wear* **2007,** *262*, 130-137.

50. Laibinis, P. E. P., B.J.; Lee, S.W.; Jennings, G.K., The synthesis of organothiols and their assembly into monolayers on gold. In *Thin Films*, Academic Press: New York, 1998; Vol. 24.

51. Liu, G. Y.; Xu, S.; Qian, Y. L., *Accounts of Chemical Research* **2000,** *33*, 457-466.

52. Kumar, A.; Whitesides, G. M., *Applied Physics Letters* **1993,** *63*, 2002-2004.

53. Lio, A.; Morant, C.; Ogletree, D. F.; Salmeron, M., *Journal of Physical Chemistry B* **1997,** *101*, 4767-4773.

54. Kim, H. I.; Koini, T.; Lee, T. R.; Perry, S. S., *Langmuir* **1997,** *13*, 7192-7196.

55. Houston, J. E.; Doelling, C. M.; Vanderlick, T. K.; Hu, Y.; Scoles, G.; Wenzl, I.; Lee, T. R., *Langmuir* **2005,** *21*, 3926-3932.

56. Singh, R. A.; Kim, J.; Yang, S. W.; Oh, J. E.; Yoon, E. S., *Wear* **2008,** *265*, 42-48.

57. Flater, E. E.; Ashurst, W. R.; Carpick, R. W., *Langmuir* **2007,** *23*, 9242-9252.

58. Hoffmann, H.; Mayer, U.; Krischanitz, A., *Langmuir* **1995,** *11*, 1304-1312.

59. Khatri, O. P.; Biswas, S. K., *Surface Science* **2006,** *600*, 4399-4404.

60. Vallant, T.; Kattner, J.; Brunner, H.; Mayer, U.; Hoffmann, H., *Langmuir* **1999,** *15*, 5339-5346.

61. Allara, D. L.; Parikh, A. N.; Rondelez, F., *Langmuir* **1995,** *11*, 2357-2360.

62. Bierbaum, K.; Kinzler, M.; Woll, C.; Grunze, M.; Hahner, G.; Heid, S.; Effenberger, F., *Langmuir* **1995,** *11*, 512-518.

63. Genzer, J.; Efimenko, K.; Fischer, D. A., *Langmuir* **2002,** *18*, 9307-9311.

64. Phillips, B. S.; Mantz, R. A.; Trulove, P. C.; Zabinski, J. S., Surface chemistry and tribological behavior of ionic liquid boundary lubrication additives in water. In *Ionic Liquids Iiia: Fundamentals, Progress, Challenges, And Opportunities, Properties And Structure*, Amer Chemical Soc: Washington, 2005; Vol. 901, pp 244-253.

65. Zhang, J. F.; Todd, B. D.; Travis, K. P., *Journal Of Chemical Physics* **2004,** *121*, 10778-10786.

66. Ye, C. F.; Liu, W. M.; Chen, Y. X.; Yu, L. G., *Chemical Communications* **2001**, 2244-2245.

67. Ye, C. F.; Liu, W. M.; Chen, Y. X.; Ou, Z. W., *Wear* **2002,** *253*, 579-584.

68. Blanchard, L. A.; Hancu, D.; Beckman, E. J.; Brennecke, J. F., *Nature* **1999,** *399*, 28-29.

69. Holbrey, J. D.; Seddon, K. R., *Clean Products and Processes* **1999,** *1*, 223-236.

70. Earle, M. J.; Seddon, K. R., *Pure and Applied Chemistry* **2000,** *72*, 1391-1398.

71. Wilkes, J. S., *Green Chemistry* **2002,** *4*, 73-80.

72. Walden, P., *Bull. Acad. Imper. Sci. (St. Petersburg)* **1914**, 1800.

73. Wilkes, J. S.; Zaworotko, M. J., *Journal of the Chemical Society-Chemical Communications* **1992**, 965-967.

74. Seddon, K. R.; Stark, A.; Torres, M. J., *Pure and Applied Chemistry* **2000,** *72*, 2275-2287.

75. Carlin, R. T.; Wilkes, J. S., Chemistry and Speciation in Room Temperature Ionic Liquids. In *Chemistry of Nonaqeous solutions*, Mamantov, G.; Popov, A. I., Eds. VCH Publisher Inc.: New York, 1994; pp 277-306.

76. Hussey, C. L., The electrochemistry of room temperature Ionic Liquids. In *Chemistry of Nonaqeous solutions*, Mamantov, G.; Popov, A. I., Eds. VCH Publisher Inc.: New York, 1994; pp 227-276.

77. Cull, S. G.; Holbrey, J. D.; Vargas-Mora, V.; Seddon, K. R.; Lye, G. J., *Biotechnology and Bioengineering* **2000,** *69*, 227-233.

78. Khan, N.; Moens, L., Room-temperature ionic liquids as new solvents for carbohydrate chemistry: A new tool for the processing of biomass feedstocks? In *Ionic Liquids*, American Chemical Society: Washington, 2002; Vol. 818, pp 360-372.

79. Welton, T., *Chemical Reviews* **1999,** *99*, 2071-2083.

80. Rosa, J. N.; Afonso, C. A. M.; Santos, A. G., *Tetrahedron* **2001,** *57*, 4189-4193.

81. Branco, L. C.; Afonso, C. A. M., *Tetrahedron* **2001,** *57*, 4405-4410.

82. Gordon, C. M., *Applied Catalysis A:General* **2001,** *222*, 101-117.

83. Roberts, N. J.; Lye, G. J., Application of room-temperature ionic liquids in biocatalysis: Opportunities and challenges. In *Ionic Liquids*, American Chemical Society: Washington, 2002; Vol. 818, pp 347-359.

84. Huddleston, J. G.; Willauer, H. D.; Swatloski, R. P.; Visser, A. E.; Rogers, R. D., *Chemical Communications* **1998**, 1765-1766.

85. Visser, A. E.; Swatloski, R. P.; Huddleston, J. G.; Rogers, R. D., *Abstracts of Papers of the American Chemical Society* **1999,** *217*, 040-IEC.

86. Visser, A. E.; Swatloski, R. P.; Reichert, W. M.; Mayton, R.; Sheff, S.; Wierzbicki, A.; Davis, J. H.; Rogers, R. D., *Chemical Communications* **2001**, 135-136.

87. Seddon, K. R., *Nature Materials* **2003,** *2*, 363-365.

88. Liu, W. M.; Ye, C. F.; Gong, Q. Y.; Wang, H. Z.; Wang, P., *Tribology Letters* **2002,** *13*, 81-85.

89. Mu, Z. G.; Liu, W. M.; Zhang, S., *Chemistry Letters* **2004,** *33*, 524-525.

90. Mu, Z. G.; Zhou, F.; Zhang, S. X.; Liang, Y. M.; Liu, W. M., *Tribology International* **2005,** *38*, 725-731.

91. Wang, H. Z.; Lu, Q. M.; Ye, C. F.; Liu, W. M.; Cui, Z. J., *Wear* **2004,** *256*, 44-48.

92. Kamimura, H.; Minami, I.; Mori, S., *Journal Of Japanese Society Of Tribologists* **2005,** *50*, 208-213.

93. Uerdingen, M.; Treber, C.; Balser, M.; Schmitt, G.; Werner, C., *Green Chemistry* **2005,** *7*, 321-325.

94. Reich, R. A.; Stewart, P. A.; Bohaychick, J.; Urbanski, J. A., *Lubrication Engineering* **2003,** *59*, 16-21.

95. Omotowa, B. A.; Phillips, B. S.; Zabinski, J. S.; Shreeve, J. M., *Inorganic Chemistry* **2004,** *43*, 5466-5471.

96. Phillips, B. S.; Zabinski, J. S., *Tribology Letters* **2004,** *17*, 533-541.

CHAPTER III

EXPERIMENTAL PROCEDURES AND CHARACTERIZATION METHODS

Experimental Procedures

Materials

Water used in all experiments was deionized (DI) and purified to 16.7 MΩ·cm with a Modu-Pure system. Ethanol (absolute) was obtained from AAPER; toluene, methylene chloride, and 2-propanol were purchased from Fisher Scientific. All reagents were used as received. 1-Butanethiol, 1-hexanethiol, 1-heptanethiol, 1-octanethiol, 1-decanethiol, 1-dodecanethiol, 1-hexadecanethiol, 1-octadecanethiol, 11-mercapto-1-undecanol, and 11-mercapto-1-undecanoic acid were purchased from Aldrich. 1-Docosanethiol was purchased from Narchem Inc. n-Octyltrichlorosilane, n-octadecyltrichlorosilane, n-octadecyl dimethylchlorosilane, and (tridecafluoro-1,1,2,2-tetrahydrooctyl)-1-trichlorosilane were purchased from United Chemical Technologies (UCT). 7-Octenyltrichlorosilane, butyltrichlorosilane, hexyltrichlorosilane, dodecyltrichlorosilane, and hexadecyltrichlorosilane were purchased from Gelest. 15 cm polished, p-doped silicon wafers (100) were purchased from Montco Silicon. The silicon wafers were rinsed with ethanol and water and then dried in a stream of nitrogen prior to use. Gold shot (99.99%) and chromium-coated tungsten filaments were obtained from J&J Materials and R. D. Mathis, respectively. Nitrogen gas was purchased from A-L Compressed Gases.

1-butyl-3-methylimidazolium hexafluorophosphate and 1-hexyl-3-methylimidazolium trifluoromethanesulfonate were purchased from Sigma Aldrich and Fluka, respectively.

Monolayer Preparation

Gold. Gold surfaces were prepared by evaporating gold shot onto silicon wafers. A chromium adhesion layer (100 Å) was deposited before gold (1250 Å) was evaporated onto the silicon wafers. Depositions were performed sequentially in a diffusion-pumped chamber with a pressure < $5x10^{-6}$ Torr at a rate < 2 Å s^{-1}. Wafers were stored at ambient conditions and typically cut into 1.5 x 4.5 cm samples. All samples were rinsed with copious amounts of absolute ethanol and dried in a stream of nitrogen before modification or testing.

Thiolate monolayers on gold. Gold substrates were immersed in a 1 mM solution of the alkanethiol in ethanol for 24 h. The resulting films were rinsed with copious amounts of absolute ethanol and dried in a stream of nitrogen before analysis and testing

Silicon. Silicon wafers were cut into 1.5 x 4.5 cm samples for surface modification and subsequent testing. Silicon substrates were sequentially sonicated in ethanol for 30 min, treated with piranha solution (70% H_2SO_4/30% H_2O_2 solution in water) for 30 min, rinsed with copious amounts of water and dried with a nitrogen stream, then immersed in a 1 mM solution of an alkyl trichlorosilane in toluene for 5 h. Samples were rinsed with toluene and dried in a stream of nitrogen.

n-Alkyltrichlorosilane monolayers on silicon. n-Alkyltrichlorosilane monolayers were formed by immersing the piranha-treated substrates into 1 mM solutions of silane precursors in toluene for 5 h. Samples were removed from solution, rinsed in ~20 mL of toluene, then rinsed with deionized water and ethanol, and dried in a stream of nitrogen.

Synthesis of hydroxyl silane monolayers via hydroboration-oxidation reaction. Piranha-treated silicon substrates were immersed in a 1 mM solution of 7-octenyltrichlorosilane in toluene for 5 h. The samples were removed from solution, rinsed with ~ 20 mL of toluene, rinsed with deionized water and ethanol, and then dried in a stream of nitrogen. The conversion of the vinyl terminal group into a hydroxyl was accomplished by immersing the samples in 0.1 M solution of borane-tetrahydrofuran complex (BH_3-THF) in a nitrogen atmosphere for 2 h. The samples were removed from solution, rinsed with THF and then deionized water, before immersion into a solution containing 10 mL of 30% hydrogen peroxide and 10 mL of 28% ammonium hydroxide in water at 60°C for 2 h. The resulting hydroxyl-terminated monolayer was rinsed with deionized water and ethanol and dried with a stream of nitrogen.

Hydroxyl monolayer on silicon via trichloroacetate conversion.[1] Piranha-treated silicon substrates were immersed in a 1 mM solution of (1-trichlorosilylundecyl) trichloroacetate in toluene for 5 h.[1] The samples were removed from solution, rinsed with ~20 mL of toluene, then rinsed with deionized water and ethanol, and dried in a stream of nitrogen. The conversion of the trichloroacetate terminal group into a hydroxyl was accomplished by immersing the sample into a solution containing 10 mL of

deionized water, 10 mL of methanol, and 0.15 g of sodium bicarbonate for 15 min.[1] The resulting hydroxyl-terminated monolayer was rinsed with deionized water and ethanol, and then dried with a stream of nitrogen.

Ionic Liquid Preparation

[1-butyl-3-methylimidazolium] [trifluoromethanesulfonate] synthesis. The procedure for the synthesis of the ionic liquid 1-butyl-3-methylimidazolium trifluoromethanesulfonate, [bmim][triflate], was adapted from a procedure reported by Bonhote et al.[2] Under a nitrogen atmosphere, ~120 mL of anhydrous dichloromethane was added to 50 g of methyl triflate (0.3 mol) to prepare a ~2.5 M solution. This methyl triflate solution was added dropwise to 42 mL (~0.3 mol, or 38 g) of 1-butylimidazole under a nitrogen atmosphere and stirred vigorously in an ice bath. Solvent was removed by placement of the single phase liquid on a rotary evaporator followed by placement of the liquid on the vacuum line overnight. The final product was stored under nitrogen atmosphere and characterized using ^{1}H NMR analysis, which revealed no water in the final product. ^{1}H NMR (400 MHz, $CDCl_3$): δ 0.916 (3H), 1.30 (2H), 1.83 (2H), 3.93 (3H), 4.16 (2H), 7.38 (2H), 9.03 (1H).

Characterization Methods

Contact Angle Goniometry

Contact angle goniometry is a simple and convenient method of evaluating the surface properties of thin films.[3] When a small drop of liquid is placed onto a surface, the

interfacial tension between the drop, the film surface, and the air determine the shape of the drop. The interfacial tensions are denoted as γ_{SG} at the solid-vapor interface, γ_{SL} at the solid-liquid interface, and γ_{LV} at the liquid-vapor interface. A force balance of these tensions involved in the surface-liquid-air interface leads to Young's equation:

$$\cos\theta = \frac{\gamma_{SG} - \gamma_{SL}}{\gamma_{LV}} \tag{3-1}$$

where θ is the angle between the line tangent to the edge of the liquid (liquid-vapor interface) and the line of solid surface beneath the drop (solid-liquid interface). The solid-vapor interfacial tension, often termed the surface energy of the solid, is affected by the chemical composition at the outermost few Angstroms of the solid phase, and the contact angle provides a relative measure of the balance between surface energy and γ_{SL}. For a given liquid, typically water or hexadecane, γ_{LV} is held constant while all other values change depending on surface composition. Using dissimilar liquids like water and hexadecane, which is a dispersive liquid that would not have significant electrostatic or polar interactions with the surface, we can develop understanding regarding the composition and integrity of the surface. A goniometer, an optical microscopy with a protractor built into the lens, is used to determine θ. Water contact angles are used to indicate the relative hydrophobicity, and hexadecane is used for oleophobitcity where larger measured angles result from more hydrophobic and oleophobic surfaces.

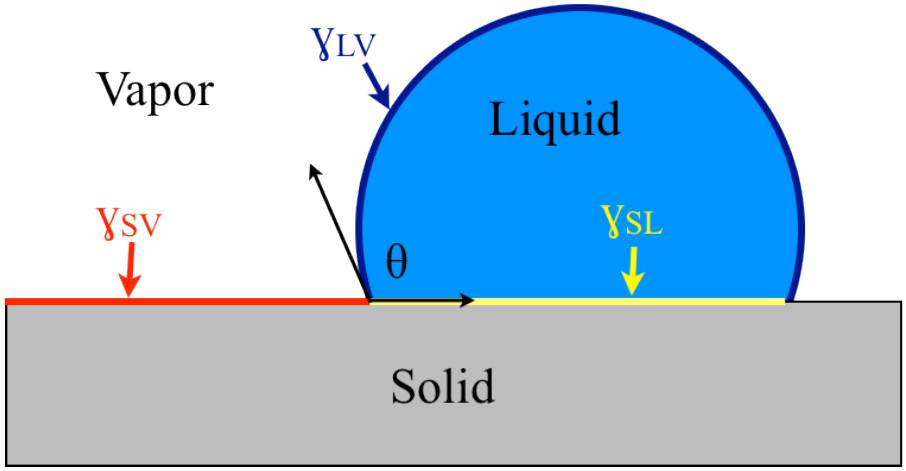

Figure 3.1. Graphical representation of interfacial energies in contact angle measurement.

Contact angles are useful in providing insight into surface roughness, chemical composition, and interfacial structure. By adding small liquid drops (~5 mL) to the surface using a syringe, the advancing contact angle and receding contact angle are measured. The advancing contact angle is measured after the liquid has been added to the drop, causing it to advance across the surface, and the receding contact angle is measured after liquid has been removed from the drop, causing it to slowly recede across the surface. The chemical composition at the surface also greatly affects the measured contact angles. Depending on whether a surface is dominated by low energy groups (-CH_2-, -CH_3, -CF_2-, -CF_3) or higher energy groups (-OH, -COOH), the contact angles will be altered.[4] By comparing subtracting the receding contact angle from the advancing contact angle, the contact angle hysteresis can be determined. Some sources for hysteresis include surface roughness, chemical surface heterogeneity, surface molecular rearrangement due to the probe fluid, and contamination that often occurs with high energy surfaces under ambient conditions. More homogeneous surfaces have a very low hysteresis while heterogeneous surfaces have a much larger hysteresis.[5]

Surface Tension

Surface tension (γ_{LV}) measurements were performed on a KSV Sigma 70 Tensiometer, which was controlled by KSV Instruments 70x software. A platinum Wilhelmy plate was suspended from an electro-balance with a measuring resolution of 1 mN. The Wilhelmy plate was lowered to touch the surface of the liquid and then submerged a specified distance into the liquid. The balance was zeroed and then, the force required to remove the plate from the liquid at a constant speed was measured and recorded. The platinum Wilhelmy plate was 0.1 mm thick and 19.6 mm long, giving a wetted length of 39.4 mm. The plate was raised and lowered at a rate of 20.0 mm/min and submerged to a depth of 5.0 mm in the liquid. Before testing of the ionic liquid, absolute ethanol (γ_{LV} = 22 mN/m), hexadecane (γ_{LV} = 27 mN/m), and water (γ_{LV} = 72 mN/m) were tested to ensure the accuracy of the instrument. Approximately 10 mL of liquid was needed to perform the experiment, and values represent 5 separate runs with each run consisting of at least 10 measurements taken at 1 min intervals.

Profilometry

A profilometer uses a stylus tip to map the surface topography and roughness by measuring height changes as the stylus tip moves across the surface. Profilometers have excellent vertical resolution (~20 nm) and lateral resolution on the order of hundreds of nanometers. A Veeco Dektak stylus profilometer with a sharp diamond coated tip was used to probe tribological wear tracks on bare substrates.

Atomic Force Microscopy (AFM)

AFM takes advantage of the deflections of a sharp tip typically made of Si_3N_4 or SiO_2 that is attached to a cantilever as the tip is moved along a surface.[6] The interactions of the tip with the sample surface as the tip scans laterally across the surface result in changes in the cantilever, which are measured by a photodiode detector that receives a signal from the deflected tip. While many types of forces can contribute to the deflection of the cantilever, typically short-range, repulsive forces account for the deflection and subsequent signal generation. The surface topology and film thickness can be obtained from AFM measurements on a variety of surfaces while operating in two modes. Contact mode AFM can be performed at high scan speeds and offers the capability of atomic resolution while tapping mode AFM vibrates the cantilever near its resonant frequency at a constant amplitude and detects deviations in the cantilever vibrations induced by the proximity of the sample surface. Tapping mode is useful for soft surfaces because it eliminates the lateral forces imposed to the sample compared to contact mode and, therefore, has a higher lateral resolution (~ 1 nm), although the vertical resolution is lower than for contact mode. Topographical images generated from AFM provide information such as film thickness and surface roughness.

Optical Microscopy

Optical microscopy is a simple and straightforward method to observe microscopic structures. Film coverage and surface morphology of IL films as well as confirmation and spatial characterization of tribology wear tracks were investigated with an Olympus BX41 microscope with Pixera camera and Pixera Viewfinder Pro image

capture software. A 10x magnification lens was used to provide images of ~350 m x ~450 m.

Spectroscopic Ellipsometry

The use of spectroscopic ellipsometry allows simple estimation of film thickness at the Angstrom scale. Film thickness up to 100 m can be measured and thicknesses < 1 m can be determined with a sensitivity of at least 0.01 nm. Linear polarized light in a specified wavelength range is reflected from a sample surface and changed into elliptically polarized light. Both the phase (Δ) and amplitude (Ψ) of the reflected light are collected by a detector, and information about the properties of the sample is contained in the complex ratio, ρ, determined from the parallel (r_p) and perpendicular (r_s) electrical field vectors.

$$\rho = \frac{r_p}{r_s} \tag{3-2}$$

The fundamental equation of ellipsometry describes the connection between the measured amplitude (Ψ) and phase (Δ) quantities and the sample properties contained in the coefficient of reflection ρ.

$$\rho = \tan(\Psi)e^{i\Delta} \tag{3-3}$$

Model layers representing the film on the substrate can be created to fit the measured data. A simple, effective model for thin organic films is the Cauchy Equation (3-4), which assumes a film to be transparent and uniform in thickness.

$$n = A + \frac{B}{\lambda^2} + \frac{C}{\lambda^4} + \ldots \tag{3-4}$$

where n is the film refractive index, A, B, and C are model fit parameters, and λ is the wavelength of incident light. Using the Cauchy model allows the refractive index and thickness both to be solved by fitting the experimental data for phase and amplitude and minimizing the mean square error. The thickness of the monolayer film is calculated with an index of refraction set to 1.46 (the second and third Cauchy coefficients were set to zero) using the software's "normal fit" application. Ellipsometric thicknesses were determined from a J. A. Woollam XLS-100 variable-angle spectroscopic ellipsometer. Thicknesses were fit to data taken at 75° from the surface normal over wavelengths from 200 to 1000 nm. The substrate was modeled as a 0.5 mm Si substrate with an oxide layer. The thickness of the oxide layer was measured from a piranha-treated silicon substrate each time samples were prepared.

Microtribology

A microtribometer enables the study of a wide variety of surfaces using any number of probe substrates that can take on a variety of geometries. In a microtrobology experiment the surface of interest is attached to a reciprocating stage beneath a probe tip that is mounted onto a two-dimensional force sensor that allows for real time recording of

forces in two directions. The coefficient of friction ( ) can be calculated by resolving the force vectors to a normal force (F_N) and a friction force (F_f) that are orthogonal to each other and provides a measure of the frictional performance of the tested surface by Amontons' laws:

$$F_f = \mu F_N + F_0 \tag{3-5}$$

where F_0 is the residual force typically arising from the adhesion between the probe tip and surface. Depending upon the interactions between the probe tip and the sample as well as the scale of the applied load, the residual force can scale with the same magnitude as applied force or can be negligible. For low energy monolayer surfaces, we have measured the residual force from adhesion to be negligible, resulting in the coefficient of friction simplifying to the ratio of friction force over normal force.

$$\mu = \frac{F_f}{F_N} \tag{3-6}$$

A Center for Tribology (CETR) UMT-2 Micro-Tribometer was used for all tribology experiments. This microtribometer enables the investigation of frictional properties of any flat surface over a large range of loads. The instrument is designed for ball on flat surface sliding experiments with a 2-D FVL or 2-D DFM-0.5 force sensor, depending on the load to be applied. The FVL sensor is capable of measuring forces from 1 to 100 mN in both dimensions with a resolution of 0.01 mN for an applied load between 5 and 30 mN, while the DFM-0.5 sensor can apply loads ranging from 50 to

5,000 mN and measure with a resolution of 0.25 mN. Tests were performed with a stainless steel ball bearing as the probe tip attached to the sensor via a suspension-mounting cantilever where the size of the tip was selected according to the magnitude of the applied load. The tip was cleaned in ethanol before use. The FVL and DFM-0.5 sensors were operated with balls of 1 mm and 4 mm diameters, respectively. The force that the tip applies to the surface was slowly ramped to the desired load and allowed to equilibrate at that load for at least 15 s before the surface was put into motion. Tests were performed at a sliding speed of 0.1 mm/s over a 15 mm track for both unidirectional and multiple cycle wear tests. Reported results represent measurements on an average of five samples each prepared independently. Due to the uncertainty of surface pressure, we report applied loads as forces in units of mN.

Electrochemical Impedance Spectroscopy (EIS)

Barrier properties of films and coatings may be measured with electrochemical impedance spectroscopy (EIS). In EIS, the film-coated substrate is an electrode in an electrochemical cell that contains a both counter and reference electrodes and is exposed to a solution containing redox probes and ions and connected to an alternating current source. During an EIS experiment, current is measured upon altering the potential of the working electrode with a sinusoidal perturbation of varying frequency. Under these conditions the following equation is applicable:

$$Z = \frac{E(t)}{I(t)} = Z_o \frac{\cos(\omega t)}{\cos(\omega t - \phi)} \tag{3-7}$$

where Z is the impedance in the system, $E(t)$ is the applied potential, and $I(t)$ is the resulting current at time t, E_0 is the amplitude of the potential and ω is the radial frequency (equal to 2 f where f is the frequency in Hz), I_0 is the amplitude of the current, ϕ is the phase shift of the output signal, and Z_0 is the magnitude of the impedance. From these equations, the impedance of a system can be characterized by a magnitude and a phase shift. An impedance plot is obtained by measuring cell current while altering the frequency of the AC source. The impedance changes due to the ability of redox probes to reach the vicinity of the working electrode of the underlying metal substrate where they can be oxidized/reduced. Impedance is directly affected by the transport of ions through a film, and lower frequencies allow more time for diffusive processes to occur. Since an electrochemical cell is used, the results can be modeled using equivalent electrical circuits consisting of resistors and capacitors that represent film, interfacial, and solution properties. Resistance and capacitance values for monolayer films may be estimated using the following equations that apply to a Randles equivalent circuit[7] shown in Figure 3.2.

$$Z_{real} = R \tag{3-8}$$

$$Z_{imag} = \frac{1}{j\omega C} \tag{3-9}$$

$$|Z| = \sqrt{\left(Z_{real}\right)^2 + \left(Z_{imag}\right)^2} \tag{3-10}$$

where Z_{real} and Z_{imag} are the respective real and imaginary components of the impedance where the real portion corresponds to resistance, R and imaginary corresponds to capacitance, C. $|Z|$ equals Z_0 and is the magnitude of the total impedance in the system. As evidenced by the impedance equations for a resistor and capacitor, higher film resistance and lower film capacitance yield higher total impedance. Higher impedance corresponds with the inhibition of ion transport to the surface and signifies a better barrier film.

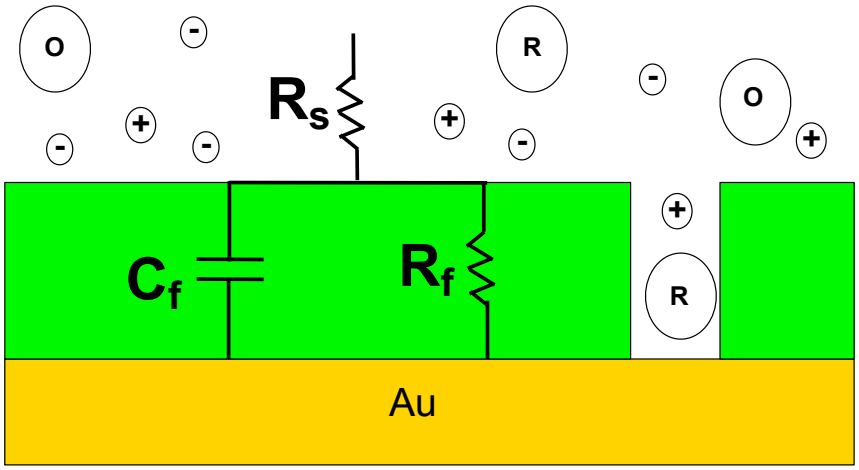

Figure 3.2. Schematic of electrochemical cell and equivalent circuit used in EIS experiments where solution resistance (R_s), film resistance (R_f), and film capacitance (C_f) can be calculated from measured current by varying frequency of applied AC perturbation.

EIS spectra were obtained with a Gamry Instruments CMS300 impedance unit. A flat cell (EG&G) was used to expose 1.0 cm^2 of each sample selectively as the working electrode to an aqueous solution of 1 mM $K_3Fe(CN)_6$, 1 mM $K_4Fe(CN)_6$, and 0.1 M $NaSO_4$. Measurements were obtained using an Ag/AgCl/saturated KCl reference electrode with evaporated gold on silicon as the counter electrode. Data were obtained by measuring the current using a 5 mV sinusoidal AC perturbation of varying frequency.

The Randles equivalent circuit has three distinct regions that are shown in the Bode plot in Figure 3.2.

At high frequencies, the resistance due to ion transfer in solution can be measured due to the rapid alternation of potential that precludes the characterization of film properties, thus measuring the resistance of the solution. At intermediate frequencies, the film often functions as a dielectric, characteristic of a straight line with a slope of -1 on the Bode plot, and enables the measurement of the capacitive properties of the film. At low frequencies, the gradual change in potential allows sufficient time for ions to penetrate defects within the thinnest SAMs, resulting in a line of zero slope on the Bode plot and enabling the measurement of the resistance provided by the film against ion transfer.[7]

When samples were tested by EIS following a pin-on-disk tribology test, 1 cm^2 of exposed sample area was centered around the tribology test track to yield an exposed track of ~1.1 cm in length and ~0.01 mm in width. Reported changes in capacitance and resistance of tested samples, therefore, were caused by tribometrically-induced changes in the monolayer along this track (~0.3 mm^2) although the entire 1 cm^2 was tested in an impedance measurement.

X-ray Photoelectron Spectroscopy (XPS)

X-ray photoelectron spectroscopy is an ultra high vacuum technique where a material is irradiated with x-rays while the kinetic energy and the number of escaping electrons is measured. The kinetic energy can be used to determine the composition, chemical state, and electronic state of the outermost ~10 nm of a material.[8] Data are

typically reported as counts per second against binding energy (E_B) that is related to the kinetic energy (E_K) by equation 3-11 where $h\nu$ is the energy of the incident photons and Φ is the work function of the spectrometer.[8]

$$E_k = h\nu - E_v - \Phi \tag{3-11}$$

X-ray photoelectron spectra (XPS) were obtained with a PHI 5000 VersaProbe spectrometer with use of a monochromatized Al Kα X-ray source (spot size of 10 μm x 20 μm) and a concentric hemispherical analyzer (pass energy = 150 eV). The detector angle with respect to the surface normal was 45° and 61 total cycles were performed. Peaks were fit with 70% Gaussian / 30% Lorentzian profiles and a Shirley background. CasaXPS (Vamas) software was used to process the XPS data.

References

1. Vilt, S. G.; Leng, Z. W.; Booth, B. D.; McCabe, C.; Jennings, G. K., *Journal of Physical Chemistry C* **2009,** *113*, 14972-14977.

2. Bonhote, P.; Dias, A.; Popageoriou, N.; Kalyanasundaram, K.; Gratzel, M., *Inorganic Chemistry* **1996,** *35*, 1168-78.

3. Laibinis, P. E.; Bain, C. D.; Nuzzo, R. G.; Whitesides, G. M., *Journal of Physical Chemistry* **1995,** *99*, 7663-7676.

4. Laibinis, P. E., B.J.; Lee, S.W.; Jennings, G.K., The synthesis of organothiols and their assembly into monolayers on gold. In *Thin Films*, Academic Press: New York, 1998; Vol. 24.

5. Zisman, W. A., *Contact Angle, Wettability, and Adhesion*. Washington, DC, 1964; Vol. 43.

6. Wang, H. Z.; Lu, Q. M.; Ye, C. F.; Liu, W. M.; Cui, Z. J., *Wear* **2004,** *256*, 44-48.

7. Bard, A. J., *Electrochemical methods : fundamentals and applications*. 2nd ed.; John Wiley: New York, 2001.

8. Briggs, D., *Practical Surface Analysis*. John Wiley & Sons Ltd.: Chichester, 1983.

CHAPTER IV

TRIBOLOGY OF MONOLAYER FILMS: COMPARISON BETWEEN N-ALKANETHIOLS ON GOLD AND N-ALKYL TRICHLOROSILANES ON SILICON

Introduction

Self-assembled monolayers (SAMs) are molecular films that can provide dense, two-dimensional sheets of surface functionality to impact interfacial properties.[1] SAMs have been used in a wide range of applications, such as the mitigation of protein adsorption,[2] promotion of selective attachments,[3, 4] generation of surfaces with varying wettability,[5] and lubrication between contacting surfaces.[6-9] In the latter regard, the lubricating properties of a variety of different monolayer films on silicon[9-11] and gold[12-15] surfaces have been investigated in an effort to reduce friction and prevent wear during operation. The ability to tailor the properties of SAMs by manipulating the composition of the precursor molecule yields a versatile class of materials with which to investigate molecularly thin lubrication schemes, particularly in micro electromechanical systems (MEMS) where surfaces are separated by as few as 1-2 nm.[16] At these small scales, the surface to volume ratio for a typical component is very high, and as a result, surface forces dominate and adhesion, stiction, friction, and wear become significant technological barriers to the successful application of durable devices. The ability to functionalize the terminus of the SAM and vary the length of the assembling molecules provides a wide range of possible films and surfaces, each with differing tribological properties and interfacial interactions.

Monolayer films offer distinct advantages over many classical strategies for lubrication[7] of MEMS devices because the molecular components can assemble onto all surfaces, even within nanoscale crevices between moving components, or onto targeted surfaces by matching the adsorbate head group with the metal or oxide surface. Silane based films are generally preferred in tribological applications[17] over thiolates because of the stronger covalent attachment of silanes compared to the weaker chemisorption of thiols on gold, silver, or copper. In addition, most MEMS devices are fabricated from silicon,[16] and therefore, interest in lubrication of silicon-based devices has led to several studies on the tribological properties of silane monolayers,[6, 8, 17-19] which are often prepared by the reaction of n-alkyltrichlorosilanes with surface silanol groups. Nonetheless, alkanethiolate SAMs on gold are also of keen interest in tribological studies due to their widespread use in the modification of many surfaces,[1, 20] and the requisite, yet varied, mechanical requirements for these films.[21-23]

Molecular films have shown promise for the lubrication of surfaces, including both alkanethiolate SAMs on coinage metals[15, 23-27] and siloxane monolayers on silicon.[6, 8, 9, 17, 18] Individual studies have focused on the effects of chain length, packing, and functionality of contacts. Specifically, Lio et al.[12] and McDermott et al.[13] demonstrated that alkanethiolate monolayers formed from longer precursor molecules are more ordered and possess denser packing than shorter molecules. Their results suggest that the higher order and degree of packing for SAMs with longer chains are correlated with a reduced coefficient of friction. In addition to monolayer thickness, the functionality of the monolayer terminus has been shown to play an important role in frictional properties.[19, 28, 29] Clear and Nealey[8] showed that adhesion and friction were dependent upon monolayer

terminus and solvent when performing chemical force microscopy with thiol-coated gold tips and trichlorosilane-coated silicon substrates. The frictional force is larger for polar termini than for nonpolar termini for all solvents studied. Evidence of probe tip influence has also been reported where similar functionalities between two contacting surfaces display greater adhesion and therefore a higher coefficient of friction than when the two have dissimilar termini.[8, 15, 30] Although studies of the frictional properties of monolayers by AFM and pin-on-disk tribometry are performed at vastly different forces and contacting areas, results from both types of testing have been shown to be consistent.[17]

Here we report frictional properties for monolayers prepared from both ω-terminated alkyl thiols on gold and n-alkyltrichlorosilanes on silicon surfaces by using microtribometry. Through our experiments we compare the tribological performance of alkanethiolates SAMs while varying chain length and terminal group functionality. We also provide a quantitative comparison of the performance of monolayers derived from n-alkanethiols on gold and n-alkyltrichlorosilanes on silicon that were subject to identical conditions. To our knowledge, the only reported comparison of n-alkanethiolate and silane monolayers was based on monofunctional hydrocarbon silanes that do not cross-link at the silicon (oxide) surface.[17] Here, we focus on the more widely studied silane monolayers on silicon (oxide) prepared from n-alkyltrichlorosilanes, which can cross-link into robust coatings, along with alkanethiolate SAMs on gold. Therefore, a direct comparison between these two monolayer systems can be made, and their differences, which have been generally accepted but rarely quantified, may be better understood. Our results demonstrate that the tribological properties of monolayer films are dependent on

their surface group as well as their internal stability, which depends on chain length and substrate-adsorbate bonding.

Experimental Section

Monolayer Preparation

Gold - Gold surfaces were prepared by evaporating gold shot onto silicon wafers. A chromium adhesion layer (100 Å) was deposited before gold (1250 Å) was evaporated onto the silicon wafers. Depositions were performed sequentially in a diffusion-pumped chamber with a pressure < $5x10^{-6}$ Torr at a rate < 2 Å s^{-1}. Wafers were stored at ambient conditions and typically cut into 1.5 x 4.5 cm samples. All samples were rinsed with copious amounts of absolute ethanol and dried in a stream of nitrogen before modification or testing. Gold substrates were immersed in a 1 mM solution of the alkanethiol in ethanol for 24 h. The resulting films were rinsed with copious amounts of absolute ethanol and dried in a stream of nitrogen before analysis and testing

Silicon - Silicon wafers were cut into 1.5 x 4.5 cm samples for surface modification and subsequent testing. Silicon substrates were sequentially sonicated in soapy water or ethanol for 30 min, treated with piranha solution (70% H_2SO_4/30% H_2O_2) for 30 min, rinsed with copious amounts of water, dried with a nitrogen stream, and then immersed in a 1 mM solution of an alkyl trichlorosilane in toluene for 5 h. Samples were rinsed with toluene and dried in a stream of nitrogen.

Microtribology

A Center for Tribology (CETR) UMT-2 Micro-Tribometer was used for all tribology experiments. The instrument was used for ball on flat surface sliding experiments with a 2-D FVL or 2-D DFM-0.5 force sensor, depending on the load to be applied. The FVL sensor is capable of measuring forces from 1 to 100 mN in both dimensions with a resolution of 0.01 mN for an applied load between 5 and 30 mN, while the DFM-0.5 sensor can apply loads ranging from 50 to 5,000 mN and measure with a resolution of 0.25 mN. Tests were performed with a stainless steel ball bearing as the probe tip attached to the sensor via a suspension-mounting cantilever where the size of the tip was selected according to the magnitude of the applied load. The tip was sonicated in acetone for 5 min and dried with nitrogen before use. The FVL and DFM-0.5 sensors were operated with balls of 1 mm and 4 mm diameters, respectively. The force that the tip applied to the surface was slowly ramped to the desired load and allowed to equilibrate at that load for at least 15 s before the surface was set into motion. Tests were performed at a sliding speed of 0.1 mm/s over a 20 mm track for both unidirectional and multiple cycle wear tests. Results represent measurements on an average of five samples each prepared independently.

Results and Discussion

Alkanethiols on Gold

To investigate the effects of SAM thickness and surface composition on frictional properties, we prepared monolayers onto gold substrates from a homologous series of

methyl-terminated alkanethiols (C_nSH where n = 4, 6, 8, 12, 16, 18, and 22) to form hydrophobic surfaces with known incremental increases in thickness, as well as monolayers of higher surface energy prepared from 11-mercaptoundecanol ($HOC_{11}SH$) and 11-mercaptoundecanoic acid (HO_2C-$C_{10}SH$). Table A.1 shows the advancing and receding water and hexadecane contact angles for each monolayer studied. For $n \geq 8$, the advancing contact angles for water and hexadecane are $\geq 106^\circ$ and $\geq 44^\circ$, respectively, and are indicative of surfaces that have a predominate $-CH_3$ composition. Alkanethiolate SAMs with shorter chains ($n < 8$) do not present such dense CH_3 surfaces upon assembly; these SAMs provide a thinner barrier and less effective screening of forces between the liquid and the underlying metal. In general, longer molecules assemble to provide more van der Waals interactions among chains and yield a more densely packed film with fewer defects.[31] The polar terminal monolayers studied (i.e., hydroxyl and carboxylic acid) are completely wet by hexadecane and have advancing water contact angles $< 40^\circ$ that are consistent with higher energy surfaces.

Polar groups that exhibit stronger interactions with liquids may also interact with solid surfaces to increase the coefficient of friction (COF), which is the ratio of friction force to normal load and can be used to describe the ability of the film to lubricate the surface. Figure 4.1 shows the relationship between terminus functionality and coefficient of friction as measured with a 9.8 mN load at 0.1 mm/s over a 20 mm linear track. The SAMs in this figure are all of similar chain length and therefore, have similar thicknesses, thus enabling investigation of the effect of the surface group on frictional performance. All SAM-modified substrates show a reduction in the coefficient of friction when compared to bare gold, regardless of the terminal functionality. Of the functionalities

studied, the methyl-terminated film exhibited the lowest frictional force for the applied normal load (9.8 mN) as shown in Figure 4.1, reflecting weak interactions between the probe and the low energy surface. Friction values for SAMs with hydroxyl and carboxylic acid termini are similar and are ~ 3x higher than those for the methyl-terminated films. The hydroxyl and carboxylic acid termini have the ability to form hydrogen bonds and possess strong dipole moments; these forces allow for greater interactions between the probe tip and the underlying surface.

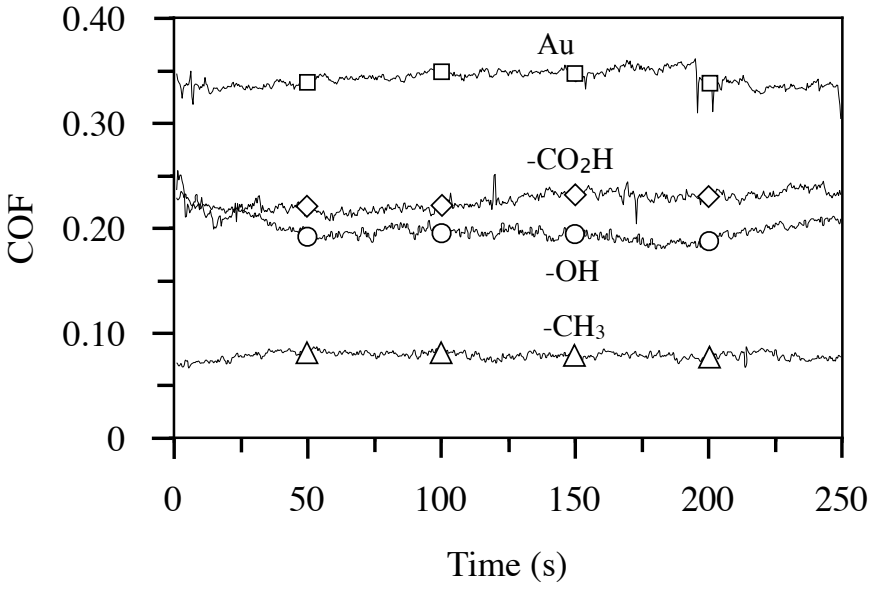

Figure 4.1. Effect of SAM terminal group on the coefficient of friction obtained with a 1 mm stainless steel ball at a sliding speed of 0.1 mm/s and a 9.8 mN applied load. SAMs were prepared from $HO_2C(CH_2)_{10}SH$, $HO(CH_2)_{11}SH$, and $CH_3(CH_2)_{11}SH$ which all yield thicknesses of ~15 Å.

In addition to forming denser monolayer films, the abilities of molecules to form more stable layers on the substrate[31] and provide effective barriers against ion penetration[32] have also been linked to the length of the adsorbing molecule. For example, an alkanethiol of at least 10 - 12 carbons is required for assembly into SAMs that provide

highly blocking barrier properties.[32] We hypothesize that the thicker films may also offer better mechanical protection to the underlying substrate because the stronger interactions between molecules provide the film with greater resistance against applied loads. The ability of the film to withstand an applied load can be characterized by measuring the friction force that results from movement of the surface against a normal load. Figure 4.2 shows the relationship between chain length of the adsorbed alkanethiolate monolayer and the coefficient of friction during a single-pass sliding test and indicates that a critical chain length of approximately 8 carbons is required to obtain low coefficients of friction at this load (9.8 mN) and sliding speed (0.1 mm/s). We observed no improvement in coefficient of friction when the surface was treated with n-alkanethiols that were longer than this critical value. This result is consistent with other tribological studies that show

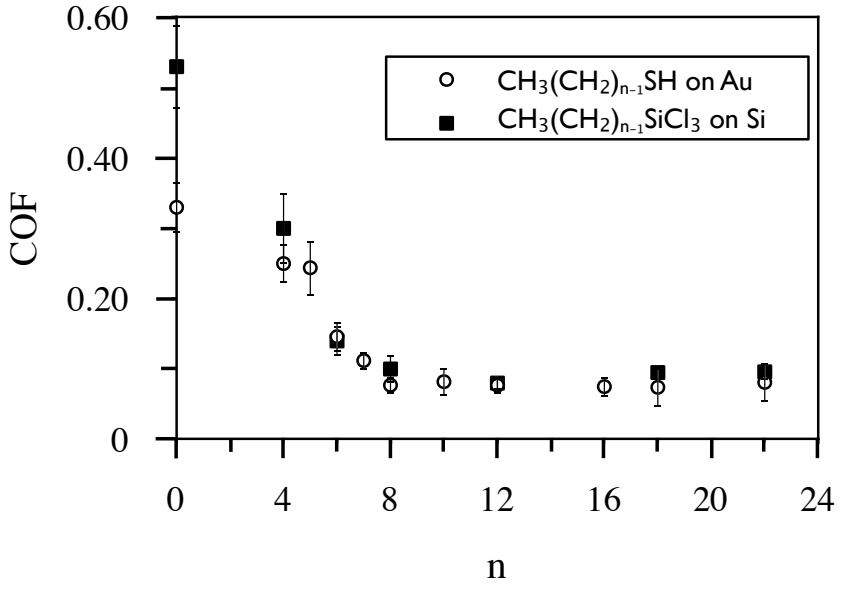

Figure 4.2. Effect of chain length (n) on the coefficient of friction for monolayers prepared from $CH_3(CH_2)_{n-1}SH$ on gold and $CH_3(CH_2)_{n-1}SiCl_3$ on silicon. Triobology tests were performed at 0.1 mm/s for a load of 9.8 mN over a length of 2 cm. Error bars represent standard deviations where tests were repeated with at least 5 independent samples for each chain length studied.

friction and adhesion forces to be independent of chain length when chains were longer than 8 carbons.[12] Above this critical value, additive van der Waals forces are sufficiently strong to stabilize the film and provide highly effective lubrication of the substrate.

The single-pass sliding test used to determine the initial coefficient of friction in Figure 4.2 does not provide information on any damage that the tip may inflict on the monolayer. To investigate the amount of monolayer deformation caused by tribological testing, we performed electrochemical impedance spectroscopy (EIS) on alkanethiol-treated gold surfaces as the working electrode in a 0.1 M Na_2SO_4 (aq) solution containing 1 mM $K_3Fe(CN)_6$ and 1 mM $K_4Fe(CN)_6$, both redox-active species that can transfer electrons with the gold electrode. A sinusoidal potential perturbation of 5 mV was applied over the range of 10,000 to 0.1 Hz while measuring the impedance at each frequency, and the results (before tribological testing) are shown as a Bode plot in Figure 4.3. At high frequencies, the resistance due to ion transfer in solution can be measured due to the rapid alternation of potential that precludes the characterization of film properties. At intermediate frequencies, the SAM functions as a dielectric, characteristic of a straight line with a slope of -1 on the Bode plot, enabling measurement of the capacitive properties of the film. At low frequencies, the gradual change in potential allows sufficient time for ions to penetrate defects within the thinnest SAMs, resulting in a line of zero slope on the Bode plot and enabling the measurement of the resistance provided by the SAM against ion transfer. As shown in Figure 4.3, the thinner films (n = 6, 8) exhibit spectra that contain a resistive plateau at low frequencies, signaling penetration of the redox probes into the SAM. The measured resistances of these thinner SAMs are 1.5–2 orders of magnitude lower than those for thicker SAMs (n > 12).

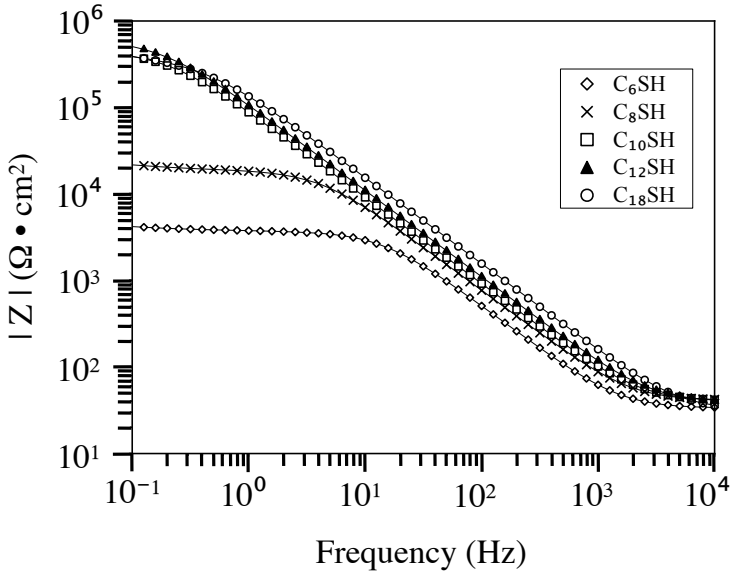

Figure 4.3. Electrochemical impedance spectra obtained prior to tribometric testing for alkanethiolate SAMs on gold in 0.1 M Na_2SO_4 (aq), 1 mM $K_3Fe(CN)_6$, and 1 mM $K_4Fe(CN)_6$. Lines represent fits of the spectra to a Randle's equivalent circuit.

To determine any damage to the monolayer caused by the single tribometer pass, after initial characterization of the SAMs by EIS as described above, we then subjected them to a single tribology test with a 9.8 mN load at a speed of 0.1 mm/s (during which contact pressures were approximately 250 MPa) for a length of 25 mm, and then characterized the films by EIS again. The tribology test resulted in contact with the sample along a very small region of approximately 10^{-2} cm^2 of the 1 cm^2 of surface tested by EIS. This small area of contact is responsible for any changes in electrochemical performance of the film and demonstrates the disruption of a monolayer by such surface pressures. As a SAM becomes damaged, the redox species can diffuse through the defects within the SAM and donate/receive electrons from the gold electrode, which reduces the measured resistance against charge transfer. Further, the easier penetration of water and aqueous ions into the SAM would result in a marked increase in capacitance

given the much higher dielectric constant of water (~78) versus that of alkyl chains (~2.1).[33] Figure 4.4 shows Bode plots before and after tribometric testing for SAMs on gold prepared from C_8SH, $C_{12}SH$, and $C_{18}SH$. Spectra for the two thinner SAMs (Figures 4.4A and 4.4B) show significant decrease in impedance at low frequency, which corresponds to a lower resistance or greater extent of defects within the SAMs after tip-SAM contact. The SAM prepared from $C_{18}SH$ (Figure 4.4C) is not affected by the tip-SAM sliding, as evidenced by impedance spectra that are nearly superimposable before and after tribometric testing. Although all three SAMs yielded indistinguishable coefficients of friction, only the thickest SAM has sufficient van der Waals interactions to maintain its integrity during the applied pressure.

By comparing the double layer capacitance before and after the tribology test (Table 4.1), conclusions about the effects of applied load on the films can be drawn. If the capacitance before and after tribology testing is similar, the film has not been significantly altered by the contact with the probe tip; however, if the tip of the microtribometer has disrupted the film by removal of molecules or alteration of the chain packing density, the capacitance will increase as a result of a less effective charge separation and/or presence of ions within defects of the SAM. Although n-alkanethiols with chain lengths greater than 8 yield similar coefficients of friction, EIS studies show that the tip significantly damages SAMs with $n \leq 12$ as evidenced by the ratio of capacitance before and after the tribology test (Table 4.1). The results suggest that SAMs with n = 16, 18, and 22 have sufficient van der Waals forces to withstand the 9.8 mN applied load while SAMs derived from shorter alkanethiols do not contain sufficient internal stability to maintain the film structure during the single pass with the tribometer.

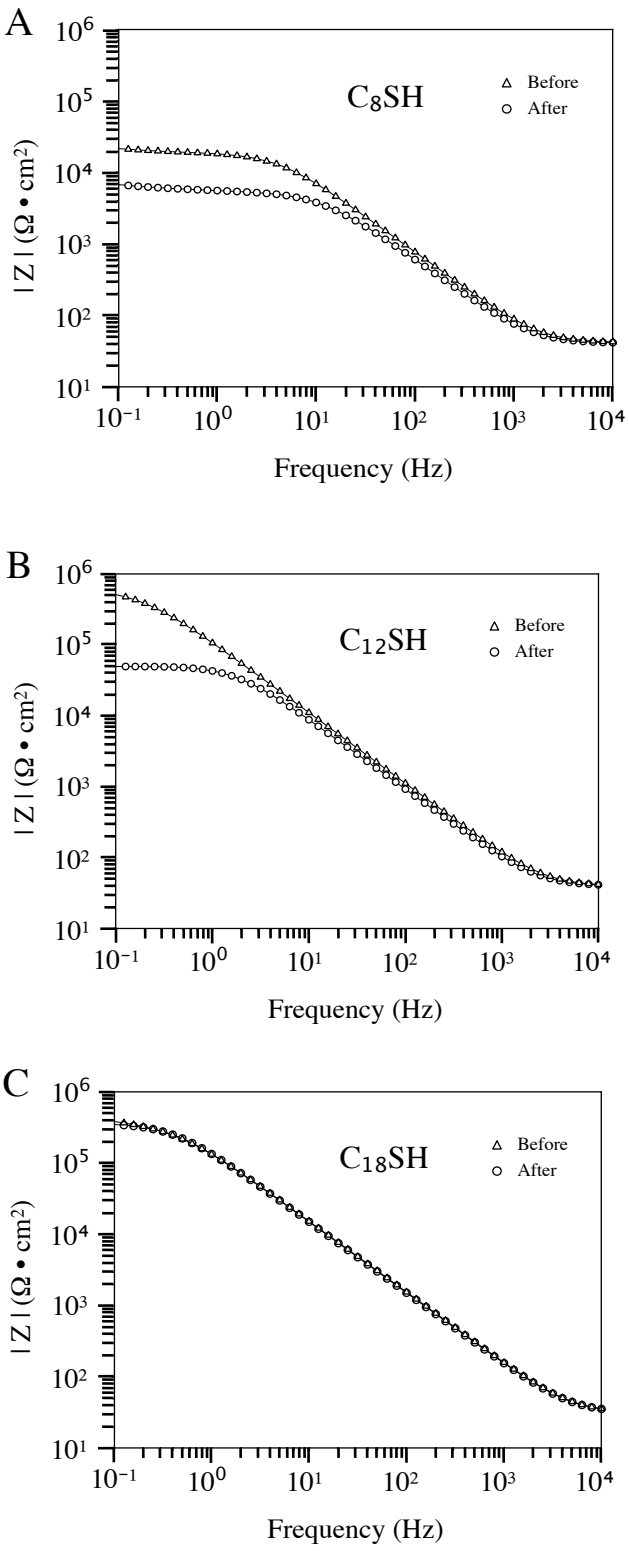

Figure 4.4. Effect of tribology testing on the impedance spectrum (Bode plot) of selected alkanethiolate SAMs on gold. SAMs were prepared from A) C_8SH, B) $C_{12}SH$, and C) $C_{18}SH$. The impedance spectrum of each SAM was obtained before and after a 1 mm stainless steel ball was slid at a velocity of 0.1 mm/s at a force of 10 mN across the sample to produce a track of ~ 10^{-2} cm^2, or 1% of the 1 cm^2 area tested by EIS. The electrolyte for impedance measurements consisted of 0.1 M Na_2SO_4 (aq), 1 mM $K_3Fe(CN)_6$, and 1 mM $K_4Fe(CN)_6$. Curves represent fits of the impedance data with a Randle's model equivalent circuit. Before tribometric testing resistances were 2 x 10^4 $\Omega \bullet cm^2$ (C_8SH), 4 x 10^5 $\Omega \bullet cm^2$ ($C_{12}SH$), 4 x 10^5 $\Omega \bullet cm^2$ ($C_{18}SH$), and after testing the resistances were 6 x 10^3 $\Omega \bullet cm^2$ (C_8SH), 5 x 10^4 $\Omega \bullet cm^2$ ($C_{12}SH$), 4 x 10^5 $\Omega \bullet cm^2$ ($C_{18}SH$).

Table 4.1. Capacitance values obtained before and after a single pass tribology test of 9.8 mN with a 1 mm stainless steel probe tip.

	Capacitance ($\mu F/cm^2$)		Ratio
Molecule	**Before**	**After**	**Before/After**
C_6SH	3.21	7.41	0.43
C_8SH	2.12	3.22	0.66
$C_{10}SH$	1.67	2.36	0.71
$C_{12}SH$	1.43	1.64	0.87
$C_{16}SH$	1.18	1.16	1.02
$C_{18}SH$	1.08	1.07	1.01
$C_{22}SH$	0.85	0.91	0.94

To further probe the tribological stability of the alkanethiolate SAMs on gold as a function of chain length (8-18), monolayers were subjected to various loads with the microtribometer (Figure 4.5). At the lowest load (9.8 mN) all monolayers displayed the capacity to withstand the applied force with a coefficient of friction of < 0.10. As the load was increased, a thicker monolayer was required to maintain the frictional properties (i.e., a coefficient of friction ≤ 0.10). However, for loads of 30 and 100 mN, no alkanethiolate monolayer tested was able to withstand the applied force. These results demonstrate that the greater cohesive interactions of the thicker SAMs cannot be disrupted unless a sufficient force is applied. For loads of 15 and 20 mN only the $C_{16}S$/Au and $C_{18}S$/Au SAMs maintained their tribological performance observed at the lower load of 10 mN. These results show the effect of van der Waals interactions on film

stability and indicate that the additivity of these relatively weak forces can stabilize monolayers, but only over modest increases in applied load.

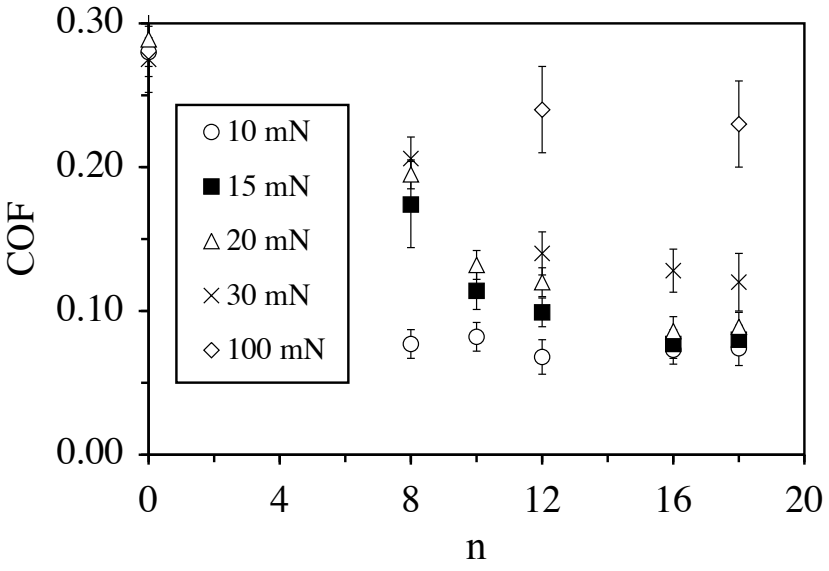

Figure 4.5. Effect of chain length (n) on the coefficient of friction for n-alkanethiolate SAMs on gold at different normal loads. Measurements reflect the average of a single pass tribology test with a 1 mm diameter stainless steel probe tip at 0.1 mm/s for a length of 2 cm. Error bars represent standard deviations based on at least 5 independently prepared films.

Lio et al.[25] and Carpick et al.[34] reported that when the force applied to the monolayer becomes large enough to overcome the cohesive interactions of the film, evidence of deformation of the SAM and underlying gold lattice have been reported. At these loads the probe tip has penetrated the SAM and has disrupted the interactions among chains, which can lead to the removal of molecules. If the load is increased above the point at which SAM disruption occurs, the tip was found to induce a transition in the lattice of the gold atoms from ($\sqrt{3}$ x $\sqrt{3}$)R30° to (1 x 1). The magnitude of this load or pressure is not well known, but the phenomenon of disruption of the SAM is supported

by our work. Liu et al[35] have designed a process referred to as "nanoshaving" where adsorbed alkanethiolate molecules are removed from the gold surface by applying a low load (0.3 nN) with an AFM tip in a solvent and molecules could re-assemble on the surface when the nanoshaving technique was performed in an appropriate solution. These studies suggest that at low loads or contact pressures the deformation of the alkanethiolates monolayer on gold is reversible; however, at normal loads above a critical point or for scans over a prolonged time, the deformation extends into the gold substrate thereby making the damage irreversible. The work presented here, where tribometric tests have been characterized by EIS, shows that for a load of 9.8 mN (~ 250 MPa) the probe tip imparts irreversible damage to monolayers with less than 16 carbon atoms. Our results show that the required load for destruction of the film depends on the cohesive energy of the SAM, and we hypothesize that the adsorbate-substrate interaction is also a key factor. A comparison between n-alkanethiolate SAMs on gold and silane monolayers is needed to test the hypothesis.

Silanes on Silicon

A covalently bound monolayer film on hydroxylated silicon oxide surfaces was formed by exposure to a solution of n-alkyl trichlorosilane or n-alkyl dimethylchlorosilane in toluene. Trichlorosilane head groups condense to form silicon-oxygen bonds with surface silanol groups generated on the native oxide layer. Similarly, dimethylchlorosilanes offer the same covalent attachment to the substrate but without the ability to form additional siloxane bonds to the surface or other adsorbing molecules. Contact angles for silane monolayers are shown in Table I and are generally consistent

with the formation of dense, methyl-terminated monolayer films derived from n-octadecyl trichlorsilane ($C_{18}SiCl_3$) molecules on silicon oxide.[8, 17] As the chain length decreases, the n-alkyl trichlorosilanes form monolayers with surfaces that are rich in $-CH_3$ groups, as supported by water contact angles of ~110°, but with some $-CH_2$ groups exposed, as indicated by reduced hexadecane contact angles. The monolayer prepared from n-octadecyl dimethylchlorosilane ($C_{18}SiMe_2Cl$) does not exhibit a dense methyl surface as indicated by the lower contact angles observed and reported in Table 1, consistent with a lower chain density as reported by Clear and Nealey.[36]

The combination of van der Waals interactions, any intermolecular cross linking, and head group attachment to the surface accounts for the cohesive energy of the alkylsilane films. While it has been generally accepted that silanes have a more robust covalent attachment than the chemisorption of alkanethiolate SAMs, the differences in these stabilities have not been quantified. We have examined the tribological properties of silane monolayers on silicon (oxide) to compare with alkanethiolate SAMs on gold (Figure 4.2). Methyl-terminated films derived from n-alkyl trichlorosilanes exhibit a chain length dependence on friction at 9.8 mN loads that is nearly identical to those for n-alkanethiolate SAMs on gold. Films formed from C_4SiCl_3 and C_6SiCl_3 molecules show a modest improvement in coefficient of friction as compared to the bare silicon oxide substrate. However, a plateau of 0.09 in the coefficient of friction was observed for molecules with 8 or more carbons, such that increasing the chain length provided no additional tribological benefit or any decrease in performance. Monolayers derived from $C_{18}SiMe_2Cl$ on silicon (oxide) yielded a coefficient of friction of 0.12, 30% higher than

those from n-octadecyl trichlorsilane ($C_{18}SiCl_3$), which we attribute to the less dense packing in the former film.[36]

To probe the difference in tribological stabilities of alkanethiolate SAMs on gold and silane monolayers on silicon, we compared the coefficients of friction for monolayers prepared from $C_{18}SH$ on gold, as well as $C_{18}SiMe_2Cl$ and $C_{18}SiCl_3$on silicon at a range of loads from 10 to 1,000 mN (Figure 4.6). The only difference between these three molecules is the assembling head group; thiol molecules self-assemble on the gold substrate by chemisorption between sulfur and gold atoms while silane monolayers are formed by a covalent siloxane bond between the silicon head group of the silane and the oxygen of the surface silanols atop the native oxide layer of the silicon substrate. Due to their identical carbon chain length, the films formed from these adsorbates should exhibit similar levels of van der Waals forces between the molecules, although the poor packing in the monolayer formed from $C_{18}SiMe_2Cl$ should result in the lowest cohesional energy of the three. While monolayers from alkanethiols and alkyl trichlorosilanes provided similar performances in initial tribological testing (Figure 4.2), the stronger covalent attachment of trichlorosilanes is demonstrated, as there is no change in the coefficient of friction for loads up to 1,000 mN while the $C_{18}S$- SAM begins to show a dramatic increase in friction at loads as low as 30 mN. Although the monolayer derived from $C_{18}Si(CH_3)_2Cl$ exhibits a higher initial coefficient of friction, this monolayer maintains its lubricity for all forces up to 1,000 mN. Therefore, improved performance for silane monolayers over thiolate SAMs can be attributed to the strong covalent attachment of the silane molecule to the substrate and, for n-alkyl trichlorosilanes, the added ability of these adsorbates to intermolecularly cross-link between molecules,[37, 38] forming a robust

siloxane network. Both features make removal or deformation of the monolayer more difficult than that for the alkanethiolate/Au system. The results presented here illustrate that silane films offer improved tribological properties over alkanethiolate SAMs on gold for high normal loads.

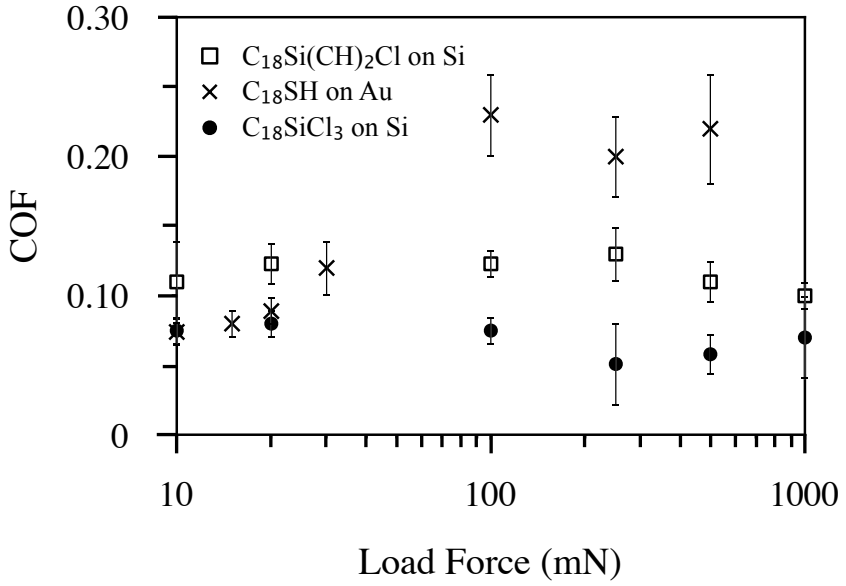

Figure 4.6. Effect of normal load, spanning two orders of magnitude, on the coefficient of friction for monolayers prepared from n-octadecanethiol on gold and both octadecyl dimethylchlorosilane and octadecyl trichlorosilane on silicon. Tribological performance was based on a single pass tribology test at 0.1 mm/s on a track of 2 cm with stainless steel probe tips of 1 mm (for loads < 100 mN) and 4 mm (for loads ≥ 100 mN).

Collectively, our results show that the tribological properties of monolayer films are dependent on their internal stabilities, which are influenced by cohesive chain interactions (van der Waals) and the adsorbate-substrate bond. For a constant load, increases in chain length yield monolayers that are more stable against tribological deformation to provide low coefficients of friction. For a constant adsorbate chain length, a more stable bonding to the substrate correlates with the most stable lubricating

monolayers. The fact that alkanethiolate SAMs on gold and silane monolayers on silicon exhibit similar chain length effects on friction at low loads (Figure 4.2), and vastly different performance at high loads (Figure 4.4), provides insight into the likely mechanism for tribological deformation of monolayer films. Stable interchain interactions can provide a buffer that prevents the probe from contacting the substrate at low loads. At higher loads, the probe disrupts these weak interchain interactions and can even dislocate adsorbates from their binding sites on the substrate. Thus, strong adsorbate-substrate bonds are required to maintain the integrity of the monolayer at these high loads.

Conclusions

These results show that the tribological properties of monolayer films depend on the surface group, chain length, and head group of the adsorbate. At low loads (9.8 mN), methyl-terminated SAMs yield coefficients of friction that are 3-fold lower than those by hydroxyl- or carboxylic acid-terminated SAMs of similar total chain length. Increasing the chain length of the adsorbate results in improved buffer properties of the monolayer to prevent probe-substrate interactions and the ability of the monolayer to withstand a higher normal load. Nonetheless, n-alkanethiolate SAMs with chain lengths $n \leq 12$ are irreparably damaged by a single pass of the probe at forces as low as 9.8 mN, whereas SAMs with longer chain lengths are more stable against the shearing forces of the probe. Monolayers prepared from n-octadecyltrichlorosilane and n-octadecyldimethylchlorosilane on silicon can withstand normal loads that are at least 30 times greater than those that disrupt $C_{18}S$/Au system, owing to the stronger siloxane

bonds of the silane monolayers. Much stronger adsorbate-substrate interactions stabilize silane monolayers against tribological degradation. The stronger covalent attachment of the silane precursor to silicon over alkanethiolates on gold is investigated for long-term tribological robustness in Chapter V.

References

1. Love, J. C.; Estroff, L. A.; Kriebel, J. K.; Nuzzo, R. G.; Whitesides, G. M., *Chemical Reviews* **2005,** *105*, 1103-1169.

2. Prime, K. L.; Whitesides, G. M., *Journal of the American Chemical Society* **1993,** *115*, 10714-10721.

3. Mrksich, M.; Chen, C. S.; Xia, Y. N.; Dike, L. E.; Ingber, D. E.; Whitesides, G. M., *Proceedings of the National Academy of Sciences of the United States of America* **1996,** *93*, 10775-10778.

4. Gujraty, K. V.; Ashton, R.; Bethi, S. R.; Kate, S.; Faulkner, C. J.; Jennings, G. K.; Kane, R. S., *Langmuir* **2006,** *22*, 10157-10162.

5. Laibinis, P. E.; Whitesides, G. M., *Journal of the American Chemical Society* **1992,** *114*, 1990-1995.

6. Ashurst, W. R.; Yau, C.; Carraro, C.; Maboudian, R.; Dugger, M. T., *Journal of Microelectromechanical Systems* **2001,** *10*, 41-49.

7. Tsukruk, V. V., *Advanced Materials* **2001,** *13*, 95-108.

8. Clear, S. C.; Nealey, P. F., *Journal of Colloid and Interface Science* **1999,** *213*, 238-250.

9. Srinivasan, U.; Houston, M. R.; Howe, R. T.; Maboudian, R., *Journal of Microelectromechanical Systems* **1998,** *7*, 252-260.

10. Maboudian, R.; Ashurst, W. R.; Carraro, C., *Sensors and Actuators A-Physical* **2000,** *82*, 219-223.

11. Sambasivan, S.; Hsieh, S.; Fischer, D. A.; Hsu, S. M., *Journal of Vacuum Science & Technology A* **2006,** *24*, 1484-1488.

12. Lio, A.; Charych, D. H.; Salmeron, M., *Journal of Physical Chemistry B* **1997,** *101*, 3800-3805.

13. McDermott, M. T.; Green, J. B. D.; Porter, M. D., *Langmuir* **1997,** *13*, 2504-2510.

14. Gellman, A. J. S., N.D. , *Proc. Inst. Mech. Engrs. Part J: Engineering Tribology* **2002**, 443-461.

15. Brewer, N. J.; Leggett, G. J., *Langmuir* **2004,** *20*, 4109-4115.

16. Maboudian, R.; Ashurst, W. R.; Carraro, C., *Tribology Letters* **2002,** *12*, 95-100.

17. Bhushan, B.; Kasai, T.; Kulik, G.; Barbieri, L.; Hoffmann, P., *Ultramicroscopy* **2005,** *105*, 176-188.

18. Singh, R. A.; Yoon, E. S.; Han, H. G.; Kong, H., *Wear* **2007,** *262*, 130-137.

19. Song, S. Y.; Zhou, J. F.; Qu, M. N.; Yang, S. R.; Zhang, J. Y., *Langmuir* **2008,** *24*, 105-109.

20. Laibinis, P. E. P., B.J.; Lee, S.W.; Jennings, G.K., The synthesis of organothiols and their assembly into monolayers on gold. In *Thin Films*, Academic Press: New York, 1998; Vol. 24.

21. Liu, G. Y.; Xu, S.; Qian, Y. L., *Accounts of Chemical Research* **2000,** *33*, 457-466.

22. Kumar, A.; Whitesides, G. M., *Applied Physics Letters* **1993,** *63*, 2002-2004.

23. Akimoto, K.; Sato, F.; Morikawa, T.; Fujihira, M., *Japanese Journal of Applied Physics Part 1-Regular Papers Short Notes & Review Papers* **2004,** *43*, 4492-4498.

24. Lee, S.; Heeb, R.; Venkataraman, N. V.; Spencer, N. D., *Tribology Letters* **2007,** *28*, 229-239.

25. Lio, A.; Morant, C.; Ogletree, D. F.; Salmeron, M., *Journal of Physical Chemistry B* **1997,** *101*, 4767-4773.

26. Sung, I. H.; Kim, D. E., *Tribology Letters* **2004,** *17*, 835-844.

27. Kim, H. I.; Koini, T.; Lee, T. R.; Perry, S. S., *Langmuir* **1997,** *13*, 7192-7196.

28. Houston, J. E.; Doelling, C. M.; Vanderlick, T. K.; Hu, Y.; Scoles, G.; Wenzl, I.; Lee, T. R., *Langmuir* **2005,** *21*, 3926-3932.

29. Singh, R. A.; Kim, J.; Yang, S. W.; Oh, J. E.; Yoon, E. S., *Wear* **2008,** *265*, 42-48.

30. Flater, E. E.; Ashurst, W. R.; Carpick, R. W., *Langmuir* **2007,** *23*, 9242-9252.

31. Porter, M. D.; Bright, T. B.; Allara, D. L.; Chidsey, C. E. D., *Journal of the American Chemical Society* **1987,** *109*, 3559-3568.

32. Jennings, G. K.; Munro, J. C.; Yong, T. H.; Laibinis, P. E., *Langmuir* **1998,** *14*, 6130-6139.

33. Peterlinz, K. A.; Georgiadis, R., *Optics Communications* **1996,** *130*, 260-266.

34. Carpick, R. W.; Salmeron, M., *Chemical Reviews* **1997,** *97*, 1163-1194.

35. Xu, S.; Liu, G. Y., *Langmuir* **1997,** *13*, 127-129.

36. Clear, S. C.; Nealey, P. F., *Journal of Chemical Physics* **2001,** *114*, 2802-2811.

37. Finklea, H. O.; Robinson, L. R.; Blackburn, A.; Richter, B.; Allara, D.; Bright, T., *Langmuir* **1986,** *2*, 239-244.

38. Allara, D. L.; Parikh, A. N.; Rondelez, F., *Langmuir* **1995,** *11*, 2357-2360.

CHAPTER V

TRIBOLOGICAL DURABILITY OF SILOXANE MONOLAYERS ON SILICON

Introduction

Silane monolayers provide the ability to tailor surface properties of silicon by varying the molecular composition and length of the adsorbing species to yield a broad range of surfaces and film thicknesses, respectively.[1-5] Despite their versatility in the modification of surfaces, these monolayers exhibit finite stabilities that limit their use in real applications.[6, 7] The thermal stability of alkylsiloxane monolayers on silicon in vacuum has been reported to exceed 400 ˚C and is independent of chain length.[8, 9] The mechanism for degradation of the monolayer has been attributed to the decomposition of the C-C bond.[8, 10] The decomposition of siloxane monolayers is also largely independent of the film's deposition method, with solution and vapor based procedures yielding similar stabilities.[8, 11, 12] While these studies have provided molecular insight toward the thermal stability of silane monolayers, molecular effects on the mechanical stability are not as well understood.

Mechanical stability or the ability of a thin film to withstand a normal load while maintaining beneficial lubrication is an important property for many applications, including coatings for microfluidics and medical implants.[13, 14] Methods for preparing thin films with beneficial tribological properties range from vapor phase deposition[6, 15, 16] to liquid-phase assembly[10, 17, 18] to multiple layers of bound and mobile molecules[19-22]. The tribological properties of a variety of different monolayer films on silicon[6, 12, 17, 23]

surfaces have been investigated in an effort to reduce friction and prevent wear during operation. Singh et al.[24] have shown that the friction force is dependent on the probe size and that a methyl-terminated film provides better tribological performance than fluorinated films. Also, they did not observe significant wear to silane based films on silicon by either AFM or microscale tribological testing for the limited number of cycles tested.

The structure and order within a monolayer is extremely important when characterizing the film's tribological properties. Several studies have focused on understanding the order and structure of silane films on silicon using infrared spectroscopy (FTIR,[25, 26] ATR,[27] and transmission IR[2, 28]) and near-edge X-ray absorption fine structure (NEXAFS)[26, 29, 30] and established the relationship between the length of the adsorbing molecule and the organization of the resulting films. Well-formed films derived from $CH_3(CH_2)_{n-1}SiCl_3$ molecules where $n \geq 12$ are known to have a highly ordered, crystalline structure with the chains extended in a trans conformation with a 7-8° tilt from the substrate.[2, 25, 27] Similarly, shorter chains ($n < 8$) exhibit liquid-like structure that can be attributed to the lack of sufficient dispersive forces between molecules.[31] Monolayer films formed from silanes with an intermediate chain length ($8 \leq n < 12$) possess both crystalline and disordered, liquid-like regions.[17, 26, 28]

In Chapter IV, I studied the initial response of monolayer films to an applied load with an emphasis on the frictional characteristics of n-alkanethiols on gold and n-alkyltrichlorosilanes on silicon.[32] My results demonstrate the dependence of the tribological properties of monolayer films on their *internal stability* i.e., the combination of dispersional chain interactions and the adsorbate-substrate bond. For a low load,

increases in chain length yield lower coefficients of friction until a plateau is reached at approximately 8 carbons, beyond which no improvement in the coefficient of friction is observed by increasing the thickness of the film. In comparison to structural studies of silane monolayers on silicon noted above, the low plateau in friction corresponds to chain lengths ($n \geq 8$) where crystalline structure begins develop in the monolayers.

Here, I report the long-term frictional properties for methyl-terminated monolayers prepared from n-alkyltrichlorosilanes along with hydroxyl- and perfluoroalkyl-terminated monolayers on silicon. A microtribometer enables the study of a broad range of sliding speeds (10 mm/s to 10 mm/s), normal loads, and tip compositions; the ability to vary both the tip parameters and the normal load, as in the current work, allows for measurements at higher forces while maintaining low to moderate surface pressures (< 400 MPa). Similar micro/macro tribology[33-36] results have been presented but typically report only the initial frictional response and do not discuss the long-term performance of the films. The use of a microtribometer here enables the long-term testing of monolayer films, which is extremely difficult to undertake using AFM measurements. Through our experiments we compare the durability of monolayers while varying chain length to tune dispersive interactions and terminal group functionality to alter surface-probe interactions. Molecular dynamics simulations have also been performed to determine the cohesive energy of methyl- and hydroxyl-terminated alkylsilane chains as related to the mechanical stability of these films. Additionally, monolayer films prepared on silicon from n-octadecyltrichlorosilane were tested at several loads to determine a critical load above which the tribological durability significantly decreases. To our knowledge we have provided the first long-term

tribological stability analysis of this monolayer system. Our results provide fundamental insight toward the molecular design of monolayer coatings for tribological applications.

Experimental Section

Monolayer Preparation

Silicon substrate. Silicon wafers were cut into 1.5 x 4.5 cm samples, sonicated in ethanol for 30 min, rinsed with ethanol, and dried in a stream of nitrogen before being treated with piranha solution (70% H_2SO_4/30% H_2O_2) for 30 min, rinsed with copious amounts of water, and dried thoroughly in a stream of nitrogen. CAUTION: Piranha solution is a strong oxidizer and can be extremely dangerous. Piranha solution should never be stored and should be disposed of properly immediately after use.

n-Alkyltrichlorosilanes monolayers. n-Alkyltrichlorosilane monolayers were formed by immersing the piranha-treated substrates into 1 mM solutions of silane precursors in toluene for 5 h. Samples were removed from solution, rinsed in ~20 mL of toluene, then rinsed with deionized water and ethanol, and dried in a stream of nitrogen.

Hydroxyl monolayer on silicon via trichloroacetate conversion.[37] Piranha-treated silicon substrates were immersed in a 1 mM solution of (1-trichlorosilylundecyl) trichloroacetate in toluene for 5 h.[37] The samples were removed from solution, rinsed with ~20 mL of toluene, then rinsed with deionized water and ethanol, and dried in a stream of nitrogen. The conversion of the trichloroacetate terminal group into a hydroxyl was accomplished by immersing the sample into a solution containing 10 mL of deionized water, 10 mL of methanol, and 0.15 g of sodium bicarbonate for 15 min.[37] The

resulting hydroxyl-terminated monolayer was rinsed with deionized water and ethanol, and then dried with a stream of nitrogen.

Hydroxyl monolayer on silicon via hydroboration-oxidation reaction. The preparation and characterization of these films followed a method that has been previously reported.[38] Piranha-treated silicon substrates were immersed in a 1 mM solution of 7-octenyltrichlorosilane in toluene for 5 h. The samples were removed from solution, rinsed with ~ 20 mL of toluene, rinsed with deionized water and ethanol, and then dried in a stream of nitrogen. The conversion of the vinyl terminal group into a hydroxyl was accomplished by immersing the samples in 0.1 M solution of borane-tetrahydrofuran complex (BH_3-THF) in a nitrogen atmosphere for 2 h. The samples were removed from solution, rinsed with THF and then deionized water, before immersion into a solution containing 10 mL of 30% hydrogen peroxide and 10 mL of 28% ammonium hydroxide in water at 60°C for 2 h. The resulting hydroxyl-terminated monolayer was rinsed with deionized water and ethanol and dried with a stream of nitrogen.

Fluorinated monolayer. (Tridecafluoro-1,1,2,2-tetrahydrooctyl)-1-trichlorosilane monolayers were formed by immersing the piranha-treated substrates into 1 mM solutions of $F_3C(CF_2)_5(CH_2)_2SiCl_3$ precursor in dichloromethane for 30 min. Samples were removed from solution, rinsed in ~20 mL of dichloromethane, then rinsed with deionized water and ethanol, and dried in a stream of nitrogen.

Microtribology

A Center for Tribology (CETR) UMT-2 Micro-Tribometer was used for all tribology experiments. The instrument was used for ball on flat surface sliding

experiments with a 2-D DFM-0.5 force sensor. The DFM-0.5 sensor can apply loads ranging from 50 to 5,000 mN and measure with a resolution of 0.25 mN. Tests were performed with a stainless steel ball bearing as the probe tip attached to the sensor via a suspension-mounting cantilever where the size of the tip was selected according to the magnitude of the applied load. The tip was sonicated in acetone for 5 min and dried with nitrogen before use. The DFM-0.5 sensor was operated with stainless steel balls of 4 mm diameters as the probe. The force that the tip applied to the surface was slowly ramped to the desired load and allowed to equilibrate at that load for at least 15 s before the surface was set into motion. Tests were performed at a sliding speed of 1.0 mm/s over a 10 mm track for cycle wear tests. Results represent measurements on an average of five samples each prepared independently unless otherwise noted as a representative data set.

X-ray Photoelectron Spectroscopy

X-ray photoelectron spectra (XPS) were obtained with a PHI 5000 VersaProbe spectrometer with use of a monochromatized Al Kα X-ray source (spot size of 10 μm x 20 μm) and a concentric hemispherical analyzer (pass energy = 150 eV). The detector angle with respect to the surface normal was 45° and 61 total cycles were performed. Peaks were fit with 70% Gaussian / 30% Lorentzian profiles and a Shirley background. CasaXPS (Vamas) software was used to process the XPS data. Spectra were obtained for monolayers prepared from $C_{16}SiCl_3$ that had been subjected to long-term durability testing and were treated post-test to a 1 mM solution of (tridecafluoro-1,1,2,2-tetrahydrooctyl)-1-trichlorosilane ($CF_3(CF_2)_5(CH_2)_2SiCl_3$) for 1 h. Wear tracks were determined on the substrate using the camera and viewing software within the XPS to

verify that spectra were obtained at the appropriate location on the sample.

Molecular Dynamics Simulations

A β-cristoballite silica surface with a thickness of ~12 Å and an area of 53.87 x 46.66 Å coated with both methyl ($Si(OH)_2(CH2)_{n-1}CH_3$, n = 4 – 22) and hydroxyl ($Si(OH)_2(CH2)_nOH$, n = 4 – 22) terminated alkylsilane chains of different lengths was studied (Figure 5.1). The silica surface and monolayer chains were described using the OPLS force field[39] adapted for simulations of silica coated with fluorocarbons.[40, 41] The silica surfaces were fully coated with 100 alkylsiloxane chains as in earlier work[42] and

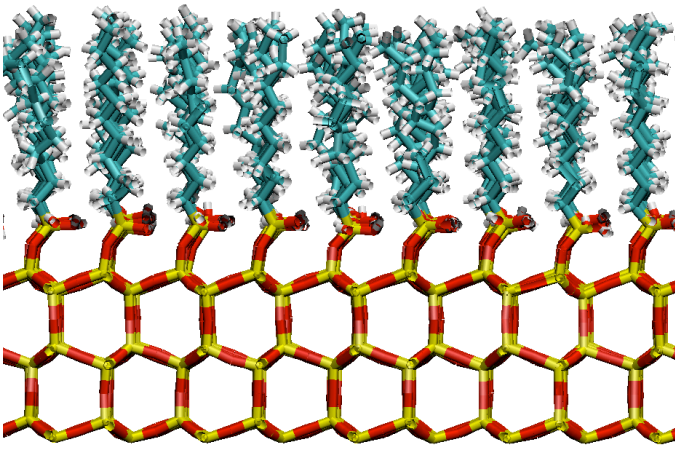

Figure 5.1. Wireframe image of $Si(OH)_2(CH_2)_9CH_3$ monolayer on a SiO_2 surface. Oxygen is red, silicon is yellow, carbon is light blue, and hydrogen is gray.

simulated under periodic boundary conditions in the surface directions in order to mimic the behavior of an infinite surface. The simulations were carried out using the LAMMPS MD code[43] with electrostatic interactions computed using the particle-particle, particle-mesh algorithm in 2D[44] and Lennard-Jones interactions computed using a cutoff radius of

10 Å. The equations of motion were integrated using the multiple time step algorithm rRESPA with time steps of 0.3 fs for bonded interactions, 0.6 fs for angle interactions (both valence and dihedral), and 1.2 fs for all intermolecular interactions. All systems were thermostated to 300 K.

For each system studied, the interchain dispersive interactions were estimated from 1 ns simulations using:

$$U = \frac{1}{m}\left[U_{SiO_2-alkylsilane} - \left(U_{SiO_2} + mU_{alkyl}\right)\right] \tag{5-1}$$

where U is the cohesive chain energy, $U_{\mathrm{SiO2\text{-}alkylsilane}}$ is the total potential energy of the simulated system (i.e., a silica surface coated with m alkylsiloxane chains), U_{SiO2} is the potential energy of the silica layer without the alkylsilane chains, and U_{alkyl} is the energy of an isolated alkane chain. In this way we can determine the contribution to the energy of the system from the chain-chain dispersive interactions. Similar approaches have been used in the work of Shimizu[45] and Xiao;[31] however, I would like to note that the simulations do not account for any effects due to cross linking between molecules.

Results and Discussion

Surface Characterization of Silane Monolayers

A covalently bound alkylsilane monolayer film on hydroxylated silicon oxide surfaces was formed by exposure to a solution of the appropriate trichlorosilane precursor molecule in toluene. Trichlorosilane head groups condense to form silicon-oxygen bonds

with surface silanol groups generated on the native oxide layer.[1] All monolayer assembly was confirmed by contact angle analysis and ellipsometric thicknesses prior to any tribological testing (Table A.2). For n-alkyltrichlorosilanes a general increase of thickness with chain length is observed, and reported values are consistent with previous results.[46] A dense, methyl-terminated silane monolayer typically yields advancing water contact angles > 108° and advancing hexadecane contact angles > 40° with a low hysteresis. Monolayers prepared from C_nSiCl_3 where n > 8 exhibit contact angles that are indicative of dense methyl surfaces that correlate with well-ordered monolayers, consistent with the structural analyses of these films by other groups.[2, 28] Thinner monolayers prepared from C_nSiCl_3 with n = 4 and 6 exhibit lower contact angles that suggest a less dense methyl surface[28, 31] with less effective screening of forces between the probe liquid and the substrate. Monolayers derived from $C_{18}Si(CH_3)_2Cl$ exhibit lower water and hexadecane contact angles than expected for a dense methyl surface, which we attribute to the steric hindrance imparted by methyl groups attached to the adsorbing silane head group to prevent formation of a dense film.[18] The monolayer prepared from $F_3C(CF_2)_5(CH_2)_2SiCl_3$ exhibits a hexadecane contact angle of 80° that is consistent with the formation of a dense CF_3-terminated surface.[30, 47]

Two approaches were used to achieve a predominately hydroxyl surface. In order to prepare films with hydroxyl termini from trichlorosilane precursors, adsorbed films must be treated post-assembly to convert the termini to the desired functionality. As one approach, surface vinyl bonds were converted to hydroxyls by a two step hydroboration-oxidation reaction.[4] The second method to achieve a hydroxyl terminus was the deprotection of the trichloroacetate terminus of a monolayer assembled from (1-

trichlorosilylundecyl) trichloroacetate by exposing the film to a solution containing methanol, water, and sodium bicarbonate.[37] The two monolayers used to obtain OH-terminated films ($H_2C{=}CH(CH_2)_6SiCl_3$ and $Cl_3C_2O_2(CH_2)_{11}SiCl_3$) exhibit wetting properties and thicknesses consistent with reported values.[37, 38] While both methods provide hydroxyl termini, the conversion of the vinyl monolayer yields films that are relatively thin due to the short assembling molecule but possess a high packing density of chains on the substrate because of the linear adsorbate that lacks a bulky head group. In contrast, the deprotection of the trichloroacetate head group yields films that have longer carbon chains (11) but a lower packing density due to the steric hindrance when assembling the bulky precursor on the substrate. The contact angles of these two films (Table A.2) demonstrate these differences in packing of the films as the hydroxyl monolayer resulting from hydroboration yields an advancing water contact angle of 39° compared to 64° for the hydroxyl monolayer derived from the deprotected trichloroacetate film.

Effect of Chain Terminus

The effect that the alkylsilane terminal group has on long-term frictional durability was investigated by preparing alkylsilane monolayer films that terminate in hydroxyl, methyl, and perfluoromethyl groups. Monolayers were prepared from n-octyltrichlorosilane to represent a methyl surface and (tridecafluor-1,1,2,2-tetrahydrooctyl)-1-trichlorosilane to represent a perfluoromethyl surface, and two types of hydroxyl surfaces were prepared as described above.

Table 5.1. Wear life for silane monolayers on silicon that terminate in different functional groups

Adsorbing Molecule	**Cycles until Failure**
$HO(CH_2)_8SiCl_3$ via hydroboration	3 ± 1
$HO(CH_2)_{11}SiCl_3$ via trichloroacetate	7 ± 2
$F_3C(CF_2)_5(CH_2)_2SiCl_3$	40 ± 10
$H_3C(CH_2)_7SiCl_3$	410 ± 160

While the impact of a film's terminus on initial frictional performance has been studied,[32, 37, 48] with more polar groups generally yielding higher frictional forces, the role of the monolayer terminus in long-term durability of a film is less understood. In this study, we compare the number of cycles at a 98 mN load to which a surface can be subjected before the film fails. We have defined failure of a film as the number of tribological cycles required for the frictional force to exceed 150% of the initial value. As shown in Table 5.1, the film prepared from octyl trichlorosilane displayed ~10 fold and ~100-fold greater stabilities than the films prepared from CF_3- and -OH termini, respectively. The hydroxyl-terminated films both performed poorly in tribology testing with neither method for hydroxyl group formation yielding a surface capable of lasting more than 10 cycles as reported in Table 5.1. The hydroxyl film obtained via the hydroboration reaction was only able to withstand 3 ± 1 cycles while the trichloroacetate conversion lasted for 7 ± 2 cycles, suggesting that longer chain length is more important than dense packing in defining the stability of these two films. We have previously shown that hydroxyl terminated monolayers yield a higher initial coefficient of friction than other functionalities studied that include carboxylic acid, methyl, and

perfluoromethyl.[32, 37] Stronger interactions between a high-energy surface and the stainless steel tip, when compared to a low energy surface, increase the adhesion between probe tip and surface, thus increasing the frictional force, and as shown here, greatly reducing tribological durability.

While the -CF_3 terminated monolayer should exhibit a low-energy surface and weak interactions with the stainless steel probe, its durability is an order of magnitude lower than the film prepared from n-octyltrichlorosilane. The CF_3 film possesses a lower packing density than monolayers derived from n-alkyltrichlorosilanes due to the larger cross section of the fluorocarbon chain, which also greatly reduces cross linking between silanol head groups. Thus, we would expect the fluorocarbon monolayer to exhibit lower cohesive and adhesive energies as compared to monolayers prepared from n-octyltrichlorosilane, which enables easier disruption of monolayer packing and displacement of the adsorbed molecules by the probe tip.

Effect of Chain Length

In addition to the functionality of the chain terminus and the extent of intermolecular cross linking, the dispersive interactions between neighboring chains could contribute toward the internal stability of the films by boosting their cohesive energy. Here, we view that the cohesive energy of a film comes only from the non-covalent chain-chain interactions among the adsorbed molecules. Thus, for a family of molecules such as n-alkyltrichlorosilanes, altering the chain length provides a means to modulate the dispersive or cohesive interactions of the film. The dependence of chain length on the structure and packing in a silane monolayer has been shown previously[17, 28,

[31] with the onset of crystallinity occurring for chain lengths (n) ≥ 8 and solidifying for n ≥ 12. In terms of tribology with 9.8 mN loads, we have shown that methyl-terminated films derived from n-alkyltrichlorosilanes exhibit a low, constant coefficient of friction of 0.09 for n ≥ 8 with increased frictional coefficients for shorter chain lengths as the thinner films do not have sufficient cohesive energy to prevent probe-substrate interactions.[32] For molecules with ≥ 8 carbons in length, sufficient dispersion forces are present to withstand the applied load so that initially measured frictional forces are independent of chain length.[49]

In this study we have investigated the long-term durability of films of increasing thickness by varying the chain length of the precursor molecule at a load of 98 mN. Films formed from C_4SiCl_3 (not shown) and C_6SiCl_3 show an initial improvement in coefficient of friction as compared to the bare silicon oxide substrate (COF = 0.60) but sustain lubrication of a 98 mN load for only 35 and 45 cycles, respectively. When longer molecules are adsorbed to form the film, the resulting monolayer is able to withstand many more cycles before failure, as shown in Figure 5.2. Thicker films such as $C_{18}SiCl_3$ are able to withstand a 98 mN load for 9,200 cycles. Since all these films have similar binding to the silicon surface, the strong dependence on chain length as observed for durability studies suggests that interchain dispersion interactions greatly influence film stability during sliding.

The effect of chain length on the cohesive energy was further probed using molecular dynamics simulations of silica surfaces covered with both methyl- ($Si(OH)_2(CH_2)_{n-1}CH_3$, n = 4 – 22) and hydroxyl- ($Si(OH)_2(CH_2)_nOH$, n = 4 – 22) terminated alkylsilane chains of different length. As shown in Figure 5.3a, a nearly linear

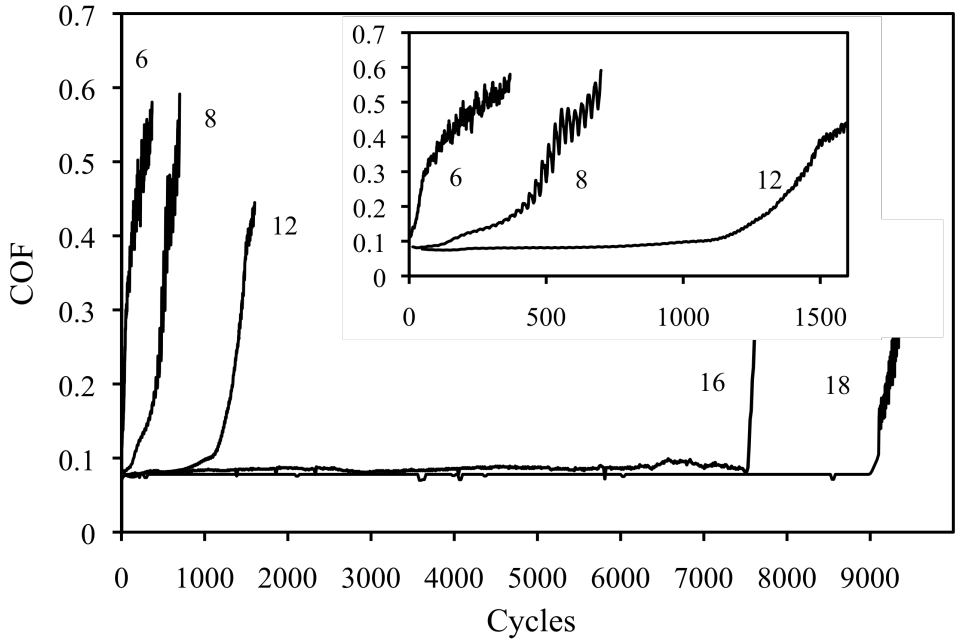

Figure 5.2. Representative tribology tests for n-alkyltrichlorosilane monolayers (C_nSiCl_3; n = 6, 8, 12, 16, 18) at a 98 mN load over a 10 mm test track with a velocity of 1 mm/s. Failure occurs at 45, 410, 1,400, 7,600, and 9,200 cycles for monolayers prepared from C_6SiCl_3, C_8SiCl_3, $C_{12}SiCl_3$, $C_{16}SiCl_3$, and $C_{18}SiCl_3$ respectively. A monolayer prepared from C_4SiCl_3 (not shown) fails after 35 cycles.

dependence of the cohesive chain energy with the length of the adsorbing molecule for both the hydrophilic and hydrophobic surfaces studied as measured by Eq. 5-1 is observed. If we consider the incremental cohesive chain energy per carbon, the cohesive energy becomes monotonically more negative with chain length for the CH_3-terminated surfaces (Figure 5.3b), increasing from -1.56 kJ/mole for C_4 chains to an asymptotic value of approximately -6 kJ/mole for C_{22} chains, which is comparable to the value of -6.8 kJ/mol based on the latent heat of melting plus vaporization for n-alkanes.[50] This result is also similar to the values reported for simulations of densely packed alkylsilane chains on mica,[31] where each CH_2 group contributes approximately -7 kJ/mole, and the observed trend is similar to the experimental observations, i.e., the cohesive energy grows with the size of the chains.

The cohesive energy for hydroxyl-terminated monolayers is slightly higher than for the hydrophobic chains (between -8 and -21 kJ/mol) due to the additional stability created by the hydrogen bond network of the terminal hydroxyl groups and passes through a minimum before reaching an asymptotic value (Figure 5.3b). The experimentally observed lower tribological stability for hydroxyl-terminated monolayers (Table 5.1) is likely due to the stronger adhesive interactions between the probe and the –OH surface, which disrupts the monolayer chain packing.

The simulation results are consistent with the experimental observations showing that the longer precursor molecules form thicker monolayers with greater dispersion forces to enhance cohesive energy. The binding energy of each molecule remains constant for all molecules since every chain, regardless of length, possesses similar binding to the surface. The greater cohesive energies of the thicker films allow these films to withstand greater normal loads[32] or an increased number of cycles without damage or plastic alteration to the individual molecules to compromise the overall integrity of the film.

The dependence of the number of cycles until failure on the thickness of the film follows an exponential trend as shown in Figure 5.4 and illustrates the importance of interchain dispersive interactions in promoting monolayer stability. This exponential dependence of chain length for mechanical degradation of silane monolayers using tribology agrees with thermal and oxidative stability studies for n-alkanethiolate systems[51, 52] and suggests that repeated cycling of the probe is required to eventually disrupt the cohesive interactions of the chains prior to probe-substrate contact.[8, 10, 53] If

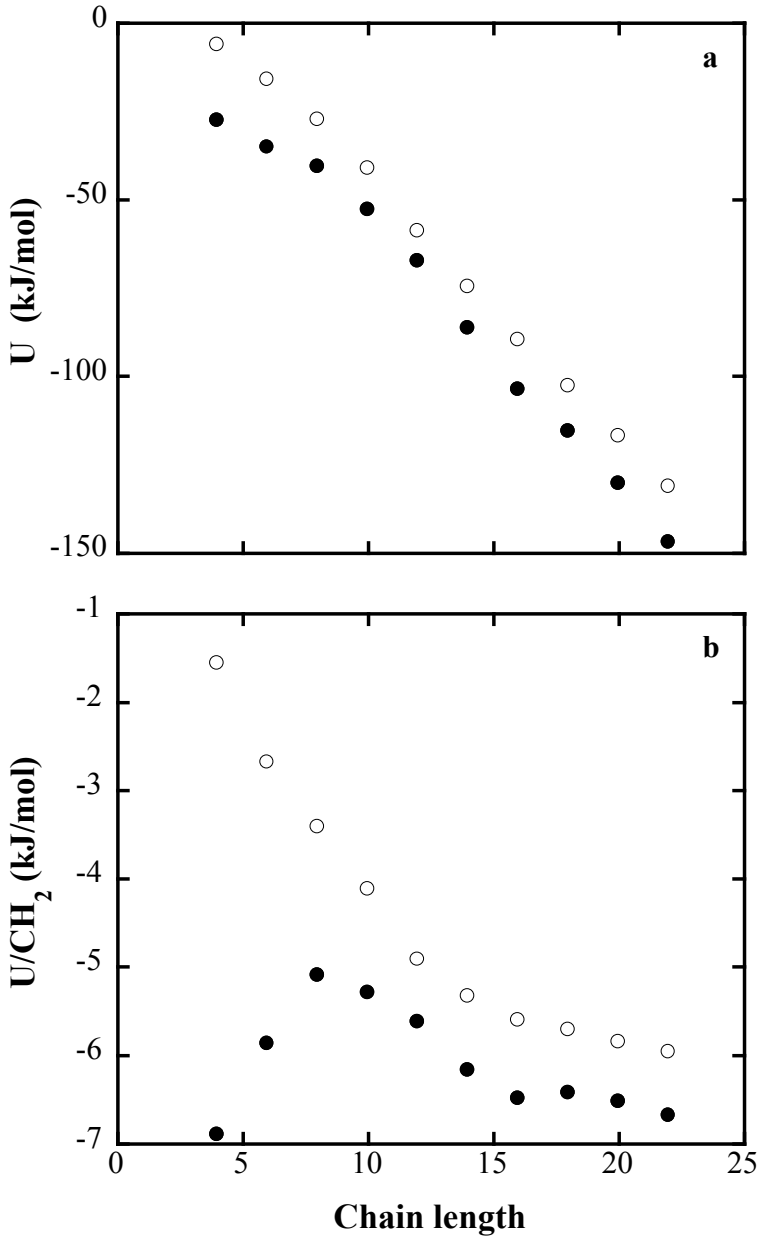

Figure 5.3. Dependence of chain length on a) cohesive chain energy and b) cohesive energy per CH_2 group as determined from molecular dynamics simulations. The closed symbols correspond to simulations of hydroxyl-terminated monolayers and the open symbols to alkyl terminated monolayers.

we assume that mechanical degradation of the monolayer occurs by mechanically assisted molecular desorption of individual components, the rate constant for mechanically assisted desorption should exhibit an Arrhenius form according to

$$k_D = k_0 e^{-\frac{E_a}{kT}} \tag{5-3}$$

where k_D is the rate of desorption, k_0 is a constant, k is the Boltzmann constant, T the temperature, and E_a is an activation energy, that should be proportional to the total internal energy within the monolayer U_{total} as

$$E_a \propto U_{total} = n\Delta U_{Dispersive} + U_b \tag{5-4}$$

where n is chain length, $\Delta U_{Dispersive}$ is the cohesive energy per carbon, and U_b is the binding energy of the molecule to the substrate. Combining equations (5-3) and (5-4), we are able to show that while the cohesive energy of the film is linear with respect to chain length, the mechanically-assisted desorption rate constant that reflects the number of cycles until failure should indeed depend exponentially on the chain length, in agreement with Figure 5.4.

$$k_D \propto k_0 e^{-\frac{n\Delta U_{Dispersive}}{kT}} \tag{5-5}$$

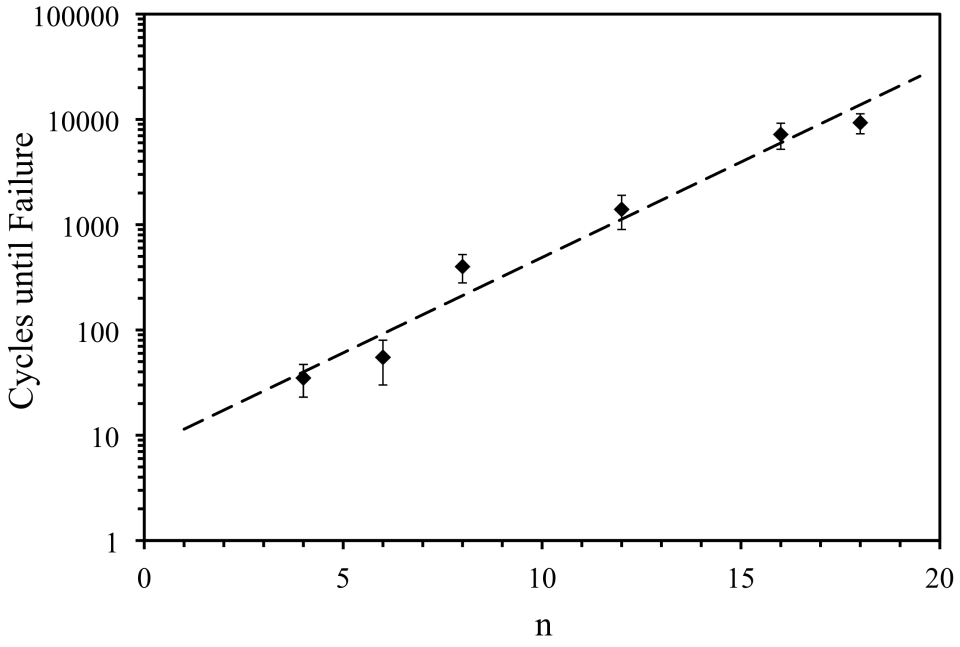

Figure 5.4. Effect of chain length on the number of cycles until failure from Figure 5.2 for monolayers prepared from C_nSiCl_3 on silicon. The dashed line represents an exponential fit of the data.

Effect of Load on Durability

For $C_{18}SiCl_3$ films that are able to withstand a load of 100 mN for over 9,000 cycles, a further study was consducted to assess the dependence of the applied load on the required time for failure. As shown in Figure 5.5, as the load increases from 100 mN to 250 mN (corresponding to a surface pressure between 180 and 250 MPa of Hertzian force), the number of cycles until failure decreases by two orders of magnitude, suggesting that the increase in pressure disrupts the stabilizing cohesive energy of the chains to provide greater tip-substrate interactions and rapidly degrade the monolayer. In general, increased normal load leads to shorter film wear life. For forces above a load of

~ 200 mN the monolayer fails within 100 cycles and at the maximum load applied, 980 mN, the monolayer film failed at 20 cycles. At these elevated loads, the monolayer is unable to maintain the cohesive energy among chains, and the molecules may be worn from the surface by direct action from the probe. We hypothesize that the mechanism for the failure of trichlorosilane films occurs as individual chains are removed from the surface by the probe tip, subsequently leading to diminished cohesive interactions and lubricating properties.

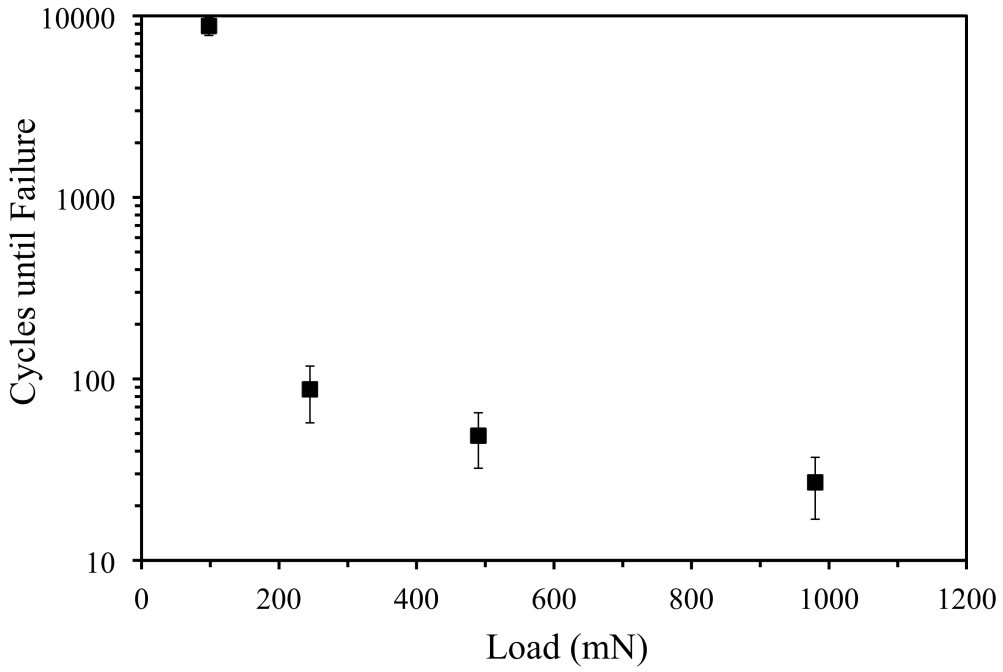

Figure 5.5. Effect of load on the number of cycles until failure for monolayers prepared from $C_{18}SiCl_3$ on silicon. These loads correspond to Hertzian pressures of 180, 240, 300 and 380 MPa.

Mechanism of Degradation

In order to investigate the mechanism for deformation of the n-alkylsilane monolayer by tribometry testing, we analyzed the subsequent wear track with X-ray photoelectron spectroscopy (XPS). Monolayers prepared from $C_{16}SiCl_3$ that had been subjected to long-term durability testing were treated post-test to a 1 mM solution of (tridecafluoro-1,1,2,2-tetrahydro octyl)-1-trichlorosilane ($CF_3(CF_2)_5(CH_2)_2SiCl_3$) for 1 h. This procedure allows for fluorinated molecules to be inserted into the wear track of the surfaces that had been damaged by tribology testing. XPS survey scans were obtained to characterize the ability and quantity of perfluorinated silane insertion into the wear track. Figure 5.6a-c shows three XPS scans obtained at several points during the tribometric testing of a $C_{16}SiCl_3$ film, the results of which are shown in Figure 5.6d. The two peaks in the XPS spectra that would reveal the extent of fluorine insertion, and thereby the extent to which the original hydrocarbon film has been damaged, are the F(1s) peak at 685 eV and C(1s) peak at 285 eV peaks. Neither the $C_{16}SiCl_3$ control sample nor the film tested before any rise in coefficient of friction (Figure 5.6a) was observed to have a fluorine peak in their respective spectra, as demonstrated by the F(1s)/C(1s) peak ratios of 0 as shown in Table 5.2. These results indicate that the fluorinated silane molecules are not inserting into the well formed alkyltrichlorosilane films and that, for the length of time in which the film demonstrates a coefficient of friction of ~0.10, no significant damage is being imparted to the monolayer by the sliding probe. After the COF doubles (point B in Figure 5.6d), exposure of the film to $CF_3(CF_2)_5(CH_2)_2SiCl_3$ results in a reduction in C(1s) intensity and the appearance of F(1s) and F(KLL) peaks in the spectrum to suggest that some hydrocarbon chains have been removed from the surface

and replaced with the fluorinated species (Figure 6b). These films have a ratio of F(1s) to C(1s) peaks that is 0.3 or two orders of magnitude less than that of a complete monolayer film prepared from $CF_3(CF_2)_5(CH_2)_2SiCl_3$, which suggests that wear occurs by the removal of individual chains and that once a small number of molecules have been worn away, the cohesive energy of the film can be more easily disrupted, leading to failure within a short number of cycles. For films where the coefficient of friction was similar to that of a bare silicon substrate (point C in Figure 5.6d), a further diminishing of the C(1s) peak and an increase of the F(1s) and F(KLL) peaks indicates that additional $CF_3(CF_2)_5(CH_2)_2SiCl_3$ molecules were able to attach to the surface where the hydrocarbon monolayer was damaged by loss of species. Even at the point where the measured friction was similar to that of the bare substrate, the F(1s)/C(1s) ratio is still an order of magnitude lower than that of a well formed film from $CF_3(CF_2)_5(CH_2)_2SiCl_3$. This result suggests that deformation of a small quantity of the surface-bound chains is sufficient to promote complete failure of the film. Sections of the monolayer that have been damaged by the probe subsequently expose more of the substrate and silanol groups to which perfluorinated silane molecules can attach. There is also the possibility that not all of the damaged film results in a surface that is capable of having a trichlorosilane molecule bond to the surface, or the film/surface is worn in a manner that destroys available silanol groups for attachment of the perfluorinated silane.

The results of Figures 5.4 – 5.6 illustrate the importance of interchain dispersion interactions in promoting the tribological longevity of silane monolayers. The dense alkyl chains represent a mechanical buffer that protects the underlying substrate from wear. Greater normal loads are able to more rapidly disrupt the buffer provided by the

chains. Once the chain buffer is disrupted, mechanical sliding provides large pressures directly at the monolayer/silicon interface to cause scission of surface bonds and promote the loss of molecular species.

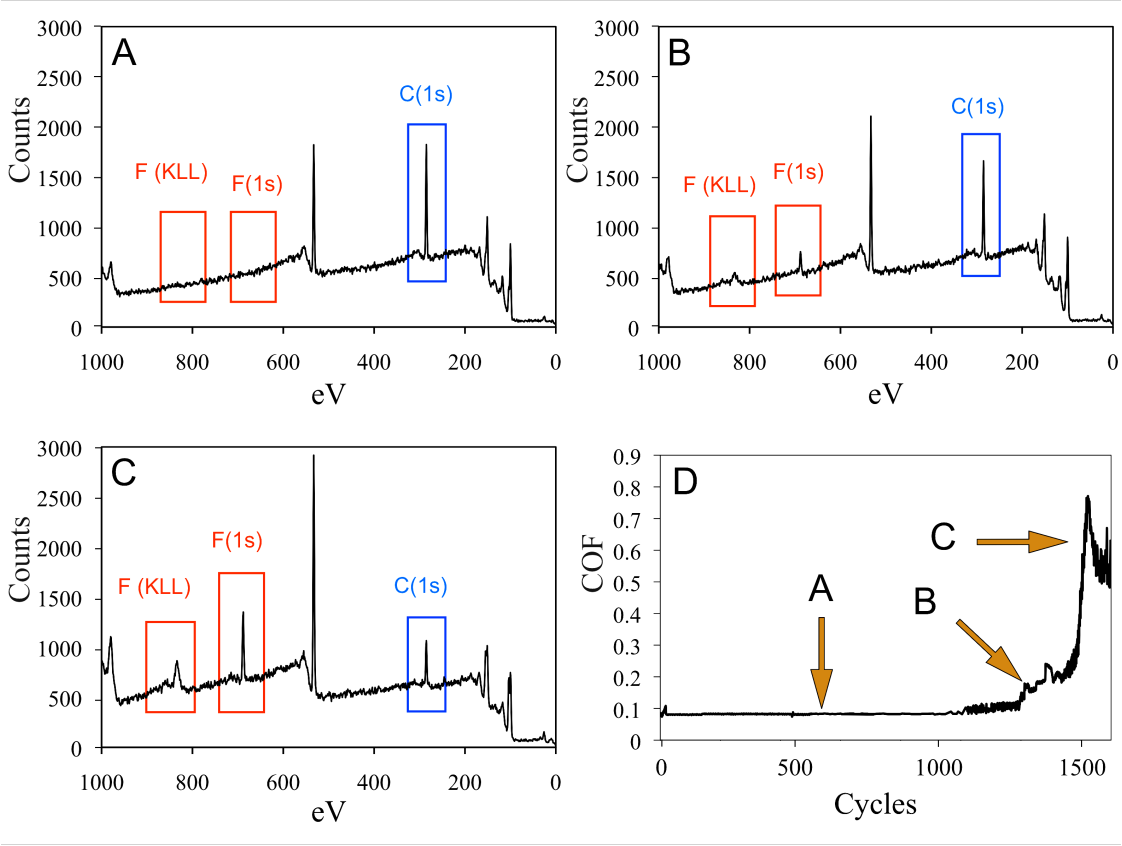

Figure 5.6. XPS survey spectra of a monolayer prepared from $C_{16}SiCl_3$ and tested with tribometry at a load of 98 mN for (A) 600 cycles, (B) 1,200 cycles, and (C) 1,500 cycles, as indicated on the COF vs. cycles curve in (D), before post-treatment with $CF_3(CF_2)_5(CH_2)_2SiCl_3$ molecules. Successful insertion of the fluorocarbon species is indicated by the evolution of F(1s) and F(KLL) peaks in the spectra. A control film at 0 cycles (no tribometry test) revealed no fluorocarbon insertion (not shown).

Table 5.2. Ratio of F(1s)/C(1s) peaks from XPS spectra after exposure of a monolayer prepared from $C_{16}SiCl_3$ to tribometric testing at 200 mN for the indicated number of cycles followed by exposure to 1 mM $CF_3(CF_2)_5(CH_2)_2SiCl_3$ for 1 h.

Monolayer Tested	Cycles	F(1s)/C(1s) Ratio from XPS Spectra
$CF_3(CF_2)_5(CH_2)_2SiCl_3$	0	30
$C_{16}SiCl_3$	0	0
$C_{16}SiCl_3$	600	0
$C_{16}SiCl_3$	1,200	0.3
$C_{16}SiCl_3$	1,500	3

Effect of Cross Linking

The effect of surface attachment on the long-term tribological properties of monolayer films was investigated by comparing silane monolayers prepared from n-octadecyl dimethylchlorosilane ($C_{18}Si(CH_3)_2Cl$) and n-octadecyltrichlorosilane ($C_{18}SiCl_3$) on silicon. Each molecule possesses an identical number of carbon atoms in the backbone as well as an identical methyl terminus. Due to their identical carbon chain length, the films formed from these adsorbates should exhibit similar levels of van der Waals forces between the molecules, although the lesser packing[18] in the monolayer formed from $C_{18}Si(CH_3)_2Cl$, indicated by a water contact angle that is 14° less than that on a monolayer prepared from $C_{18}SiCl_3$ (Table I), should result in weaker intermolecular interactions when comparing the two films. The monolayer derived from $C_{18}SiCl_3$ survived for 9,200 ± 300 cycles in comparison to 1,615 ± 680 for the monolayer from $C_{18}Si(CH_3)_2Cl$. The capability of films prepared from n-octadecyltrichlorosilane on

silicon to consistently provide good wear protection for many thousands of cycles at 98 mN loads indicates that these films have large internal energies to stabilize the film. While the $C_{18}Si(CH_3)_2Cl$ based film attaches to the silicon substrate by the same covalent bond as alkyltrichlorosilane molecules, $C_{18}Si(CH_3)_2Cl$ molecules are not able to form additional cross linked bonds during monolayer formation. Furthermore, the methyl groups attached to either side of the chain limit the ability of the molecules to pack into a dense film.[18, 54] Both of these factors reduce the internal energy of the subsequent film and dramatically reduce the long-term lubricating ability as compared to a monolayer prepared from $C_{18}SiCl_3$.

Conclusions

We have presented results from experimental and computational studies investigating the long-term durability, cohesive energy, and tribological failure mechanisms of silane monolayer films on silicon. Collectively, our results show that the long-term tribological properties of silane monolayer films are dependent on their internal stabilities, which are influenced by dispersive chain interactions and cross linking, as well as their outer terminus that interacts with the sliding probe. For a constant load, increases in chain length yield monolayers that are dramatically more stable against tribological deformation to provide low coefficients of friction over much longer periods of time. For a constant adsorbate chain length, a more stable bonding to the substrate through cross linking correlates with the most stable lubricating monolayers capable of lasting several orders of magnitude longer than those with weaker substrate-adsorbate binding. For the most robust films in this study, monolayers prepared from

$C_{18}SiCl_3$, a load dependence was observed where a load of 250 mN (~240 MPa) is required to significantly damage the film in fewer than 100 cycles. The proposed mechanism of deformation whereby disruption of the cohesive buffer leads to desorption of monolayer components is supported by XPS analysis of the reinsertion of silane molecules into the tribometry wear track. Overall, we have found that films with low energy surfaces and greater internal stabilities through a high degree of cross linking and longer, densely packed chains to increase dispersion interactions are more stable against tribological damage.

References

1. Sagiv, J., *Journal of the American Chemical Society* **1980,** *102*, 92-98.

2. Allara, D. L.; Parikh, A. N.; Rondelez, F., *Langmuir* **1995,** *11*, 2357-2360.

3. Banga, R.; Yarwood, J.; Morgan, A. M.; Evans, B.; Kells, J., *Langmuir* **1995,** *11*, 4393-4399.

4. Wasserman, S. R.; Tao, Y. T.; Whitesides, G. M., *Langmuir* **1989,** *5*, 1074-1087.

5. Ruhe, J.; Novotny, V. J.; Kanazawa, K. K.; Clarke, T.; Street, G. B., *Langmuir* **1993,** *9*, 2383-2388.

6. Maboudian, R.; Ashurst, W. R.; Carraro, C., *Sensors and Actuators A-Physical* **2000,** *82*, 219-223.

7. Ashurst, W. R.; Carraro, C.; Maboudian, R.; Frey, W., *Sensors and Actuators a-Physical* **2003,** *104*, 213-221.

8. Kluth, G. J.; Sung, M. M.; Maboudian, R., *Langmuir* **1997,** *13*, 3775-3780.

9. Sung, M. M.; Kluth, G. J.; Yauw, O. W.; Maboudian, R., *Langmuir* **1997,** *13*, 6164-6168.

10. Kulkarni, S. A.; Mirji, S. A.; Mandale, A. B.; Vijayamohanan, K. P., *Thin Solid Films* **2006,** *496*, 420-425.

11. Zhuang, Y. X.; Hansen, O.; Knieling, T.; Wang, C.; Rombach, P.; Lang, W.; Benecke, W.; Kehlenbeck, M.; Koblitz, J., *Journal of Micromechanics and Microengineering* **2006,** *16*, 2259-2264.

12. Srinivasan, U.; Houston, M. R.; Howe, R. T.; Maboudian, R., *Journal of Microelectromechanical Systems* **1998,** *7*, 252-260.

13. Kaufmann, C. R.; Mani, G.; Marton, D.; Johnson, D. M.; Agrawal, C. M., *Biomedical Materials* **2010,** *5*, -.

14. Sackmann, E., *Science* **1996,** *271*, 43-48.

15. Bhushan, B.; Kulkarni, A. V.; Koinkar, V. N.; Boehm, M.; Odoni, L.; Martelet, C.; Belin, M., *Langmuir* **1995,** *11*, 3189-3198.

16. Bhushan, B.; Cichomski, M., *Journal of Vacuum Science & Technology A* **2007,** *25*, 1285-1293.

17. Sambasivan, S.; Hsieh, S.; Fischer, D. A.; Hsu, S. M., *Journal of Vacuum Science & Technology A* **2006,** *24*, 1484-1488.

18. Clear, S. C.; Nealey, P. F., *Journal of Chemical Physics* **2001,** *114*, 2802-2811.

19. Choi, J.; Morishita, H.; Kato, T., *Applied Surface Science* **2004,** *228*, 191-200.

20. Cione, A. M.; Mazyar, O. A.; Booth, B. D.; McCabe, C.; Jennings, G. K., *Journal of Physical Chemistry C* **2009,** *113*, 2384-2392.

21. Hu, Y. Z.; Granick, S., *Tribology Letters* **1998,** *5*, 81-88.

22. Gellman, A. J.; Spencer, N. D., *Proceedings of the Institution of Mechanical Engineers Part J-Journal of Engineering Tribology* **2002,** *216*, 443-461.

23. Singh, R. A.; Kim, J.; Yang, S. W.; Oh, J. E.; Yoon, E. S., *Wear* **2008,** *265*, 42-48.

24. Singh, R. A.; Yoon, E. S.; Han, H. G.; Kong, H., *Wear* **2007,** *262*, 130-137.

25. Hoffmann, H.; Mayer, U.; Krischanitz, A., *Langmuir* **1995,** *11*, 1304-1312.

26. Khatri, O. P.; Biswas, S. K., *Surface Science* **2006,** *600*, 4399-4404.

27. Vallant, T.; Kattner, J.; Brunner, H.; Mayer, U.; Hoffmann, H., *Langmuir* **1999,** *15*, 5339-5346.

28. Masuko, M.; Miyamoto, H.; Suzuki, A., *Tribology International* **2007,** *40*, 1587-1596.

29. Bierbaum, K.; Kinzler, M.; Woll, C.; Grunze, M.; Hahner, G.; Heid, S.; Effenberger, F., *Langmuir* **1995,** *11*, 512-518.

30. Genzer, J.; Efimenko, K.; Fischer, D. A., *Langmuir* **2002,** *18*, 9307-9311.

31. Xiao, X. D.; Hu, J.; Charych, D. H.; Salmeron, M., *Langmuir* **1996,** *12*, 235-237.

32. Booth, B. D.; Vilt, S. G.; McCabe, C.; Jennings, G. K., *Langmuir* **2009,** *25*, 9995-10001.

33. Song, S. Y.; Zhou, J. F.; Qu, M. N.; Yang, S. R.; Zhang, J. Y., *Langmuir* **2008,** *24*, 105-109.

34. Lee, S.; Heeb, R.; Venkataraman, N. V.; Spencer, N. D., *Tribology Letters* **2007,** *28*, 229-239.

35. Nakano, M.; Ishida, T.; Numata, T.; Ando, Y.; Sasaki, S., *Japanese Journal of Applied Physics Part 1-Regular Papers Short Notes & Review Papers* **2003,** *42*, 4734-4738.

36. Bhushan, B.; Kasai, T.; Kulik, G.; Barbieri, L.; Hoffmann, P., *Ultramicroscopy* **2005,** *105*, 176-188.

37. Vilt, S. G.; Leng, Z. W.; Booth, B. D.; McCabe, C.; Jennings, G. K., *Journal of Physical Chemistry C* **2009,** *113*, 14972-14977.

38. Clear, S. C.; Nealey, P. F., *Journal of Colloid and Interface Science* **1999,** *213*, 238-250.

39. Jorgensen, W. L.; Maxwell, D. S.; TiradoRives, J., *Journal of the American Chemical Society* **1996,** *118*, 11225-11236.

40. Lorenz, C. D.; Webb, E. B.; Stevens, M. J.; Chandross, M.; Grest, G. S., *Tribology Letters* **2005,** *19*, 93-99.

41. Padua, A. A. H., *Journal of Physical Chemistry A* **2002,** *106*, 10116-10123.

42. Mazyar, O. A.; Jennings, G. K.; McCabe, C., *Langmuir* **2009,** *25*, 5103-5110.

43. Plimpton, S., *Journal of Computational Physics* **1995,** *117*, 1-19.

44. Crozier, P. S.; Rowley, R. L.; Henderson, D., *Journal of Chemical Physics* **2001,** *114*, 7513-7517.

45. Shimizu, K.; Tariq, M.; Gomes, M. F. C.; Rebelo, L. P. N.; Lopes, J. N. C., *Journal of Physical Chemistry B* **2010,** *114*, 5831-5834.

46. Schreiber, F., *Progress in Surface Science* **2000,** *65*, 151-256.

47. Weinstein, R. D.; Moriarty, J.; Cushnie, E.; Colorado, R.; Lee, T. R.; Patel, M.; Alesi, W. R.; Jennings, G. K., *Journal of Physical Chemistry B* **2003,** *107*, 11626-11632.

48. Kim, H. I.; Graupe, M.; Oloba, O.; Koini, T.; Imaduddin, S.; Lee, T. R.; Perry, S. S., *Langmuir* **1999,** *15*, 3179-3185.

49. Lio, A.; Charych, D. H.; Salmeron, M., *Journal of Physical Chemistry B* **1997,** *101*, 3800-3805.

50. Israelachvili, J. N., *Intermolecular and Surface Forces*. 2nd ed.; Academic Press London: London, 1992.

51. Jennings, G. K.; Munro, J. C.; Yong, T. H.; Laibinis, P. E., *Langmuir* **1998,** *14*, 6130-6139.

52. Jennings, G. K.; Yong, T. H.; Munro, J. C.; Laibinis, P. E., *Journal of the American Chemical Society* **2003,** *125*, 2950-2957.

53. Bain, C. D.; Troughton, E. B.; Tao, Y. T.; Evall, J.; Whitesides, G. M.; Nuzzo, R. G., *Journal of the American Chemical Society* **1989,** *111*, 321-335.

54. Helmy, R.; Fadeev, A. Y., *Langmuir* **2002,** *18*, 8924-8928.

CHAPTER VI

TRIBOLOGICAL CHARACTERIZATION OF OCTADADECYL TRICHLOROSILANE GRADIENT MONOLAYER FILMS

Introduction

In many applications, the ability to control the surface energy of a substrate with a high degree of positional precision, such as creating surface energy gradients, is an essential requirement. The ability to achieve gradients in silane monolayer films was first demonstrated by Chaudhury and Whitesides,[1] and since then, many researchers have investigated gradient monolayer films. The potential application of these gradient monolayers ranges from biological detection and selective attachment[5, 7, 8, 10] to microfluidics[7] and chemical sensing.[6] The formation and characterization of gradient films has been reported in the literature[ref] and there have been several techniques that yield consistent gradients of one or two component monolayers using alkanthiolate[5, 6] or n-alkyl trichlorosilane precursors, depending upon the substrate.[3, 7] Groups have assembled gradient monolayers of thiolates on gold using diffusion through chromatography media,[6] ink –jet printing,[4] and solution assembly[8] approaches. Choi and Newby[7] have reported a contact printing procedure for octadecyl trichlorosilane that results in a surface of varying surface energy that is easily controlled by varying the physical contact of a PDMS stamp in the printing process. Wijesundara[9] used polyatomic fluorocarbon ion bombardment of a PMMA film to obtain surface energy gradients on a substrate. The Whitesides group[10, 11] has developed an elegant process utilizing laminar

flow in microfluidic channels to fabricate spatially and temporally stable gradient films from a wide variety of precursors including both alkanethiols and silanes.

The use of gradients to improve lubrication has focused in diamond-like coatings (DLC)[12, 13] particularly for the use in hard drives[14] and space applications.[15] The work with DLCs has focused on the ability of gradient layers to mediate the indentation or damage to a surface during the initial contact between two dissimilar materials[16, 17] and the reduction of adhesion during the processing of DLC layers.[14] Since silane based monolayer films have begun to emerge due to the rise in demand for more intricate MEMS device components,refs the implementation of monolayer gradients as a technique to alleviate stiction and adhesion during fabrication and operation is promising. Some of the first work using thin films for the reduction of friction utilized surfactants[18] and Langmuir-Blodgett monolayers[19] to demonstrate the promise of monolayers for lubrication. More robust attachment schemes were then characterized for frictional performance, namely alkanethiols on gold[20] and silanols on silicon[20, 21] that showed beneficial coefficients of friction and long-term wear properties. Chapter III focused on investigating the initial frictional behavior of dense monolayers prepared from n-alkanethiols on gold and n-alkyl trichlorosilanes on silicon. In addition the tribological performance of two component silane monolayer films using a microtribometer has been reported[22] and suggests that with the proper pairing of components, these systems can provide beneficial frictional properties. While one and two component silane monolayer films have been studied for lubrication applications,[20-23] gradient silane films have not been characterized in tribological testing. The ability to prepared precise, robust

gradients is an important aspect in the future technological development and application of MEMS technologies.

Here we report the formation and characterization of octadecyl trichlorosilane gradient monolayer films using a simple solution-based assembly method. We also report the tribological performance of gradient monolayer films with a microtribometer using a 4 mm stainless steel ball bearing as the probe for tests conducted over the length of the gradient subjected to a load of 98 mN at a speed of 0.1 or 1.0 mm/s. Friction tests were also performed cyclically to investigate the reproducibility of the film's performance. We believe this is the first detailed study into the frictional performance of silane gradient monolayer films using a microtribometer.

Experimental Section

Monolayer Preparation

Octadecyltrichlorosilane gradient monolayers. Octadecyl trichlorosilane monolayers were formed by immersing the 4.5 cm piranha-treated substrates into solutions of silane precursors in toluene. Assembly was carried out in a 20 mL vial that initially contained 0.5 mL of 0.5 mM octadecyl trichlorosilane in toluene so that only the bottom of the substrate was immersed (~0.3 cm). Toluene was added to the vial via a peristaltic pump at a rate of 1 mL/min for approximately 20 min using the setup as shown in Figure 6.1. The concentration and time allowed for assembly varied with respect to position on the substrate in order to obtain a gradient of surface energy along the sample. Samples were removed from solution immediately upon the solution fully immersing the sample, rinsed

in ~ 20 mL of toluene, then rinsed with deionized water and ethanol, and then dried in a stream of nitrogen. The characterization of densely packed monolayer prepared from octadecyl trichlorosilane similar to ones used in this study by contact angle analysis and ellipsometry was discussed in Chapter III and IV and values for these measurements are reported in Appendix A.

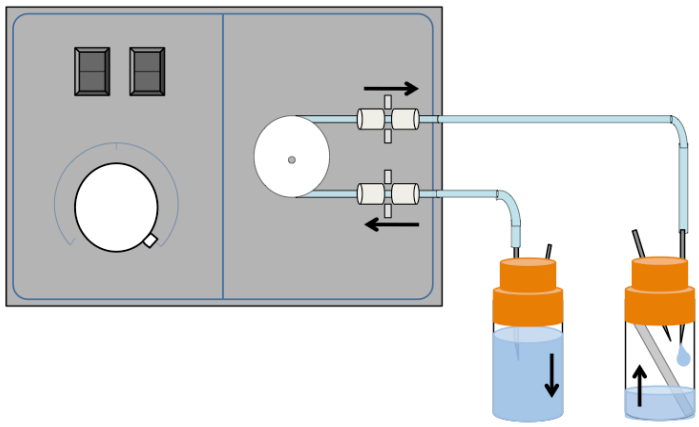

Figure 6.1. Schematic of silane gradient assembly setup where a peristaltic pump was used to add solvent at 1 mL/min to an initial starting solution of ~0.5 mL containing 0.5 mM $C_{18}SiCl_3$ precursor for assembly on a silicon substrate.

Microtribology

A Center for Tribology (CETR) UMT-2 Micro-Tribometer was used for all tribology experiments. The instrument was used for ball on flat surface sliding experiments with a 2-D DFM-0.5 force sensor. The DFM-0.5 sensor can apply loads ranging from 50 to 5,000 mN and measure with a resolution of 0.25 mN. Tests were performed with a stainless steel ball bearing as the probe tip attached to the sensor via a suspension-mounting cantilever where the size of the tip was selected according to the

magnitude of the applied load. The tip was sonicated in acetone for 5 min and dried with nitrogen before use. The DFM-0.5 sensor was operated with stainless steel balls of 4 mm diameters as the probe. The force that the tip applied to the surface was slowly ramped to the desired load and allowed to equilibrate at that load for at least 15 s before the surface was set into motion. Tests were performed at a sliding speed of 0.1 mm/s over a 10 mm track for surface energy tests and at a sliding speed of 0.1 mm/s over a track of 25 mm for probing of the gradient. Results represent measurements on an average of five samples each prepared independently unless otherwise noted as a representative data set.

Results and Discussion

Formation of Gradient Monolayers

In this study I investigated the formation and tribological properties of one-component gradient monolayers formed from an octadecyl trichlorosilane precursor on silicon. I used a unique deposition technique that provides a high degree of control while maintaining a simple design. Samples were placed in a vial with ~0.5 mL of 0.5 mM octadecyl trichlorosilane in toluene and capped with a rubber septum. Toluene was subsequently added dropwise at a rate of ~1 mL/min using a peristaltic pump as shown in Figure 6.1 until the entire sample was completely submerged in solution that typically requires ~20 min. Through this process of gradually increasing the level of precursor solution while simultaneously diluting the active trichlorosilane concentration, higher points on the vertically oriented sample are exposed to lower precursor concentrations for shorter periods of time. Thus, by adding solvent using a perstaltic pump during the

monolayer assembly process, we have varied the precursor concentration and substrate exposure time, thereby controlling the number of molecules that are adsorbed to the substrate dynamically.

Characterization of the films was performed using contact angle goniometry, ellipsometry, and microtribology. Water contact angles and ellipsometric thicknesses were taken at 5 mm increments across the sample to analyze the monolayer and confirm the formation of a gradient. Figure 6.2 shows the measured thickness of the substrate at various points in the assembly process and demonstrates a thickness of 2.5 nm at a relative distance ≤ 0.2 consistent with a densely packed $C_{18}SiCl_3$ monolayer. In the intermediate portion of the substrate (relative distance 0.2 to 0.8) the thickness decreases linearly until there is no measured thickness at high relative distances (≥ 0.8). In the intermediate region the decrease in number of silane molecules allows for conformational states other than the trans extended conformation from the surface and results in a decrease in measured thickness. At high relative distances where no thickness is measured, some molecules have assembled on the substrate to form a sparse film in a conformation that maximizes interactions and minimizes free energy by lying down to cover the substrate. There is potential for the octadecyl trichlorosilane precursor to assemble into islands on the substrate as reported for gradient alkanethiols on gold,[5] but, as described below, these gradient films do not form islands on the surface.

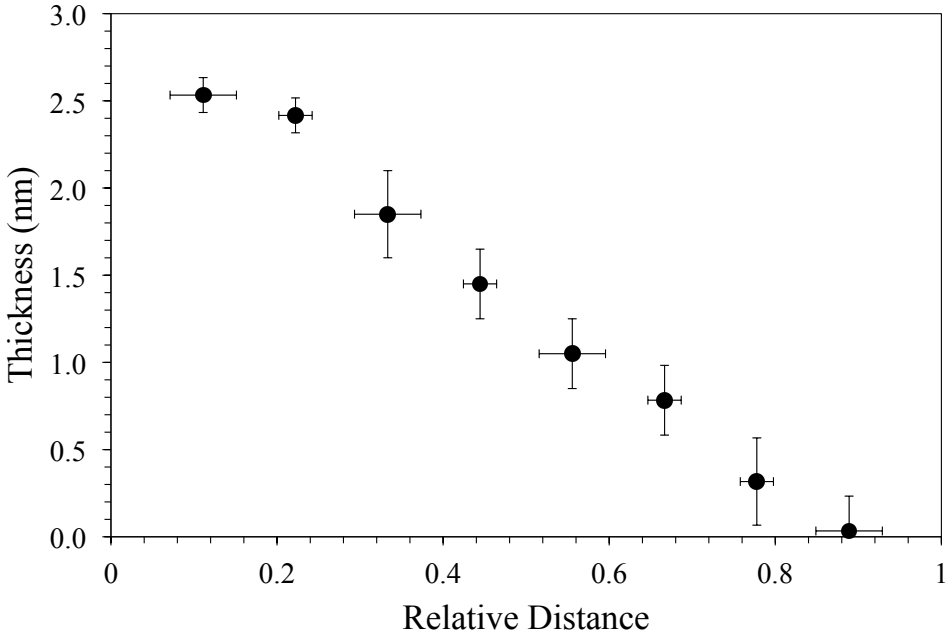

Figure 6.2. The observed dependence of ellipsometric thickness on the relative distance along the substrate demonstrating the formation of a gradient film.

Through water contact angle measurements shown in Figure 6.3, we demonstrate the hydrophobic and hydrophilic character of a gradient with an intermediate wetting region. The hydrophilic end of the substrate reaches a contact angle of ~45° that is similar to the value for a bare silicon substrate exposed to pure toluene solvent for the same time as the experiments, while the hydrophobic end has a value of 110° consistent with a well formed methyl-terminated monolayer.[24]

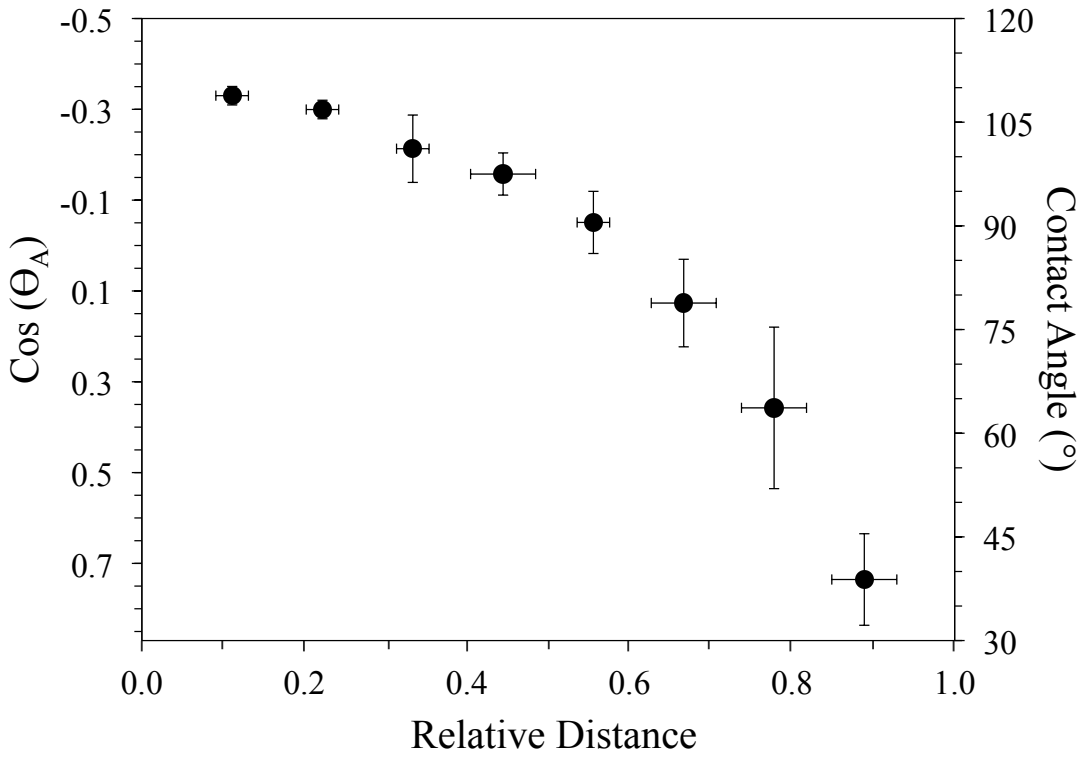

Figure 6.3. Water contact angle measured at relative distances along substrate showing the change in surface energy along the substrate resulting from gradient assembly process.

Two methods have been used to determine the area coverage of octadecyl trichlorosilane in the gradient monolayer. First, the equation proposed by Cassie[25] was used to estimate the area coverage based on advancing water contact angles of the silane precursor on the substrate using methyl terminated and control bare substrate contact angle measurements:

$$\cos\theta = \sigma_{Cassie}\cos\theta_1 + \left(1 - \sigma_{Cassie}\right)\cos\theta_2 \qquad (6\text{-}1)$$

where θ is the measured water contact angle on the gradient monolayer, σ_{Cassie} is the area coverage of octadecyl trichlorosilane, θ_1 is the water contact angle of a pure octadecyl trichlorosilane monolayer (113°), and θ_2 is the water contact angle of a bare substrate that has been exposed to solvent (40°). Next, the ratio of measured ellipsometric thickness (d) to the thickness of a dense octadecyl trichlorosilane monolayer (d_{pure}):

$$\sigma_{thickness} = \frac{d}{d_{pure}} \tag{6-2}$$

where $\sigma_{thickness}$ is the area coverage as determined by thicknesses and d_{pure} is 2.5 nm (Table A.1). Figure 6.4 shows correlation between $\sigma_{thickness}$ and σ_{Cassie}. If sparse regions exist as islands of silane molecules, we would expect these two coverages to agree. For the majority of the gradient film (relative distances of > 0.1 and < 0.9) the area coverage of bound octadecyl silane molecules as estimated by these two methods does not agree. The deviation between the two coverage calculations suggests that adsorbates in the intermediate region of the film adopt conformations where the chains are more canted as opposed to extending normal from the substrate. The higher cant of the bound molecules results in molecules occupying more space on the substrate to provide a greater hydrophobic footprint than the coverage as determined by ellipsometric thickness would suggest. Thus, the area coverage as determined from wetting tends to overestimate the number of molecules on the surface since Cassie's equation describes the behavior of a surface with discrete, segmented areas (CH_3 versus bare), and does not fully describe a gradual transition (CH_3, CH_2, bare) between states. This discrepancy indicates the

molecules do not form islands on the substrate but assemble into a film with a continuous gradient of surface energy.

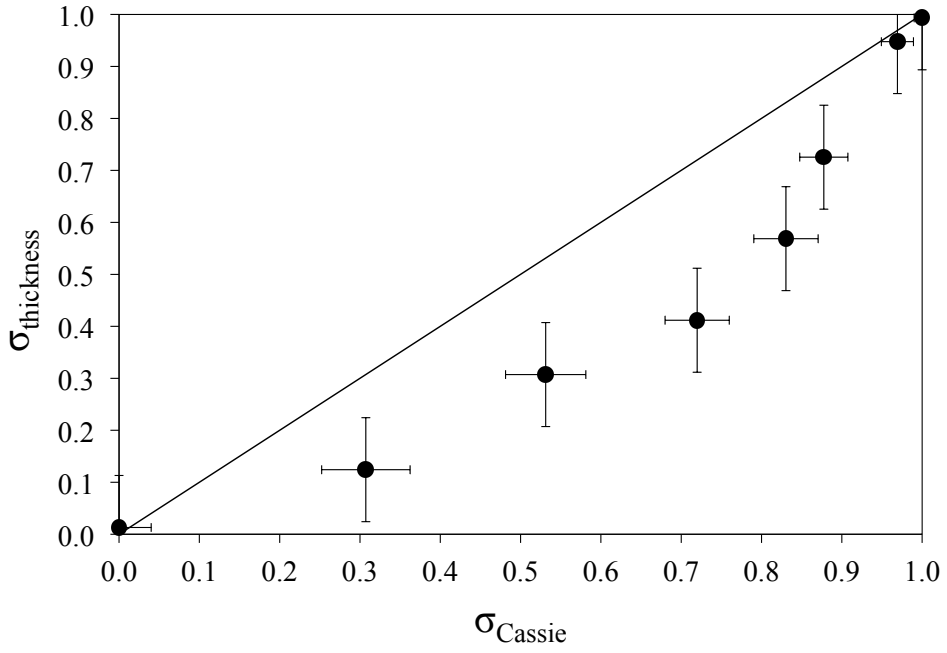

Figure 6.4. Comparision between coverage as determined by thickness versus contact angles and Eq. 6-1. Deviation between the two techniques indicates that molecules do no assemble into islands on the substrate.

The gradient monolayers prepared by our solution method demonstrate similar thicknesses and wetting behavior to previously reported silane gradient monolayers[1, 3, 7, 26] while being simple to perform, repeatable, and easily tuned. The loosely packed, sparse monolayer present at relative distances between 0.3 and 0.8 offers unique surface energies that have previously not been studied in tribological testing.

Tribology of Gradient Monolayers

Figure 6.5A shows the coefficient of friction of a one-component gradient monolayer of octadecyl trichlorosilane on silicon at specific relative distances that correspond to differing surface energies. The CH_3 rich portions of the substrate (relative distance < 0.3), as indicated by water contact angles and ellipsometric thicknesses (shown in Figures 6.2 and 6.3) display a COF of 0.08 that is consistent with the COF of a densely packed octadecyl trichlorosilane film.[23] When the conditions of assembly are manipulated to yield a film that is less dense and lacks necessary dispersive forces to provide a stable barrier to the tribological load, the coefficient of friction increases due to higher probe-substrate interactions. The methyl deficient end of the sample has a COF that is significantly higher than that of a well formed film, but due to the presence of a small number of chains on the surface, does not reach the value of a bare silicon substrate (0.6). This behavior is expected for one component gradient films since the COF is directly affected by the number of silane molecules on the surface. At relative distances > 0.7 where the coverage of molecules is well less than half a monolayer, the molecules minimize free energy by adopting a highly canted conformation to interact with other sparse molecules and even completely horizontal in some cases to interact with the substrate and thereby provide a thinner lubricating barrier. Figure 6.5B shows how the frictional performance of the gradient film compares with that of well formed monolayers assembled from precursors of a fixed length. At low relative distances, the films behave identically to a well formed $C_{18}SiCl_3$ monolayer due to the fact that in this regime a densely packed monolayer has formed. As we have shown in Chapter IV, a chain length of about 8 carbons (~1 nm) is required to provide a sufficiently cohesive monolayer that

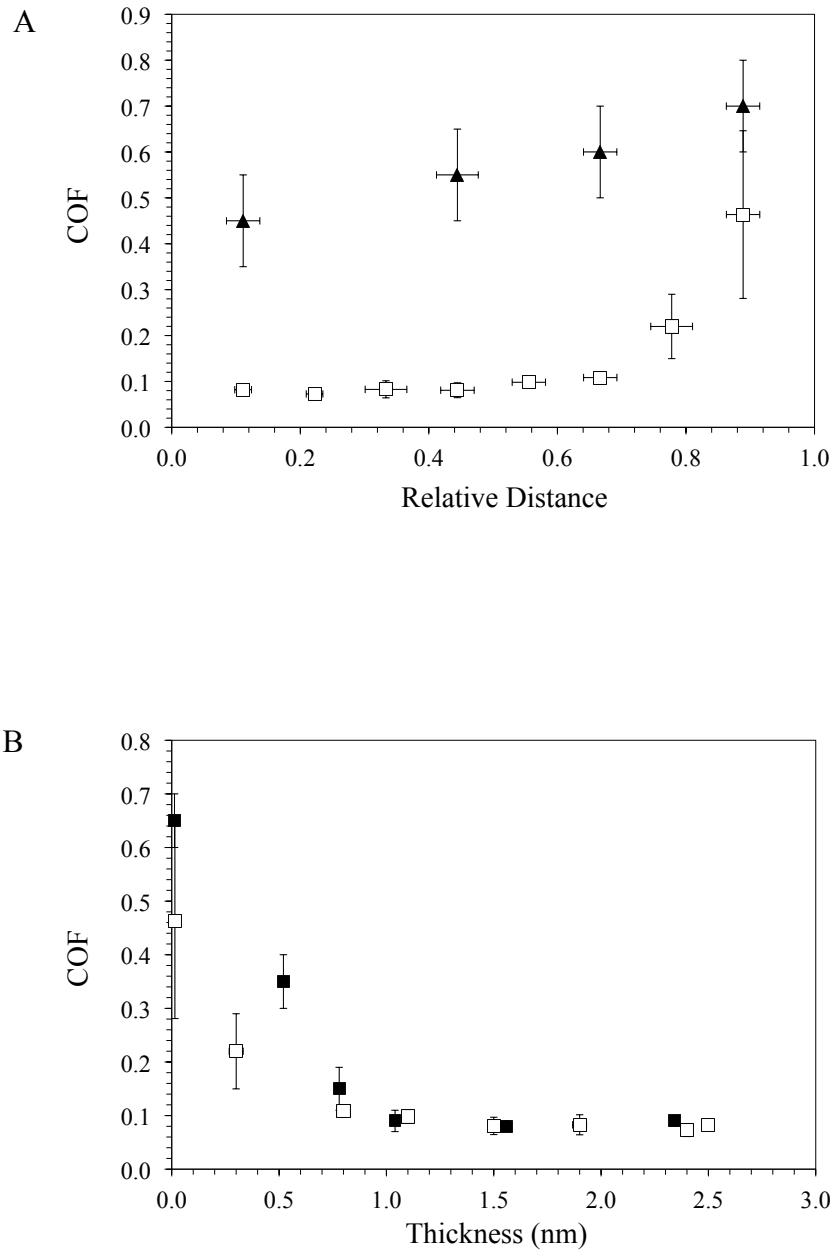

Figure 6.5. (A) Dependence of the coefficient of friction on the relative distance for gradient monolayers. Gradient monolayers are shown as open squares and control sample (not exposed to silane precursor) are shown as triangles. (B) Dependence of COF on thickness for gradient monolayer (open squares) and monolayers prepared from n-alkyl trichlorosilanes (n = 4, 6, 8, 12, 16, and 18) that are shown as closed squares.

prevents probe-substrate interactions to achieve low coefficients of friction at this load and speed.[23] The gradient monolayer behaves similarly, demonstrating the same plateau in COF at 0.08 for thicknesses > 1 nm that is observed for well formed monolayers with lengths ≥ 8 carbons. When the thickness of the film is less than 1 nm, which corresponds to a chain length of < 8 carbons, the lubricating performance of the monolayer begins to decrease, as the film is not robust enough to sustain the applied 98 mN tribological load. The first evidence of diminished performance is the rise in COF to a value of 0.12 at a thickness of 0.8 nm (corresponding to a relative distance of ~ 0.7) that is similar to the performance of a C_6SiCl_3 film that is known to assemble into a film that possess liquid like order not sufficient to withstand these frictional loads. Figure 6.5A also shows the control samples that were exposed to solvent without monolayer precursor and is consistent with the known COF of silicon (0.6) for the entire example except at high relative distances (> 0.8). This result suggests that the high energy bare substrate exposed to solvent is partially passivated by a very small number of physisorbed molecules resulting in a COF of 0.4 that is slightly lower than the known value of 0.6 for a bare silicon substrate.

In order to determine the repeatability of the tribological performance of gradient films, frictional tests were run for several cycles, and the results are shown in Figure 6.6. These tribology tests focus on the performance of the portion of the gradient film (relative distance between 0.2 and 0.7) that exhibits behavior different from the tribological results for dense octadecyl trichlorosilane monolayers described in Chapters IV and V. These tribology tests were performed to follow the surface energy of the gradient from low (relative distance of 0.7) to high (relative distance 0.2) and then retrace

the same path. The much steeper slope of the COF during the initial scan and at the beginning of the second scan demonstrates the probe is altering the film. Similarly, the peak between the first and second scans rises to a COF of 0.4 that is greater than at any other time during the wear test. We believe during the first scan the probe tip aligns or equilibrates the film, demonstrated by the different shape and higher COF values in the

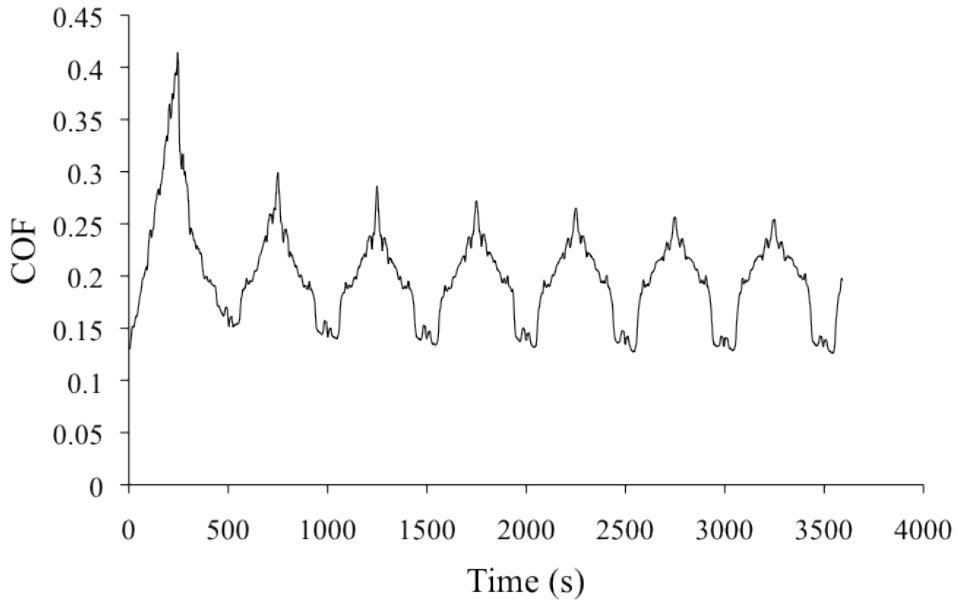

Figure 6.6. Cyclic tribological scans focusing on the sparse end of a gradient film (relative distance from 0.2 to 0.7) that demonstrates a broadening of monolayer deficient region by frictional testing.

initial tribological scan. The tribology passes following this initial equilibration exhibit more consistent behavior with a more regular sawtooth pattern for subsequent cycles. The portion of the gradient that has a higher surface energy due to fewer adsorbed molecules exhibits an increase in the coefficient of friction rising to a value of 0.3. Towards this sparsely populated end of the sample, the monolayer exhibits worse frictional performance as the barrier between the probe and substrate is diminished. As

discussed in Chapter V, the likely mechanism for tribological failure of silane monolayer films is the removal of individual molecules from the substrate. The broadening of the shoulder on each cycle is indicative of the rearrangement and possible removal of molecules from the substrate by the probe.

Conclusions

We have demonstrated a simple and effective approach to assemble gradient monolayer films of silane precursors onto a silicon substrate. Characterization of these gradient films by water contact angles and ellipsometric thicknesses confirm gradient formation with a high degree of repeatability. These results show that the tribological properties of gradient monolayer films prepared from octadecyl trichlorosilane on silicon are dependent upon the surface coverage and surface energy of the gradient monolayer. We have shown that the thickness of a low energy hydrocarbon monolayer is a critical aspect of the frictional response of the film by relating the tribological performance of gradient monolayers to that of monolayers with known thicknesses. Sparse monolayer regions are more prone to frictional failure by exposing more of the underlying substrate and further enabling the probe tip to impart the normal load to fewer adsorbed molecules to greatly increase the pressure per adsorbate. Further investigation as to the durability of silane monolayers and the mechanism for their failure is discussed in Chapter V.

References

1. Chaudhury, M. K.; Whitesides, G. M., *Science* **1992,** *256*, 1539-1541.

2. Sackmann, E., *Science* **1996,** *271*, 43-48.

3. Cai, Y. J.; Yun, Y. H.; Newby, B. M. Z., *Colloids and Surfaces B-Biointerfaces* **2010,** *75*, 115-122.

4. Sankhe, A. Y.; Booth, B. D.; Wiker, N. J.; Kilbey, S. M., *Langmuir* **2005,** *21*, 5332-5336.

5. Morgenthaler, S.; Lee, S. W.; Zurcher, S.; Spencer, N. D., *Langmuir* **2003,** *19*, 10459-10462.

6. Liedberg, B.; Tengvall, P., *Langmuir* **1995,** *11*, 3821-3827.

7. Choi, S. H.; Newby, B. M. Z., *Langmuir* **2003,** *19*, 7427-7435.

8. Morgenthaler, S. M.; Lee, S.; Spencer, N. D., *Langmuir* **2006,** *22*, 2706-2711.

9. Wijesundara, M. B. J.; Fuoco, E.; Hanley, L., *Langmuir* **2001,** *17*, 5721-5726.

10. Dertinger, S. K. W.; Chiu, D. T.; Jeon, N. L.; Whitesides, G. M., *Analytical Chemistry* **2001,** *73*, 1240-1246.

11. Jeon, N. L.; Dertinger, S. K. W.; Chiu, D. T.; Choi, I. S.; Stroock, A. D.; Whitesides, G. M., *Langmuir* **2000,** *16*, 8311-8316.

12. Enke, K.; Dimigen, H.; Hubsch, H., *Applied Physics Letters* **1980,** *36*, 291-292.

13. Erdemir, A.; Switala, M.; Wei, R.; Wilbur, P., *Surface & Coatings Technology* **1991,** *50*, 17-23.

14. Ueng, H. Y.; Guo, C. T., *Journal of Vacuum Science & Technology B* **2003,** *21*, 2540-2544.

15. Donnet, C.; Fontaine, J.; Le Mogne, T.; Belin, M.; Heau, C.; Terrat, J. P.; Vaux, F.; Pont, G., *Surface & Coatings Technology* **1999,** *120*, 548-554.

16. Liu, Y.; Meletis, E. I., *Surface & Coatings Technology* **2002,** *153*, 178-183.

17. Pauschitz, A.; Kvasnica, S.; Jisa, R.; Bernardi, J.; Koch, T.; Roy, M., *Diamond and Related Materials* **2008,** *17*, 2010-2018.

18. Yoshizawa, H.; Chen, Y. L.; Israelachvili, J., *Journal of Physical Chemistry* **1993,** *97*, 4128-4140.

19. Bhushan, B.; Kulkarni, A. V.; Koinkar, V. N.; Boehm, M.; Odoni, L.; Martelet, C.; Belin, M., *Langmuir* **1995,** *11*, 3189-3198.

20. Xiao, X. D.; Hu, J.; Charych, D. H.; Salmeron, M., *Langmuir* **1996,** *12*, 235-237.

21. Srinivasan, U.; Houston, M. R.; Howe, R. T.; Maboudian, R., *Journal of Microelectromechanical Systems* **1998,** *7*, 252-260.

22. Vilt, S. G.; Leng, Z. W.; Booth, B. D.; McCabe, C.; Jennings, G. K., *Journal of Physical Chemistry C* **2009,** *113*, 14972-14977.

23. Booth, B. D.; Vilt, S. G.; McCabe, C.; Jennings, G. K., *Langmuir* **2009,** *25*, 9995-10001.

24. Wang, M.; Liechti, K. M.; Wang, Q.; White, J. M., *Langmuir* **2005,** *21*, 1848-1857.

25. Cassie, A. B. D., *Discussions of the Faraday Society* **1948,** *3*, 11-16.

26. Bierbaum, K.; Grunze, M.; Baski, A. A.; Chi, L. F.; Schrepp, W.; Fuchs, H., *Langmuir* **1995,** *11*, 2143-2150.

CHAPTER VII

DEPOSITION AND WETTABILITY OF IONIC LIQUIDS AS A MOBILE PHASE FOR TRIBOLOGICAL APPLICATIONS

Introduction

Room temperature ionic liquids (ILs) typically contain a bulky, asymmetric organic cation that inhibits crystalline packing and results in low melting temperatures.[1] ILs can exhibit other significant properties including negligibly low vapor pressure, non-combustibility, and a broad range of electrochemical stability.[2] ILs are uniquely flexible chemicals in that their properties can be tuned by varying the cation or anion. Thus, by altering the structure of the ions or choosing different cation-anion combinations, an ionic liquid with desirable properties for a specific application can be designed or selected. Because of their useful properties and tunability, ILs have found many applications including as nonvolatile solvents,[3] electrolytes,[4] chromatographic stationary phases,[5] and lubricants.[6-8] In addition to lubrication, the versatility and unique properties of ILs make them good candidates for many applications that involve interactions of liquids with surfaces. For these applications to be realized, efficient methods of depositing thin films of ILs must be developed.

In this work, we investigate the deposition and spreading of 1-butyl-3-methylimidazolium triflate ([bmim][triflate]), 1-butyl-3-methylimidazolium hexafluorophosphate ([bmim][PF_6]), and 1-hexyl-3-methylimidazolium triflate ([hmim][triflate]) on surfaces generated by the assembly of thiol- and silane-based

monolayers on gold and silicon, respectively. Imidazolium-based ILs are the most commonly studied IL system to date because of their air and moisture stability.[2, 9] While the bulk-phase viscosity of ILs can be comparable to traditional hydrocarbon lubricants, ILs have been shown to exhibit superior anti-wear and friction-reducing properties in lubrication settings.[10-12] In particular, ILs with the 1-alkyl-3-methylimidazolium cation and either the BF_4 or PF_6 anion have proven to be effective lubricants in many studies;[7, 8, 13-15] however, these anions can hydrolyze upon exposure to water. More recently, Jimenez et al.[15] have shown that the triflate anion, CF_3SO_3, has even better wear-reducing properties than BF_4 or PF_6 and that cations with longer side chains ($n > 2$) improve wear properties even more than changing the anion. In the selection of ionic liquids for this study, several factors were considered including tribological benefit, ease of preparation,[3] as well as viscosity and surface tension.[5]

Gao and McCarthy[16] have reported the wettability of four different ILs with surface tensions ranging from 49 – 66 mN/m on various hydrophobic and superhydrophobic surfaces. They noted the complexity of contact angle analysis with ILs since either ion of the probe liquid can interact with the surface. For the ultralow energy surfaces, the contact angles of the ILs were often indistinguishable from those of water. For a typical smooth polymer, the contact angles of the ILs were lower than that of water, owing to their lower surface tensions. In this work, we use contact angle goniometry to measure the wettability of [bmim][triflate] on several surfaces, ranging from low energy to high energy, prepared by the assembly of normal and ω-terminated alkyl thiols on gold and trichlorosilanes on silicon (oxide) and determine a critical surface energy using monolayers of mixed functionality. Finally, we address the issues regarding spreading of

IL films drop cast on high energy surfaces and several techniques to improve continuous IL film formation.

Experimental Section

[bmim][triflate] Preparation.

The procedure for the synthesis of [bmim][triflate], was adapted from a procedure reported by Bonhote et al.[17] Under nitrogen atmosphere, ~120 mL of anhydrous dichloromethane was added to 50 g of methyl triflate (0.3 mol) to prepare a ~2.5 M solution. This methyl triflate solution was added dropwise to 42 mL (~0.3 mol, or 38 g) of 1-butylimidazole under a nitrogen atmosphere and stirred vigorously in an ice bath. Solvent was removed by placement of the single phase liquid on a rotary evaporator followed by placement of the liquid on the vacuum line overnight. The final product was stored under nitrogen atmosphere and characterized using ^{1}H NMR analysis, which revealed no water in the final product. ^{1}H NMR (400 MHz, $CDCl_3$): δ 0.916 (3H), 1.30 (2H), 1.83 (2H), 3.93 (3H), 4.16 (2H), 7.38 (2H), 9.03 (1H).

Ionic liquid drop casting.

Solutions of an ionic liquid in solvent were prepared in various concentrations (0.1-5% (v/v)) for drop casting based on the desired thickness of the resulting film. In order to prepare films of [bmim][PF_6] of ~25 and ~150 nm, solutions of 0.1% (v/v) and 1.0% (v/v) in acetone, ethanol, or 2-propanol were used. A 20 μL amount of the appropriate solution was placed on a silicon surface that had been treated with piranha solution

immediately prior to IL deposition, and then IL-coated silicon sample was placed in a vacuum chamber with a pressure of ~30 mTorr. The chamber was sealed and left under vacuum until the solvent was fully evaporated. Removal of the samples was accomplished by slowly filling the chamber with a stream of nitrogen. Samples were then placed in a vacuum oven for 1 h at 150°C and subsequently allowed to cool before characterization.

XPS

XPS was performed using a Physical Electronics (PHI) 5000 VersaProbe. Monochromatic Al Kα x-rays (1486.6 eV) were used. Photoelectrons were collected into a spherical capacitor analyzer in constant pass energy mode and a take-off angle of 45 degrees to sample normal. Analysis was performed with a 200 μm diameter, 44.1 W x-ray spot. Electrons neutralization was done with 1.1 eV electrons, and the Ar^+ ion neutralization was done with 10 eV Ar. Linearity was calibrated to the $Ag3d^5/_2$ peak at 368.28 eV. The work function was adjusted such that the $Au4f^7/_2$ and $Cu2p^3/_2$ peaks were separated by 848.6 eV, at 84.05 and 932.65 eV respectively. Data reduction was done in CasaXPS and PHI Multipak.

Time dependent analysis was performed and charging time will refer to the amount of time between XPS analysis under various conditions. XPS scans consisted of high resolution scans were taken of F1s, C1s, N1s, Si2p, and O1s. The regions were scanned for 1 cycle, and the cycle took 2.5 minutes to complete. Analysis of the freshly piranha cleaned substrate revealed less than 3 atomic percent carbon present.

Results and Discussion

Wettability of [bmim][triflate] on Monolayer Films

To investigate the wetting properties of monolayers formed on gold or silicon, the advancing and receding contact angles of water, hexadecane, dicyclohexyl, and [bmim][triflate] were measured and are reported in Table 7.1. Monolayers of varying surface functionality were assembled onto gold from alkanethiolate precursors ($CH_3(CH_2)_{n-1}SH$ where n = 8, 12, 18) and 11-mercapto-1-undecanol ($HO(CH_2)_{11}SH$)) and on silicon using n-alkyl trichlorosilanes ($CH_3(CH_2)_{n-1}SiCl_3$ where n = 8, 12, 18), (tridecafluoro-1,1,2,2-tetrahydrooctyl)-1-trichlorosilane ($F_3C(CF_2)_5(CH_2)_2SiCl_3$), and 7-octenyltrichlorosilane ($H_2C=CH(CH_2)_6SiCl_3$), both before and after hydroboration/oxidation. Water, hexadecane (HD), and dicylohexyl (DCH) were selected as probe liquids due to their widespread use in other studies[18] and to compare with values obtained from [bmim][triflate]. Hexadecane (γ = 27 mN/m) and dicyclohexyl (γ = 33 mN/m)[18,19] are both dispersive liquids although the surface tension of DCH is comparable to that of [bmim][triflate] (γ = 34 mN/m) while water has strong hydrogen bonding and a significantly higher surface tension (γ = 72 mN/m) than the other liquids studied.

The large variation in contact angles reflects the composition of the chain termini and indicates that these adsorbates assemble to form oriented monolayers that effectively alter the surface properties of the substrate. The highest surface energy was achieved using a hydroxyl-terminated precursor, while the lowest surface energy was achieved

using a CF_3-terminated precursor. Methyl-terminated surfaces also yielded hydrophobic and oleophobic surfaces with low surface energies to typically yield water contact angles

Table 7.1. Contact Angles (Advancing, Receding) for SAMs on Au and Si

Adsorbate/Substrate	θ_{H2O}[a] (°)	θ_{HD}[b] (°)	θ_{DCH}[a] (°)	θ_{IL}[a] (°)
$C_{18}SH/Au$	112, 102	49, 40	56, 45	69, 64
$C_{12}SH/Au$	109, 96	46, 30	54, 44	64, 60
C_8SH/Au	106, 98	43, 32	47, 38	66, 58
$HOC_{11}SH/Au$	28, 19	<15	20	17
$C_{18}SiCl_3/SiO_2$	110, 103	44, 40	49, 44	69,65
$C_{12}SiCl_3/SiO_2$	110, 103	37, 32	45, 40	72, 64
C_8SiCl_3/SiO_2	109, 100	32, 26	38, 31	67, 56
$F_3C(CF_2)_5(CH_2)_2SiCl_3/SiO_2$	120, 195[c]	80, 61[d]	81, 57	91, 57
$H_2C{=}C_5H_9SiCl_3/SiO_2$	96, 84[c]	<15[d]	<15	50, 33
(HB-O) $HO\text{-}C_6H_9SiCl_3/SiO_2$	32, 18	<15[d]	<15	19

Standard deviation = a) ± 4; b) ± 1, c) ± 10; d) ± 5;

of 109-114°[20] and hexadecane contact angles of ~45° - 50°;[21] thus, the advancing water and hexadecane contact angles on monolayers formed from n-alkanethiols in Table 7.1 are indicative of dense methyl surfaces. The hexadecane contact angles on n-alkyl trichlorosilane monolayers are lower than those on n-alkanethiolate monolayers suggesting that the n-alkanethiolate monolayers formed on Au exhibit a more homogeneous methyl surface than the monolayers formed from n-alkyl trichlorosilanes on silicon. Contact angles with DCH support this assertion as the methyl-terminated SAMs on gold exhibit advancing DCH contact angles that are 7 - 9° greater than those

for methyl-terminated monolayers on silicon. The surface exposed to a precursor solution of $H_2C=C_5H_9SiCl_3$ exhibits wetting properties expected from a vinyl-terminated monolayer; it is hydrophobic ($\theta_{H2O} > 90°$), though its water contact angle is lower than that of a methyl-terminated monolayer, and it is wet by HD and DCH because the surface is composed of methylene groups that are abundant in these liquids. After undergoing a hydroboration-oxidation (HB-O) reaction, we estimate from the Cassie equation (Eq 7-1) that approximately 90% of the vinyl termini are converted to hydroxyl termini, resulting in a much lower water contact angle.

Since the surface tension of [bmim] [triflate] (34 mN/m) is similar to that of DCH (33 mN/m), one might expect the contact angles of the IL to be similar to those of DCH. However, [bmim][triflate] contact angles are ~10° higher than those of DCH on methyl-terminated alkanethiolate SAMs and 20 - 30° higher than those of DCH on methyl-terminated silane monolayers. Further, the IL shows no trend with chain length for either methyl-terminated system, unlike DCH and HD. As the HD and DCH contact angles fall significantly for thinner n-alkyl silane SAMs, the IL contact angle remains high. The decrease in HD and DCH contact angles for these surfaces is attributed to a greater extent of structural defects within the methyl-terminated monolayer that expose oleophilic methylene groups as the chain length is reduced. This absence of a trend in the [bmim][triflate] contact angle suggests that this IL is less sensitive to these defects and is consistent with its presumed weak interaction with both methyl and methylene groups. Whereas the hexadecane contact angle changes from ~55° on a dense methyl surface to <15° on a vinyl- (CH_2) terminated surface, indicating extreme sensitivity to these functional groups, the IL contact angle decreases only from 69° to 50° for the same

monolayers. The weaker sensitivity to slight changes in hydrophobic functional groups for [bmim][triflate] is more closely related to that of water and may reflect the strong electrostatic interactions between ions in the IL. Higher energy surfaces (-OH) can effectively compete for interactions with the ions of the IL, and as shown in Table 7.1, the values of [bmim][trifate] and DCH contact angles are similar for these surfaces. In general, the higher energy surfaces are wet more effectively by all liquids, and thus, the variation between the three probe liquids is compressed.

Wettability of [bmim][triflate] on Mixed Monolayers on Gold and Silicon

In order to determine the critical surface energy required for the spreading of ionic liquids on a surface, [bmim][triflate] was selected as a representative probe fluid for contact angle analysis. The advancing water contact angle of each sample was measured to estimate the fractional surface coverage of the monolayer from the equation proposed by Cassie,[22]

$$\cos(\theta_{mixed}) = \sigma_1 \cos(\theta_1) + \sigma_2 \cos(\theta_2) \qquad (7\text{-}1)$$

where θ_{mixed} is the water contact angle on the mixed monolayer, σ_1 is the fractional coverage of methyl monolayer, σ_2 is the fractional coverage of hydroxyl monolayer, θ_1 is the water contact angle of pure methyl monolayer (110°), and θ_2 is the water contact angle of pure hydroxyl monolayer (10°). For mixed thiolate based monolayers, precursor solutions of n-dodecanethiol ($C_{12}SH$) with varying proportions of 11-mercapto-1-undecanol ($HOC_{11}SH$) were prepared such that each mixture had a total thiol

concentration of 1 mM. Initially, mixtures of 60%, 80%, and 100% (molar) $HOC_{11}SH$ were prepared from stock solutions of $C_{12}SH$ and $HOC_{11}SH$ followed by the preparation of 65%, 70%, 75%, and 90% (molar) mixtures of $HOC_{11}SH$ from new stock solutions. Contact angle analysis was performed immediately upon removing samples from solution and rinsing with water and drying in a stream of nitrogen and is shown in Figure 7.1.

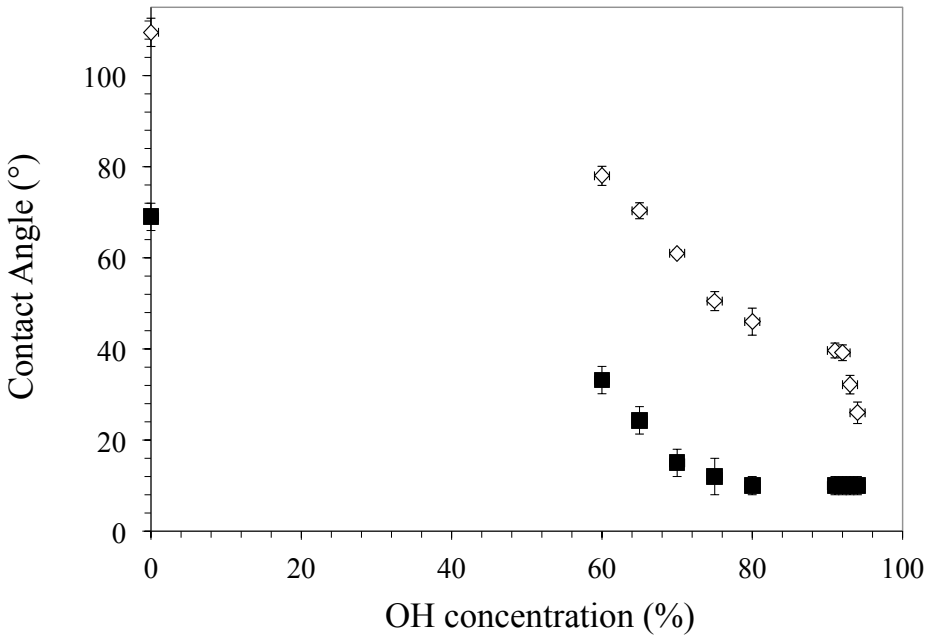

Figure 7.1. Contact angles of water (shown as open diamonds) and [bmim][triflate] (shown as closed squares) on mixed monolayers of dodecanethiol and 11-mercaptoundecanol to determine the surface energy required to obtain complete wetting of [bmim][triflate].

Figure 7.2 shows optical microscopy images of [bmim][triflate] films that were cast onto monolayers prepared from $C_{12}SH/HOC_{11}SH$ mixtures on gold. Ethanol was selected as the solvent for ILs due to its polarity to aid in solvating the IL and due to its

low surface tension of 22 mN/m,[23] which should aid in spreading. Spreading of the IL drop solution (IL + solvent) did not occur on surfaces with a fractional $C_{12}SH$ coverage

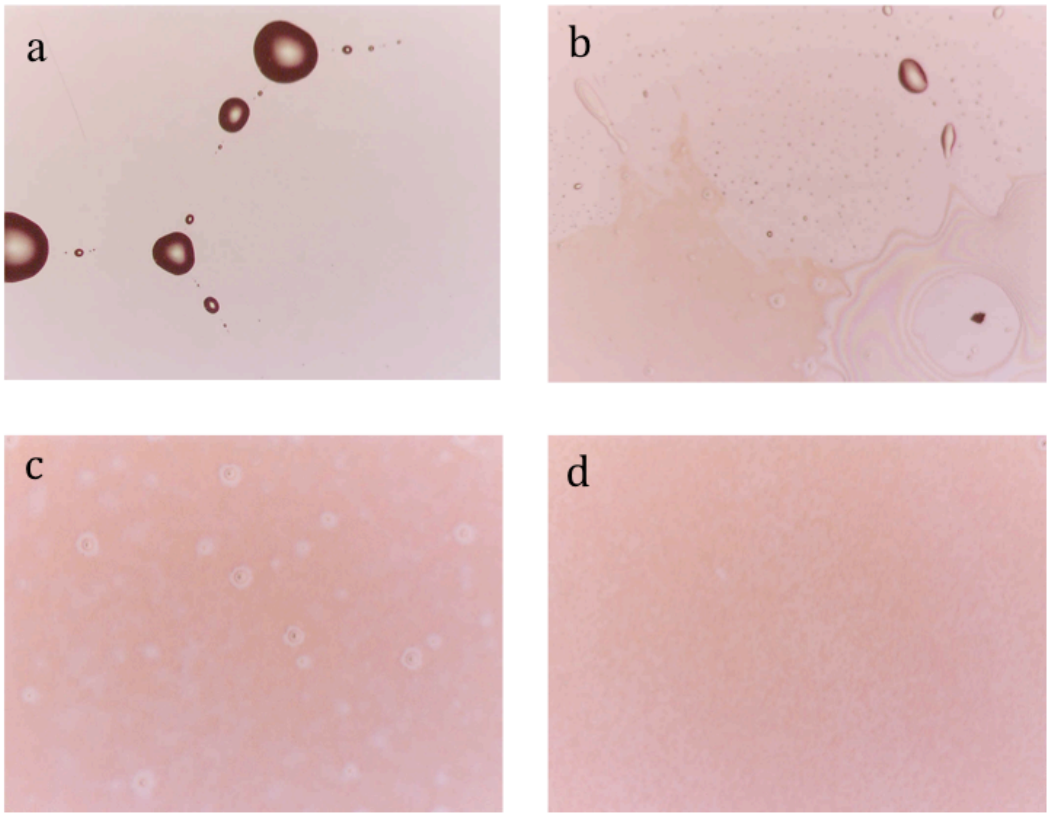

Figure 7.2. Optical images (10x) of IL films on mixed monolayers of methyl- and hydroxyl- terminated alkanethiols on gold. Hydroxyl surface concentration of a) 20%, b) 60%, c) 80%, d) 85%. Data are from multiple experiments. The images shown here depict the most prevalent region in the specified film.

of greater than 75%. Under vacuum, the IL/ethanol drop shrunk into a smaller drop of IL as the ethanol evaporated. In order to form an IL film on the surface, the drop solution must spread across the surface, and upon evaporation, the IL should remain as a film on the surface, as depicted in Figure 7.3. Thus, by Eqs 7-2 and 7-3, the surface tension of the solution (IL and ethanol) must be low enough for spreading to occur, and the surface energy of the substrate must be high enough to prevent the IL from coalescing into small droplets or a large droplet upon solvent evaporation. However, two different wetting regimes were observed for monolayers in which the solution wet the surface. For monolayers between 30% and 75% $C_{12}SH$, the IL coalesced into tiny droplets scattered across the surface rather than spreading out into a film due to the higher surface tension of the IL as compared to the IL drop solution (IL + solvent) after the solvent was evaporated. Thus, the surface energies of these two regimes ($C_{12}SH$ concentration >

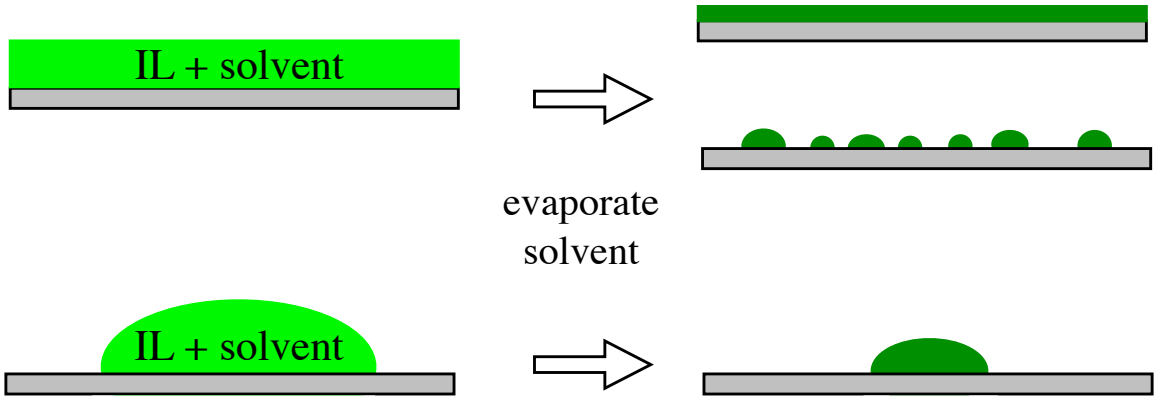

Figure 7.3. Behavior of IL when drop casting to a substrate. The morphology of the ionic liquid film after solvent evaporation is dependent upon both the initial solution coverage and the energetics of wetting (surface energy of the substrate and surface tension of the IL).

30%) are too low to yield a homogenous IL film of [bmim][triflate]. However, below this critical concentration of 30% the [bmim][triflate] demonstrated wetting of the surface and formed the desired uniform film. Therefore, the critical fractional $C_{12}SH$ coverage in a monolayer, below which the monolayer could be coated by an IL thin film, was 30%, which corresponds to a water contact angle of ~60° and an IL contact angle of 20°(+/-3°) as shown in Figure 7.1.

To determine if this critical surface condition translated to silicon substrates, we prepared variations in surface energy on silicon substrates by assembling mixed vinyl/methyl-terminated silane monolayers and oxidizing the vinyl groups of the monolayer via the hydroboration-oxidation reaction. Upon drop casting and removing solvent, the IL beaded up into distinct droplets on the samples with IL contact angles greater than 30°, as shown in Figure 7.4a. The sample with 60% hydroxyl concentration (Figure 7.4b) showed a transition state in film formation as [bmim][triflate] neither beaded up nor formed a continuous film. To the unaided eye, the surface appeared to have a continuous film, but microscope images showed that it consisted of tiny, closely-spaced but disconnected islands of IL. Because the IL formed closely spaced islands rather than droplets, this surface must be close to the target surface energy at which a continuous film begins to form. Indeed, a more continuous film was formed on the surface with a hydroxyl concentration of 70% (Figure 7.4c) and a continuous film was formed on the surface with a hydroxyl concentration of 80% (Figure 7.4d). Similar to the results from IL deposition on thiolate SAM gold substrates, surfaces below a critical IL contact angle of 20° support a sufficient IL coating by drop casting from ethanol at the reported concentration.

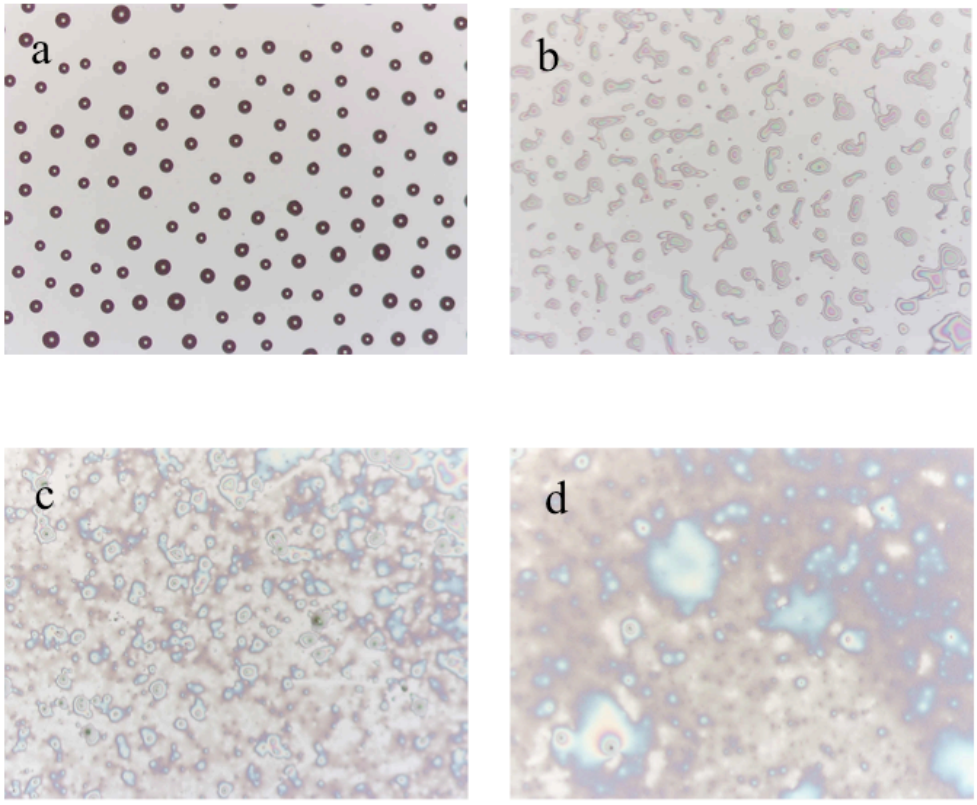

Figure 7.4. Optical microscopy images at 10x of [bmim][triflate] drop cast films onto monolayers with differing surface energies. IL films where concentration of hydroxyl monolayer is: (a) 60%, (b) 70%, (c) 80%, (d) 90%.

Molecular Simulations

Analysis of the droplet structure from molecular simulation of [bmim] [triflate] on CH_3- and OH-terminated SAMs provides support for the experimental observations. As shown in Figure 2, in both drops, the butyl chains on the cations point outwards, while the imidazolium rings tend to be shielded within the surface of the drop. Similarly, a strong orientation effect is evident for anions located in the outer shells of both drops. As shown in Figure 7.5 the SO_3 groups of the anions are directed toward the center of the

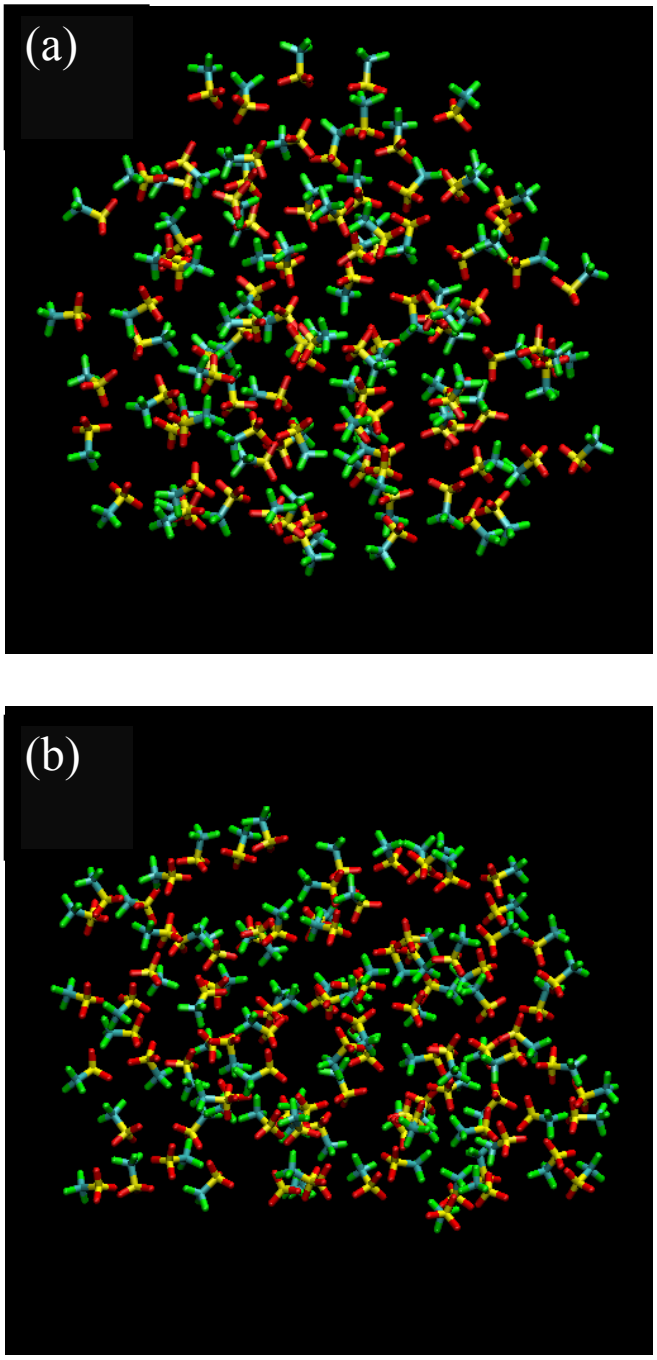

Figure 7.5. Snapshots showing the orientation of triflate anions within the [bmim][triflate] droplet on (a) CH_3-terminated and (b) OH-terminated monolayer surfaces on silica.

drop with the corresponding CF_3 groups pointing outwards. However, in the region of contact with the OH-terminated SAM surface the anions appear more randomly distributed (see the IL-SAM interface shown in Figure 7.5b). Similar preferred orientation of the cations and anions was observed in simulations of the vapor-phase of [bmim][triflate] clusters containing up to 30 ion pairs[24] and is likely due to the charge distribution in these ions, i.e., the positive charge of the bmim cation is concentrated on the methyl-imidazolium group[25] and the negative charge of the triflate anion is concentrated on the SO_3 group.[26] In the outer shell, these ions can move and assume the orientation in which their fragments with the higher charge density are directed toward the center of the IL drop. The observed orientation of the triflate anions in the radial direction with the SO_3 groups pointing towards the center of the drop in the outer shells of the IL may induce greater structuring in ultrathin IL films.

Cation/anion Variation in Ionic Liquids

In order to determine how different ion pairs of an IL affect spreading on a substrate, 1-hexyl-3-methylimidazolium trifluoromethanesulfonate ([hmim][triflate]) and 1-butyl-3-methylimidazolium hexafluorophosphate ([bmim][PF_6]) were cast into films on a bare substrate and analyzed with optical microscopy. The surface tension of [hmim][triflate] (30 mN/m) is lower than that of [bmim][triflate] due to the longer alkyl side chain on the imidazolium ring that helps dissociate the ion pair because of the greater interaction among alkyl chains[27] and [bmim][PF_6] has a higher surface tension (45 mN/m) but has shown more promise in lubrication applications.[7, 8, 13-15] The same solutions of IL (0.1%(v/v) in ethanol) were used for deposition onto high energy

substrates. In order to further promote spreading on the surface, a post deposition heat treatment at 150°C for 1 h was evaluated to determine if such a treatment would enable the formation of a homologous thin film instead of the droplet formation demonstrated to be effective in previous studies. It was observed that for non-heated films of [bmim][PF_6] (Figure 7.6a) and [hmim][triflate] (Figure 7.6c) that the IL formed droplets on the substrate similar to that demonstrated by [bmim][triflate] on low energy surfaces (Figure 7.4a). Since [bmim][PF_6] has a higher surface tension than the other ILs previously tested, a homologous film was not expected to form by drop casting this IL from solution. The drop casting solution completely wets the substrate, but upon removal of solvent the [bmim][PF_6] forms droplets along the surface as shown in Figure 7.6a. The [hmim][triflate] exhibited better spreading in forming a morphology that, while not continuous, does optically appear to be on the verge of forming a homogeneous film. While the heat treatment did successfully lower the surface tension of the IL so that limited spreading occurred along the substrate as shown in Figure 7.6b and 7.6d, once the IL cooled to room temperature, both the [bmim][PF_6] and [hmim][triflate] films reverted into droplets on the surface.

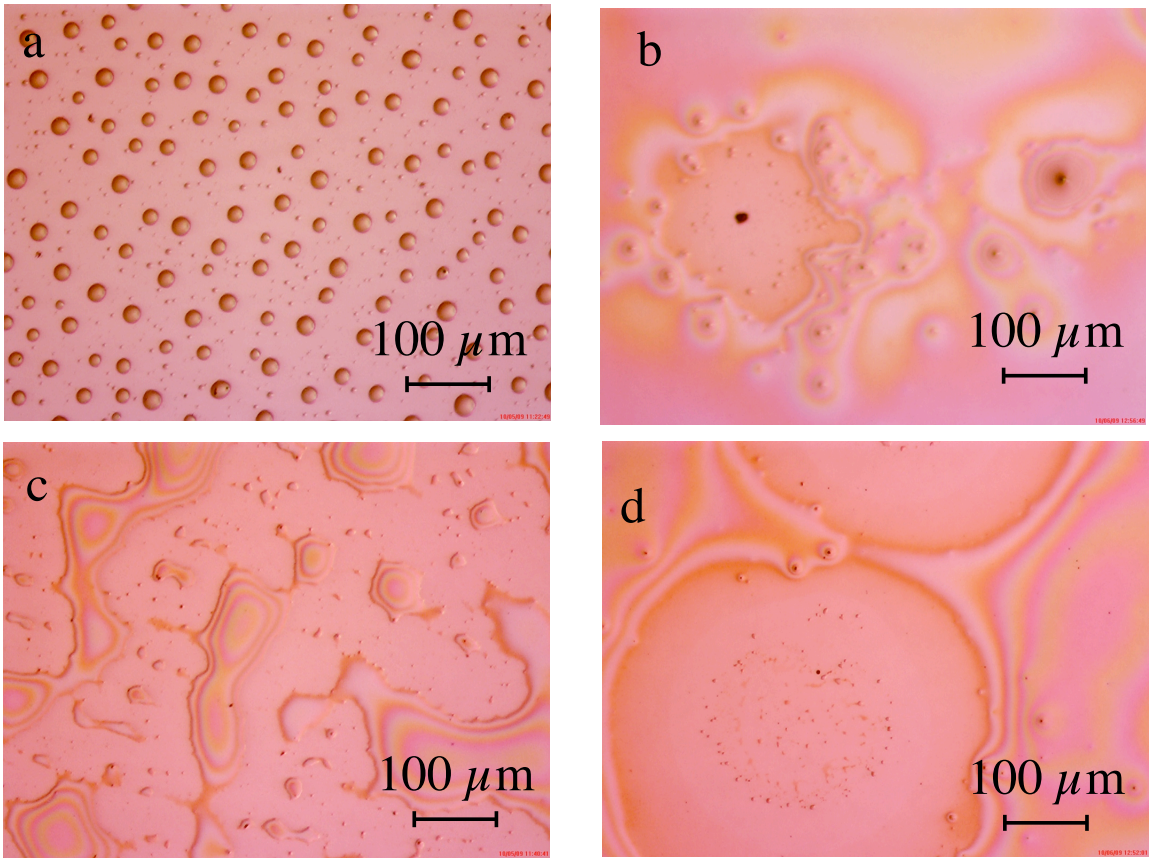

Figure 7.6. Optical microscopy images (10x) of drop casted films of [bmim][PF_6] and [hmim][triflate]. Samples were heat treated post-deposition to 150°C for 1 h and images were obtained immediately deposition before heating (a and c), and after the sample was heated to 150°C for 1 h (b and d).

XPS Modification of ILs

In order to help determine the structure of the droplet films formed from [bmim][PF_6], angle resolved x-ray photoelectron spectroscopy (ARXPS) was performed on ~150 nm films. IL films were drop cast onto bare, piranha-treated silicon substrates that possess the highest surface energy that can be fabricated in the laboratory. These IL films were heated post deposition to promote spreading of the IL on the substrate before XPS analysis. In the course of these ARXPS experiments, interesting charging effects from the XPS analysis were observed. The IL films that were exposed to XPS analysis

demonstrated a decrease in the intensity of both silicon and oxygen with an increase in nitrogen and fluorine intensity (Figure 7.7) indicative of the IL film becoming more homogeneous which was confirmed by optical microscopy (Figure 7.8). In order to further investigate the exact conditions that resulted in the morphological change of the IL films, experiments focusing on the species used in XPS analysis (electrons and Ar^+ used for charge neutralization in addition to x-rays) were performed. These experiments revealed that the charge neutralization during XPS analysis drives the change in morphology of the IL film. We believe that the bombardment of ionic liquid

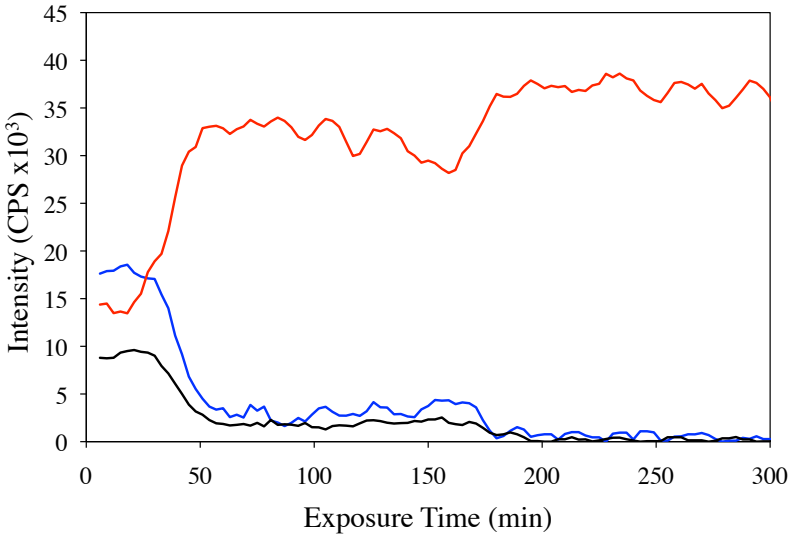

Figure 7.7. Intensity of selected elements: silicon (blue), oxygen (black), and fluorine (red) that indicate conformational changes within IL films during XPS analysis. The decrease in silicon and oxygen intensities from the substrate combined with the increase in fluorine intensity (and decrease in nitrogen intensity, not shown) demonstrates the alteration of droplets to a film that more uniformly covers the substrate.

microdroplets with the charged species during XPS disrupts the surface tension of these droplets and ion pairing between molecules to help promote spreading along the surface. The proposed mechanism for changes within the film involves charged XPS species providing additional electrostatic interactions that disrupt the cation-anion pairs in the liquid and impart more energy to the liquid aiding in the spreading of the IL across the substrate. The process of morphological changes to the IL film occurs slowly (~1 h of XPS exposure time) as the ions in each droplet interact with the XPS species. The literature is divided on which ion preferentially migrates to the liquid-air interface (PF_6[28] or butyl side chain[29-31]) in the bulk phase with no investigations into the structure of IL thin films (< 1 m). The role of XPS in altering film morphology makes it an unreliable technique to investigate which ion may dominate the interface. Also, at this time, it is unclear the role that each individual species used in XPS plays in changing the morphology but is an important detail to improve the method of obtaining a homogenous film as well as insight into the mechanism that causes these morphology changes.

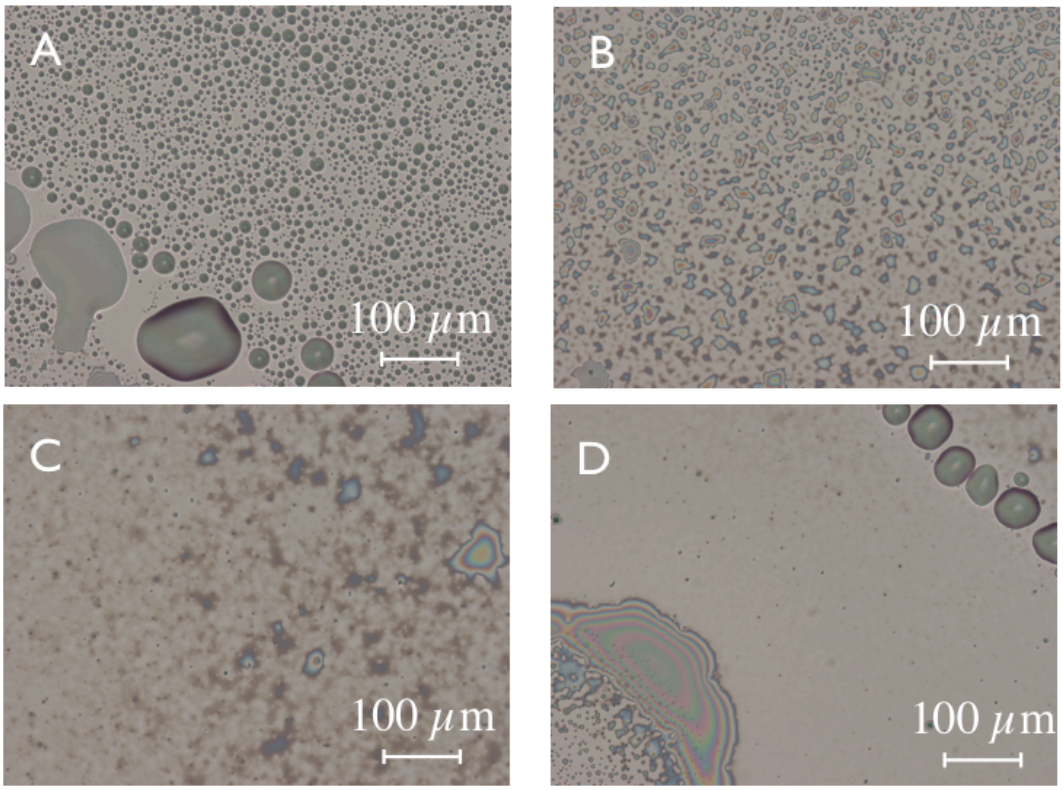

Figure 7.8. 10x optical microscopy images of [bmim][PF6] films after XPS analysis for ~400 min that induces a morphological change in the film in regions that have been exposed to XPS analysis. (A) is an unaffected portion of the film ~ 1.5 cm from the analysis area, (B) transition region of the film where the shape of droplets has been altered ~ 1 cm from analysis area, (C) coalesced ionic liquid film in the analysis area, (D) demonstrates portions at the interface of droplets and uniform film near the edge the of substrate.

Conclusions

Ionic liquids exhibit contact angles that are strongly influenced by ion pairing within the droplets and are distinct from those exhibited by dicyclohexyl, a dispersive liquid with similar suface tension as the IL. On both Au and Si substrates, the critical surface energy required for the formation of an IL film was characterized by a [bmim][triflate] contact angle of $\leq$ ~20°, which corresponds to an advancing water contact angle of $\leq$ 60°. Molecular simulation of [bmim] [triflate] droplets on hydroxyl- and methyl-terminated SAMs are qualitatively consistent with the experimental observations and show that the higher energy hydroxyl surface induces a perturbation of the characteristic charge alternation of the IL, decreasing the forces of attraction between the ions in the outer shells and reducing the local surface tension in the drop. Heat treatment was observed to aid in the spreading of [bmim][PF6] on a hydroxyl substrate, but wetting behavior reverts to non-continuous droplets upon returning the sample to ambient conditions. XPS-induced spreading of [bmim][PF_6] was observed and has shown promise in both modifying film morphology to a more homogenous layer and in improving the wear properties of the resulting film. More investigation is needed into the mechanisms for changes in morphology for IL films through XPS analysis; specifically, the role of each species (x-rays, Ar^+, and electrons) plays in changing the wetting of the IL on the substrate.

References

1. Weingaertner, H., *Angew. Chem. Int. Ed.* **2008,** *47*, 654-670.

2. Hoffmann, M.; Heitz, M.; Carr, J.; Tubbs, J., *Journal of Dispersion Science and Technology* **2003,** *24*, 155-171.

3. Bonhote, P.; Dias, A. P.; Papageorgiou, N.; Kalyanasundaram, K.; Gratzel, M., *Inorganic Chemistry* **1996,** *35*, 1168-1178.

4. Li, J.; Shen, Y.; Zhang, Y.; Liu, Y., *Chem. Comm.* **2005**, 360-362.

5. Anderson, J. L.; Armstrong, D. W.; Wei, G.-T., *Analytical Chemistry* **2006,** *78*, 2892-2902.

6. Liu, X.; Zhou, F.; Liang, Y.; Liu, W., *Wear* **2006,** *261*, 1174-1179.

7. Mu, Z.; Zhou, F.; Zhang, S.; Liang, Y.; Weimin, L., *Tribology International* **2005,** *38*, 725-731.

8. Liu, W.; Ye, C.; Gong, Q.; Wang, H.; Wang, P., *Tribology Letters* **2002,** *V13*, 81-85.

9. Wilkes, J. S.; Zaworotko, M. J., *J Chem Soc - Chemical Comminications* **1992**, 965-967.

10. Liu, W. M.; Ye, C. F.; Gong, Q. Y.; Wang, H. Z.; Wang, P., *Tribology Letters* **2002,** *13*, 81-85.

11. Ye, C. F.; Liu, W. M.; Chen, Y. X.; Yu, L. G., *Chemical Communications* **2001**, 2244-2245.

12. Ye, C. F.; Liu, W. M.; Chen, Y. X.; Ou, Z. W., *Wear* **2002,** *253*, 579-584.

13. Phillips, B. S.; Mantz, R. A.; Trulove, P. C.; al, e., *American Chemical Society: Washington 2005* **2005,** *901*, 244-253.

14. Yu, G. Q.; Zhou, F.; Liu, W. M.; al, e., *Wear* **2006,** *260*, 1076-1080.

15. Jimenez, A. E.; Bermudez, M. D.; Iglesias, P.; Carrion, F. J.; Martinez-Nicolas, G., *Wear* **2006,** *260*, 766-782.

16. Gao, L.; McCarthy, T. J., *J. Am. Chem. Soc.* **2007,** *129*, 3804-3805.

17. Bonhote, P.; Dias, A.; Popageoriou, N.; Kalyanasundaram, K.; Gratzel, M., *Inorganic Chemistry* **1996,** *35*, 1168-78.

18. Laibinis, P. E.; Bain, C. D.; Nuzzo, R. G.; Whitesides, G. M., *J. Phys. Chem.* **1995,** *99*, 7663-7676.

19. Grobe, G. L.; Valint, P. L.; Ammon, D. M., *J. Biomedical Materials Research A* **1996,** *32*, 45-54.

20. Wang, M.; Liechti, K. M.; Wang, Q.; White, J. M., *Langmuir* **2005,** *21*, 1848-1857.

21. Gupta, V. K.; Abbott, N. L., *Physical Review E* **1996,** *54*, R4540.

22. Cassie, A. B. D., *Discussions of the Faraday Society* **1948,** *3*, 11-16.

23. quest@surface-tension.de, Surface tension values of common test liquids for surface energy analysis. In www.surface-tension.de/: 2006.

24. Ballone, P.; Pinilla, C.; Kohanoff, J.; Del Popolo, M. G., *Journal of Physical Chemistry B* **2007,** *111*, 4938-4950.

25. Cadena, C.; Maginn, E. J., *Journal of Physical Chemistry B* **2006,** *110*, 18026-18039.

26. Lopes, J. N. C.; Padua, A. A. H., *Journal of Physical Chemistry B* **2004,** *108*, 16893-16898.

27. Carvalho, P. J.; Freire, M. G.; Marrucho, I. M.; Queimada, A. J.; Coutinho, J. A. P., *Journal of Chemical and Engineering Data* **2008,** *53*, 1346-1350.

28. Faulkner, C. J.; Fischer, R. E.; Jennings, G. K., *Macromolecules* **2010,** *43*, 1203-1209.

29. Bhargava, B. L.; Balasubramanian, S., *Journal of the American Chemical Society* **2006,** *128*, 10073-10078.

30. Fitchett, B. A.; Conboy, J. C., *Journal of Physical Chemistry B* **2004,** *108*, 20255-20262.

31. Iimori, T.; Iwahashi, T.; Ishii, H.; Seki, K.; Ouchi, Y.; Ozawa, R.; Hamaguchi, H.; Kim, D., *Chemical Physics Letters* **2004,** *389*, 321-326.

CHAPTER VIII

CONCLUSIONS AND FUTURE WORK

In this work, we aimed to evaluate the frictional performance of monolayer films for potential lubrication applications. The results from Chapter IV show that the initial tribological properties of monolayer films depend on the surface group, chain length, and head group of the adsorbate. At low loads (9.8 mN), methyl-terminated SAMs from alkanethiol precursors yielded coefficients of friction that are 3-fold lower than those by hydroxyl- or carboxylic acid-terminated SAMs of similar total chain length. We determined that increasing the chain length of the adsorbate results in improved frictional properties of the monolayer and works to prevent probe-substrate interactions for monolayers derived from both n-alkanethiols on gold and n-alkyl trichlorosilanes on silicon. n-Alkanethiolate SAMs with chain lengths $n \leq 12$ are irreversibly damaged by a single pass of the probe at forces as low as 9.8 mN, whereas SAMs with longer chain lengths are more stable against the shearing forces of the probe. Monolayers prepared from n-octadecyltrichlorosilane and n-octadecyldimethylchlorosilane on silicon can withstand normal loads that are at least 30 times greater than those that disrupt $C_{18}S$/Au system, as a result of the stronger siloxane bonds of the silane monolayers demonstrating that stronger adsorbate-substrate interactions stabilize silane monolayers against tribological degradation.

We have presented results investigating the long-term durability, cohesive energy, and tribological failure mechanisms of silane monolayer films on silicon. The concept of

internal stability of a monolayer discussed first in Chapter IV is investigated further in Chapter V where the results show that the long-term tribological properties of silane monolayer films are dependent on their internal stabilities, which are influenced by dispersive chain interactions and cross linking, as well as their outer terminus that interacts with the sliding probe. For a constant load, increases in chain length yield monolayers that are dramatically more stable against tribological deformation to provide low coefficients of friction over much longer periods of time. For a constant adsorbate chain length, a more stable bonding to the substrate through cross linking correlates with the most stable lubricating monolayers capable of lasting several orders of magnitude longer than those with weaker substrate-adsorbate binding. For the most robust films in this study, monolayers prepared from $C_{18}SiCl_3$ that were capable of withstanding a 98 mN load for 9,200 cycles, a load dependence was observed where a load of 250 mN (~240 MPa) is required to significantly damage the film in fewer than 100 cycles. The proposed mechanism of deformation whereby disruption of the cohesive buffer leads to desorption of monolayer components is supported by XPS analysis of the reinsertion of silane molecules into the tribometry wear track.

In order to better understand the importance of surface energy on tribological properties more closely, gradient silane films were assembled onto silicon substrates. The characterization of a unique, simple, and effective approach to assemble gradient films is shown through water contact angles and ellipsometric thicknesses that confirm gradient formation with a high degree of repeatability. The tribological properties of gradient monolayer films prepared from octadecyl trichlorosilane on silicon were found to be dependent upon the surface coverage and, therefore, surface energy of the gradient

monolayer. Figure 8.1 shows how the coefficient of friction varies with surface energy as measured from advancing water contact angles. While, generally, a low energy surface yields a low coefficient of friction, a requisite thickness still must be achieved in order to observe a low frictional force. This necessity is displayed by the film formed from a C_4SiCl_3 precursor having a coefficient of friction of 0.3 despite being a hydrophobic surface and for the two surfaces of highest surface energy ($\cos(\theta_{Adv}) = 0.78$) giving very different frictional performance due to the negligible thickness of the sparse gradient compared to the hydroxyl terminated monolayer. We have shown that the thickness of a

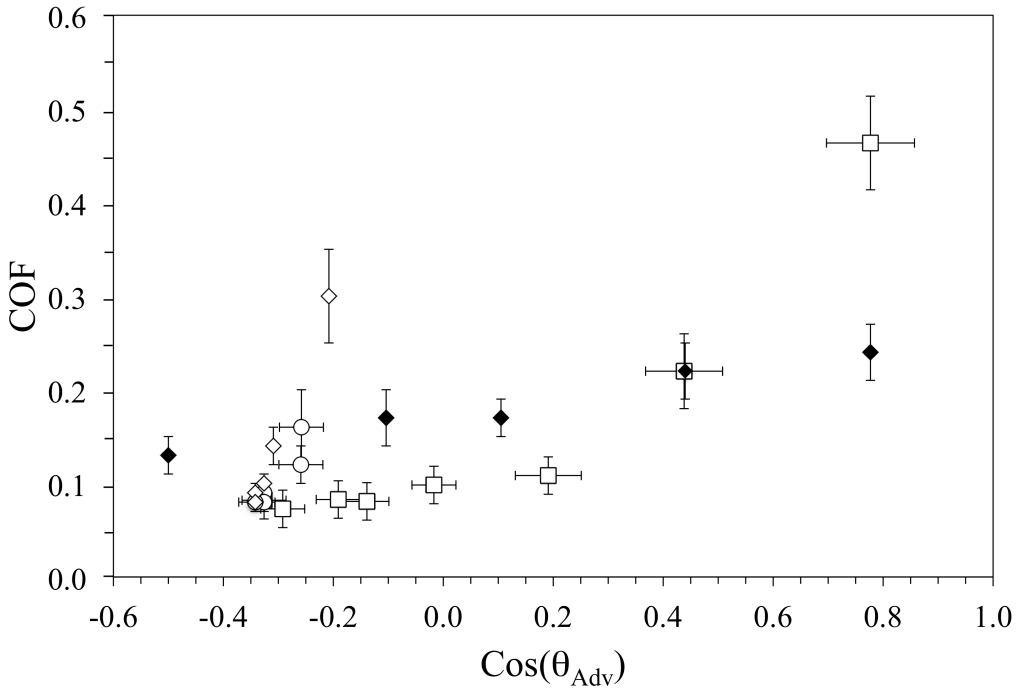

Figure 8.1. The dependence of coefficient of friction on the measured surface energy of a monolayer is shown for a 98 mN load. Diamonds represent single component trichlorosilane precursors with open and closed symbols corresponding to methyl and non-methyl terminated precursors, respectively. Open squares reprsent gradient samples and open circles represent two-component mixed monolayers consisting of methyl terminated precursors of different chain lengths.

low energy hydrocarbon monolayer is a critical aspect of the frictional response of the film by relating the tribological performance of gradient monolayers to that of monolayers with known thicknesses. Sparse monolayer regions have also been shown to be dependent upon the conditions of tribology testing due to the higher degrees of freedom for each molecule. These sparse regions are more prone to frictional failure by exposing more of the underlying substrate and further enabling the probe tip to impart the normal load to fewer adsorbed molecules to greatly increase the pressure per adsorbate.

Finally, a mobile phase of ionic liquids was investigated to improve the tribological wear on a substrate. We found that ILs exhibit contact angles that are strongly influenced by ion pairing within the droplets and are distinct from those exhibited by dicyclohexyl, a dispersive liquid with similar surface tension as the ionic liquid [bmim][triflate]. The critical surface energy required for the formation of an IL film was characterized by wettability of [bmim][triflate] and were qualitatively consistent with molecular simulations of [bmim] [triflate] droplets on hydroxyl- and methyl-terminated SAMs showing that the higher energy hydroxyl surface induces a perturbation of the characteristic charge alternation, reducing the local surface tension in the drop. Heat treatment was observed to aid in the spreading of [bmim][PF_6] and [hmim][triflate] on a bare substrate, but wetting behavior reverts to non-continuous droplets upon sample returning to ambient conditions. The spreading of [bmim][PF_6] was observed during XPS analysis, and more homogneous films have shown promise in improving the wear properties of the resulting film.

Future Work

Tribology of Longer Monolayers

In this work we have investigated the classical monolayer systems of alkanethiolates on gold and silanes on silicon using commercially available precursors. The observed plateau for monolayers greater than 8 carbons should be further investigated to determine if this behavior holds for thicker monolayer films such as $C_{22}SiCl_3$ and $C_{29}SiCl_3$ precursors on gold and silicon, respectively. The synthesis of longer trichlorosilane precursors can be achieved through the Grignard synthesis of a long ω-terminated olefin and its subsequent reaction with tetrachlorosilane by using a platinum catalyst. These molecules would allow for the determination if the observed plateau in frictional coefficient and the observed exponential increase in tribological durabilitiy extend to chain lengths greater than 18 or 22 carbons.

Gradient Silane Monolayers

The gradient films assembled for study in Chapter VI offer several interesting future studies. The initial characterization provided in this work offers a basis of understanding a straightforward assembly method for gradient silane films that can be built upon to probe monolayers of varying surface energies. The incorporation of a tunable terminal group into the gradient provides a unique group of films that could have the surface energy varied by an external stimulus to completely change the wetting, thickness, and tribological properties of the resulting film. Such films could be implemented where the functionality could be modified through changes in pH or even

load. The gradient films in Chapter VI were prepared from only octadecyl trichlorosilane so a natural extension of this work would be to develop two component films. We have shown that the coefficient of friction depends on terminal group and thickness; thus, by incorporating a second precursor or back filling the gradient after the first assembly process a more robust film with a longer wear life could be produced. The ability to vary the surface energy independent of thickness may produce more consistent tribological behavior.

IL Films Modified by XPS

In Chapter VII we demonstrated the ability to modify thin films of ionic liquid using XPS. There are many aspects of this procedure that need to be investigated in more depth starting with the mechanism for changing film morphology, as this is not fully understood at this time. Studies varying each species used in XPS analysis, x-rays, Ar atoms, and electrons, should be completed. Also varying the energy of these species may provide insight into the mechanism and reveal a more efficient method to produce homogeneous IL films. The thickness limit for IL films formed in the manner is not known, and the possibility of fabricating ultra thin ionic liquid films (< 50 nm) should be studied to extend IL lubrication into applications where the ~150 nm films explored in this work may not be beneficial. The partitioning of anion or cation to the air/vacuum interface could be important not only in wetting phenomena but also for future use in lubrication applications. Finally, extending the XPS method to obtain homogenous films can be tested to examine if IL films could be used in more complex two phase systems

where the IL coats an underlying monolayer or polymer to further enhance frictional properties.

APPENDIX A

CHARACTERIZATION OF MONOLAYERS

n-Alkanethiols on Gold

The characterization of alkanethiolates on gold and trichlorosilanes on silicon has been reported previously in the literature. In order to ensure that the films tested for this work were comparable with previous studies, characterization of monolayers is provided here. Table A.1 shows the characterization of alkanethiols on gold by water and hexadecane contact angles. The hydroxyl and carboxcylic acid funtionalities were hydrophilic and all methyl terminated films yield hydrophobic surfaces with films where n > 6 displaying strong oleophobic character.

Table A.1. Water (θ_{H2O}) and hexdecane (θ_{HD}) contact angles for monolayers prepared from n-alkanethiols on Au and both octadecyl dimethylchlorosilane and n-alkyl trichlorosilanes on silicon oxide.

Adsorbate/Substrate	θ_{H2O}[a] (°)	θ_{HD}[b] (°)
$C_{22}SH/Au$	110, 103	48, 40
$C_{18}SH/Au$	112, 102	48, 40
$C_{16}SH/Au$	106, 100	46, 37
$C_{12}SH/Au$	109, 96	45, 32
$C_{8}SH/Au$	106, 98	44, 30
$C_{6}SH/Au$	100, 94	28, <15
$C_{4}SH/Au$	98, 85	<15
$HOC_{11}SH/Au$	28, 19	<15
$HO_2C_{11}SH$	38, 24	<15

[a] Standard deviation ±4. [b] Standard deviation ±2.

Figure A.1 shows the inverse capacitances of n-alkanethiols on gold measured by electrochemical impedance spectroscopy in 0.1 M Na_2SO_4 (aq), 1 mM $K_3Fe(CN)_6$, and 1 mM $K_4Fe(CN)_6$. Since the capacitance of a film (*c*) can serve as a measure of the film thickness, the chain length of the n-alkanethiol should be reflected in the capacitance of the SAM.[1] Using a Randles equivalent circuit and a Helmholtz model the relationship between capacitance and thickness is related by the following equation:

$$\frac{1}{c} = \frac{d_{SAM}}{\varepsilon_{SAM}\varepsilon_o} = \frac{d_{CH_2}n}{\varepsilon_{CH_2}\varepsilon_o} + \frac{d_s}{\varepsilon_s\varepsilon_o} \qquad \text{(A-1)}$$

where d_{SAM} is the thickness of the monolayer, d_S is the effective thickness of the sulfur layer ($d_{SAM} = d_{CH2}n + d_S$), ε_{SAM} is the permittivity of the total film, ε_{CH2} and ε_S are the permittivities of the hydrocarbon and sulfur portions of the film, respectively, and ε_o is the permittivity of vacuum. The slope for a linear fit through the data gives a dielectric constant of 2.4 that compares favorable to the hydrocarbon value of 2.3.[2]

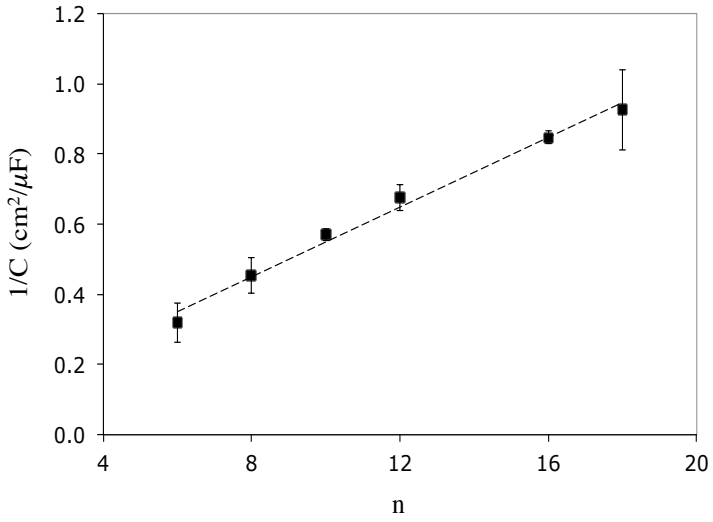

Figure A.1. Inverse capacitances of SAMs of CnSH on gold. Capacitance values were determined by fitting impedance data to a Randle equivalent circuit. The dashed line is a linear fit of the data and corresponds to a dielectric constant of 2.4

Silane Monolayers on Silicon

Table A.2 shows the characterization of silanol based films on silicon. Since trichlorosilanes have a tendacy to polymerize vertically, [3] the ellipsometric thicknesses of films prepared from silane based precursors were measured and exhibited the appropriate monolayer thicknesses. Our results agree with known values for the family of C_nSiCl_3 monolayers where all films display hydrophobic wetting. Monolayers prepared from C_nSiCl_3 where n > 8 exhibit contact angles that are indicative of dense methyl surfaces that correlate with well-ordered monolayers. [4, 5] Thinner monolayers prepared from C_nSiCl_3 with n = 4 and 6 exhibit lower contact angles that suggest a less dense methyl surface[4, 6] with less effective screening of forces between the probe liquid and the substrate. The conversion of the vinyl terminus to hydroxyl was demonstrated previously and these results agree with that work. [7] The deprotection of the trichloroacetate head

group was developed in our group and compares well with other loosely packed hydroxyl monolayers.[8] The monolayer prepared from $F_3C(CF_2)_5(CH_2)_2SiCl_3$ exhibits a hexadecane contact angle of 80° that is consistent with the formation of a dense CF_3-terminated surface.[9, 10]

Table A.2. Characterization of silane monolayers on silicon: advancing and receding water contact angles (θ_{H2O}), advancing and receding hexadecane contact angles (θ_{HD}) and ellipsometric thicknesses (d).

Adsorbate	θ_{H2O}[a] (°)	θ_{HD}[b]	d[c] (nm)
C_4SiCl_3	102, 88	20, <15	0.7
C_6SiCl_3	108, 96	29, 18	0.9
C_8SiCl_3	109, 100	36, 28	1.1
$C_{12}SiCl_3$	110, 103	40, 35	1.4
$C_{16}SiCl_3$	110, 104	43, 41	1.9
$C_{18}SiCl_3$	110, 103	44, 40	2.4
$C_{18}Si(CH_3)_2Cl$	96, 80	32, 16	1.5
$F_3C(CF_2)_5(CH_2)_2SiCl_3$	120, 105	80, 61	1.0
$H_2C{=}CH(CH_2)_6SiCl_3$	96, 84	<15	1.1
$HO(CH_2)_8SiCl_3$ via hydroboration	39, 22	<15	--
$Cl_3C_2O_2(CH_2)_{11}SiCl_3$	84, 76	<15	1.7
$HO(CH_2)_{11}SiCl_3$ via trichloroacetate	64, 55	<15	1.5

[a] Standard deviation ±4. [b] Standard deviation ±2. [c] Standard deviation ±0.1.

References

1. Porter, M. D.; Bright, T. B.; Allara, D. L.; Chidsey, C. E. D., *Journal of the American Chemical Society* **1987,** *109*, 3559-3568.

2. Brandrup, J.; Immergut, E. H.; Grulke, E. A., *Polymer Handbook*. 4th ed.; Wiley: New York, 1989.

3. Fadeev, A. Y.; McCarthy, T. J., *Langmuir* **2000,** *16*, 7268-7274.

4. Masuko, M.; Miyamoto, H.; Suzuki, A., *Tribology International* **2007,** *40*, 1587-1596.

5. Allara, D. L.; Parikh, A. N.; Rondelez, F., *Langmuir* **1995,** *11*, 2357-2360.

6. Xiao, X. D.; Hu, J.; Charych, D. H.; Salmeron, M., *Langmuir* **1996,** *12*, 235-237.

7. Wasserman, S. R.; Tao, Y. T.; Whitesides, G. M., *Langmuir* **1989,** *5*, 1074-1087.

8. Berron, B.; Jennings, G. K., *Langmuir* **2006,** *22*, 7235-7240.

9. Weinstein, R. D.; Moriarty, J.; Cushnie, E.; Colorado, R.; Lee, T. R.; Patel, M.; Alesi, W. R.; Jennings, G. K., *Journal of Physical Chemistry B* **2003,** *107*, 11626-11632.

10. Genzer, J.; Efimenko, K.; Fischer, D. A., *Langmuir* **2002,** *18*, 9307-9311.

APPENDIX B

INVESTIGATION INTO MECHANISM OF MICROTRIBOLOGICAL FAILURE OF N-ALKANETHIOLS ON GOLD

The effect of surface attachment on the long-term tribological properties of monolayer films was investigated by comparing alkanethiolate SAMs on gold and silane monolayers on silicon. The alkanethiolate molecules self assemble on the gold surface by chemisorption whereas silane molecules form covalent siloxane bonds with exposed silanol groups from the silicon (oxide) substrate. To properly compare the differences in attachment to the surface, octadecanethiol ($C_{18}SH$), octadecyl dimethylchlorosilane ($C_{18}SiMe_2Cl$), and octadecyl trichlorosilane ($C_{18}SiCl_3$) were selected as adsorbates for comparison where each molecule possesses an identical number of carbon atoms in the backbone as well as an identical methyl terminus. Due to their identical carbon chain length, the films formed from these adsorbates should exhibit similar levels of van der Waals forces between the molecules, although the lesser packing[1] in the monolayer formed from $C_{18}SiMe_2Cl$ should result in the weakest intermolecular interactions of the three films indicated by a water contact angle 14° and 16° less than $C_{18}SiCl_3$ and $C_{18}SH$, respectively (shown in Appendix A).

Table B.1. Average wear life for monolayer systems that have similar extents of dispersive interactions subjected to a 98 mN load with a 4 mm stainless steel probe

Monolayer System	Average Wear Life (Cycles)
$C_{18}S/Au$	5 ± 3
$C_{18}SiMe_2Cl/SiO_2$	1,615 ± 680
$C_{18}SiCl_3/SiO_2$	9,200 ± 300

The capability of films prepared from octadecyl trichlorosilane on silicon to consistently provide good wear protection for 9,200 cycles indicates that these films have the largest cohesive energy (Table B.1). While the $C_{18}SiMe_2Cl$ based film attaches to the silicon substrate by the same covalent bond as alkyltrichlorsilane molecules, $C_{18}SiMe_2Cl$ molecules are not able to form additional cross-linked bonds during monolayer formation. Furthermore, the methyl groups attached to either side of the chain limit the ability of the molecules to pack into a dense film.[1, 2] Both of these factors reduce the cohesive energy of the subsequent film and dramatically reduce the long-term lubricating ability by an order of magnitude compared to a monolayer prepared from $C_{18}SiCl_3$. The thiolate monolayers, despite having a high packing density that maximizes the dispersion interactions among chains, perform poorly in tribological durability testing lasting for only 5 cycles at a 98 mN load.

While it is possible the poor wear performance of octadecanethiol is due to the fact that the alkanethiolate monolayer is chemisorbed to the gold surface by the strong association between the gold and sulfur head group, rather than forming a covalent bond; the difference in adsorbate-substrate attachment may not be the main cause of failure for thiol/gold systems subjected to cyclic tribological testing. In order to understand the mechanism in which alkanethiol/gold system failed during stability testing, optical microscopy images were taken of the tribological wear track at different numbers of

cycles. Images at 10x magnification were taken of both a bare gold substrate and a $C_{18}S$/Au substrate and are presented in Figure B.1A. Figure B.1A shows the wear track of the bare gold substrate after a single tribological pass and qualitatively demonstrates the damage done by the stainless steel probe tip to the gold substrate. Subsequent tribological cycles broaden the wear track and produce a greater number of striations indicative of the gold being scratched and eventually worn away by 50 cycles (Figure B.2). The soft, malleable gold is easily displaced by the 98 mN load from the tribology test track during wear testing. Figure B.1B shows an optical image confirming the onset of damage to a $C_{18}S$/Au sample at 5 cycles where the outline of a weak track has formed. Further damage to this coated sample can be seen in Figure B.1C where, at 10 cycles, more scratches are observed as the $C_{18}S$/Au surface yields a coefficient of friction similar to bare gold, 0.30, suggesting that the monolayer no longer provides tribological benefit. Evidence that the gold substrate is being damaged can be more easily seen in Figure B.1D with an increase in the number of scratches and their depth, as indicated by the darkening of each scratch. By comparing optical images from bare gold sample and octadecanthiol/gold sample at similar numbers of wear cycles we are able to investigate how the system fails. As shown in Table 6.3, frictional data indicate that the monolayer is able to provide lubrication and protection to the gold surface for approximately 5 cycles where, as Figure B.1A shows, the onset of damage to the gold substrate can be observed. Additionally, when comparing the octadecanethiol/gold at 10 cycles (Figure B.1C) to the bare gold at 1 cycle (Figure B.1A) it is clear that the monolayer, although deemed to have failed by coefficient of friction values, has offered beneficial protection to the gold substrate. The $C_{18}S$/Au system at 20 cycles (Figure B.1D) does closely

resemble the bare gold at 1 cycle (Figure B.1A), which is indicative of complete tribological failure of the monolayer and the deformation of the gold substrate. A quantitative investigation was performed using electrochemical impedance spectroscopy (EIS) of samples before and after tribology testing[3] to determine any damage to the monolayer film as EIS is a well-known, sensitive technique for analysis of monolayer film defects. Using a Randles equivalent circuit to fit the data, film capacitance and resistance values were obtained for monolayers before and after 10 and 20 cycles.

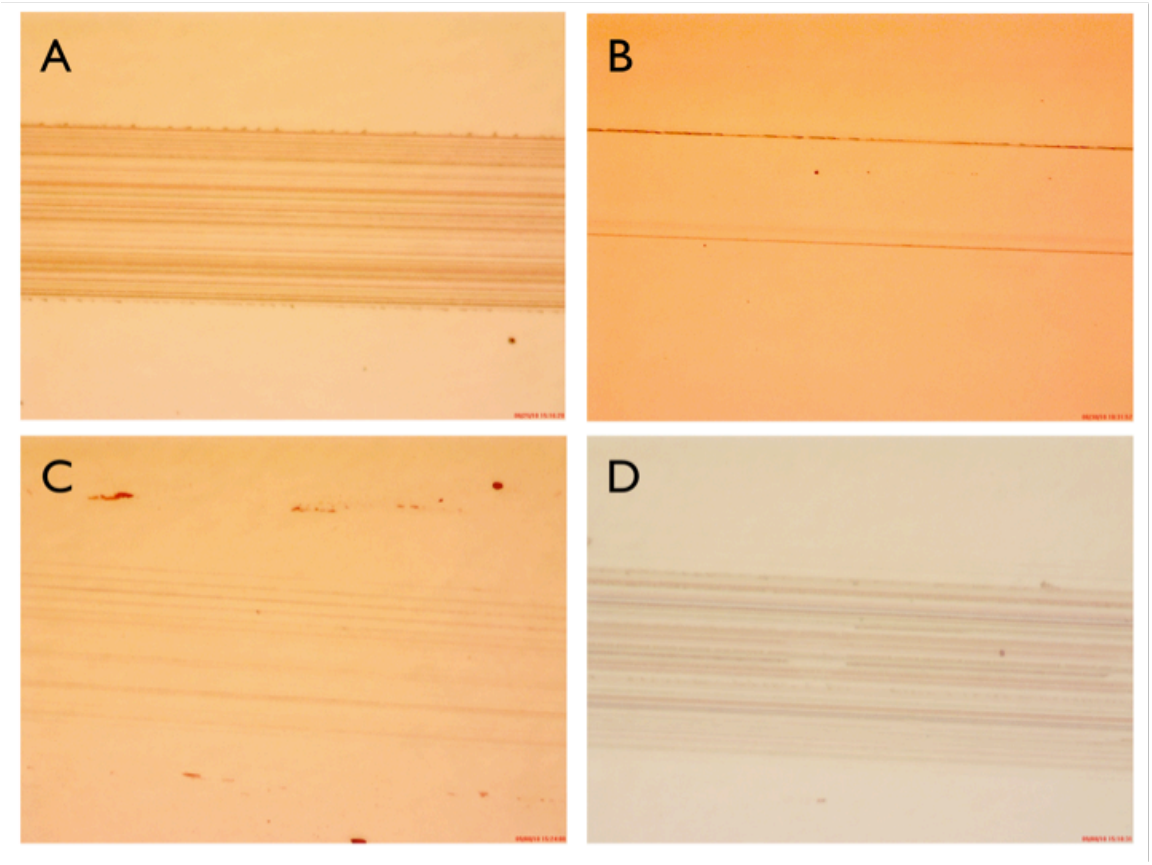

Figure B.1. Optical microscopy images at 10x of tribological wear tracks performed on unmodified gold and $C_{18}S$/Au that were subjected to a 98 mN load. (A) Bare Au for 1 cycle, (B) $C_{18}S$/Au for 5 cycles, (C) $C_{18}S$/Au for 10 cycles, (D) $C_{18}S$/Au for 20 cycles.

Before tribology testing the film capacitance for each monolayer was 1 μF/cm^2 and had a film resistance of 360 and 290 kΩ, respectively. After 10 cycles the film capacitance increased to 1.1 μF/cm^2 and after 20 cycles increased 1.3 μF/cm^2. The film resistance dropped to 50 kΩ and 20 kΩ, respectively for 10 and 20 cycles. These EIS results indicate that a significant number of molecules remain on the surface but the underlying gold substrate has been deformed by the probe tip as shown in the optical images (Figure B.1B-C). The damage to the underlying gold may disrupt the packing in the SAM to create defects for the transport of redox species during impedance testing. Thus, the SAM provides a buffer layer to inhibit tribological deformations to the gold surface, and the SAM remains attached after such deformation has created grooves in the underlying substrate. The roughness of the stainless steel probe (13 nm) is almost an order of magnitude higher than the substrate and also contributes to the type of wear imparted to the monolayer/Au system. The rearrangement of the gold substrate is also manifested in a higher COF as the monolayer begins to be rearranged along with gold and still provides some frictional benefit by continuing to mitigate against probe/gold contact.

Optical microscopy images of tribological wear tracks for increasing number of cycles were obtained at 50x magnification. In Figure B.1 we showed that even after 1 cycle the gold substrate is damaged, here we have extended the tribological testing to 5, 10, and 50 cycles. For 5 and 10 cycles (Figure B.2A-B) numerous striations are observed in the substrate indicative of significant damage to the gold. At 50 cycles (Figure B.2C) the stainless steel probe tip has displaced a significant amount of the gold layer (~125 nm) as the underlying silicon wafer is exposed. Similarly, for the substrate treated with a monolayer and subjected to 50 cycles the silicon substrate can be seen in the center of the

wear track demonstrating the removal of gold from the tribological wear track by the probe tip (Figure B.2D).

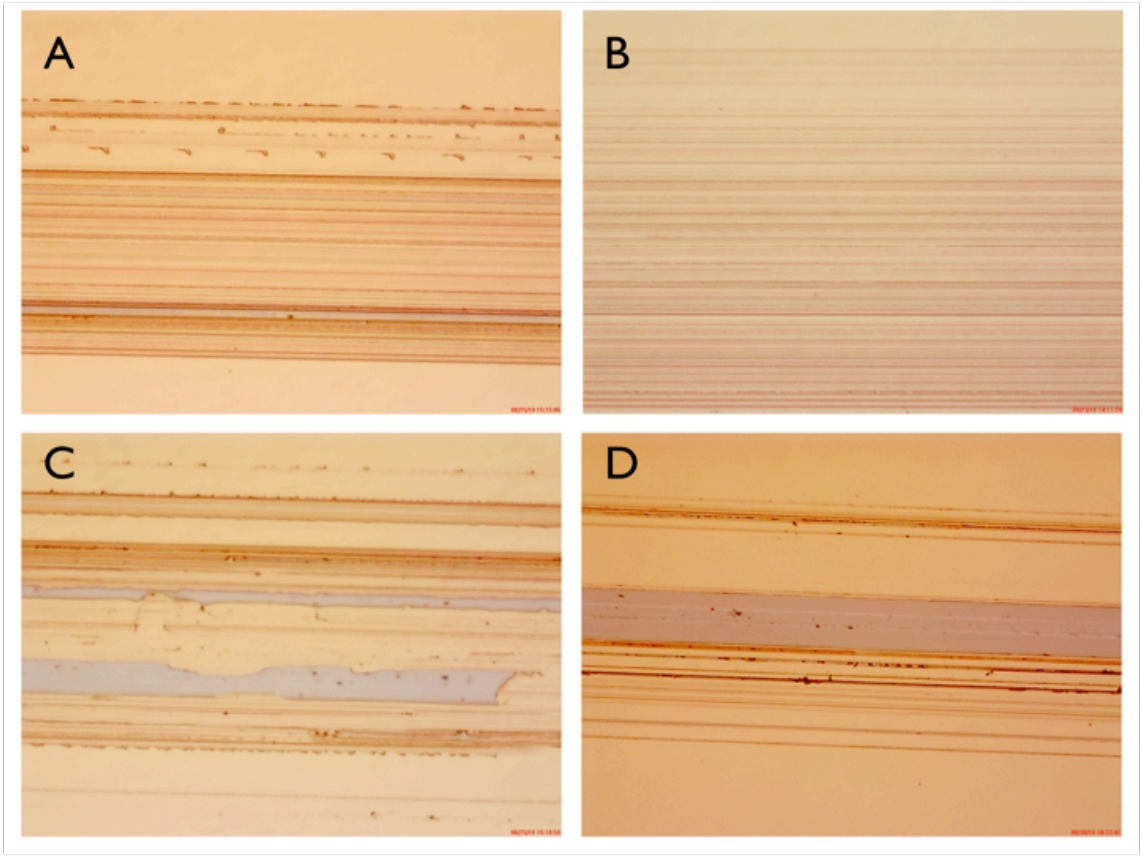

Figure B.2. Optical microscopy images obtained at 50x demonstrating damage to the bare gold substrate subjected to a 98 mN load at (A) 5 cycles, (B) 10 cycles, (C) 50 cycles and (D) damage to an octadecanethiol monolayer on gold at 50 cycles.

Scanning electron microscopy (SEM) was performed on the tribological wear tracks of films prepared from both octadecanthiol on gold and octadecyl trichlorosilane on silicon after 10 cycles at a 98 mN applied load (Figure B.3) to investigate any discrepancies in the interaction between the probe tip and surface. We first compared the tribological track of bare gold (Figure B.3A) and bare silicon oxide (Figure B.3C) to determine if the substrate had an influence in the applied load. We have found that the

wear tracks left after tribology testing are similar in size indicating that the load and surface pressure are consistent for both systems and suggesting that the substrate itself does not influence test results. When comparing bare gold (Figure B.3A) and the failed octadecane thiol on gold (Figure B.3B), the two wear tracks are also similar in size and appearance indicating that the monolayer has been completely removed from the surface. However, the monolayer prepared from octadecyl trichlorosilane (Figure B.3D) shows no wear track after 50 cycles demonstrating the ability of the film to withstand the 98 mN applied normal load. The more favorable tribological performance for silane monolayers over thiolate SAMs can be attributed to the strong covalent attachment of the silane molecule to the substrate and, for n-alkyl trichlorosilanes, the added ability of these adsorbates to intermolecularly cross-link between molecules,[4, 5] forming a robust siloxane network. Both the adsorbate-substrate attachment and cross-linking make removal or deformation of the trichlorosilane monolayer more difficult than that for the alkanethiolate/Au system demonstrated by the reduction in several orders of magnitude in the number of cycles required for the thiolate-based monolayer on gold to fail. The results presented here illustrate that silane films, and in particular trichlorosilane-derived monolayers, offer superior tribological durability when comparing these two widely studied monolayer systems.

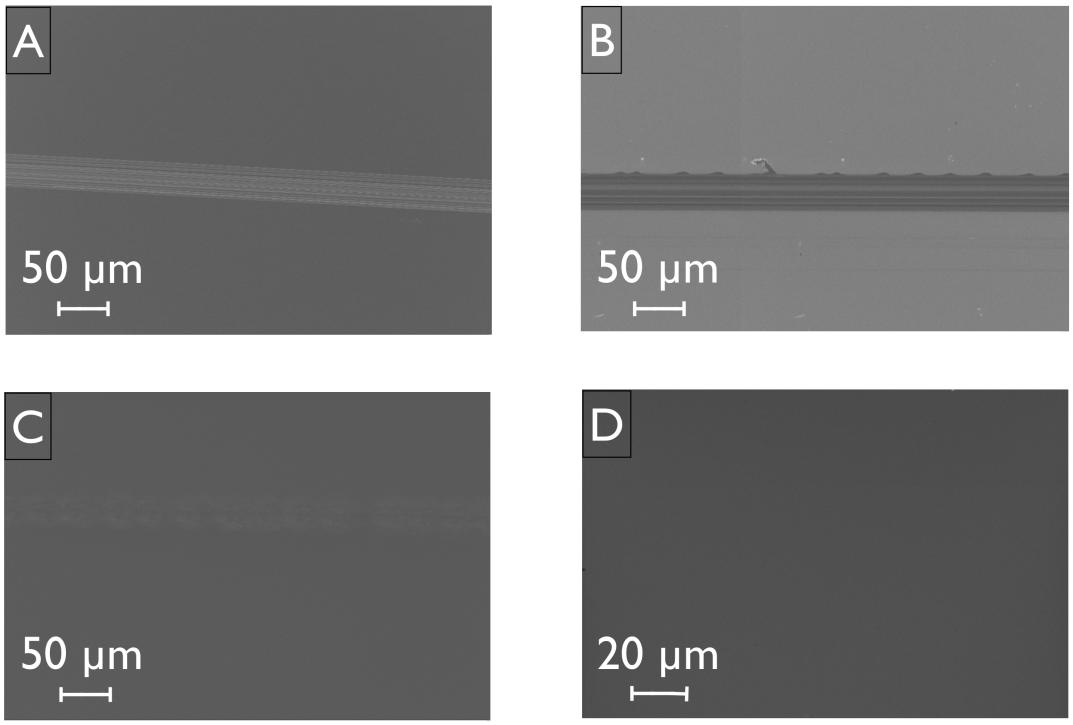

Figure B.3. SEM images of tribological wear path on different surfaces at a 98 mN load. Bare substrates (A and C) exposed to 1 cycle and monolayers (B and D) tested for ~ 50 cycles. A: bare gold substrate (30 µm wear track), B: octadecanethiol on gold (32 µm wear track), C: bare silicon oxide substrate (28 µm wear track), D: octadecyl trichlorosilane on silicon substrate (no wear track).

References

1. Clear, S. C.; Nealey, P. F., *Journal of Chemical Physics* **2001,** *114*, 2802-2811.

2. Helmy, R.; Fadeev, A. Y., *Langmuir* **2002,** *18*, 8924-8928.

3. Booth, B. D.; Vilt, S. G.; McCabe, C.; Jennings, G. K., *Langmuir* **2009,** *25*, 9995-10001.

4. Finklea, H. O.; Robinson, L. R.; Blackburn, A.; Richter, B.; Allara, D.; Bright, T., *Langmuir* **1986,** *2*, 239-244.

5. Allara, D. L.; Parikh, A. N.; elez, F., *Langmuir* **1995,** *11*, 2357-2360.